Doctoral Dissertation

Analysis and Design of Zeolite-based Catalysis for Production of Benzene Derivatives

ベンゼン誘導体製造のためのゼオライトに立脚する触媒作用の解析と設計

January 2020

Koshiro Nakamura

Department of Chemistry and Biotechnology

Graduate School of Engineering

Tottori University

Preface

The studies presented in this thesis were carried out under the direction of Professor Naonobu Katada, Senior Associate Professor Etsushi Tsuji, and Associate Professor Satoshi Suganuma, Course of Applied Chemistry, Department of Chemistry and Biotechnology, Graduated School of Engineering, Tottori University, during 2017-2020.

The object of this thesis is to analyze and understand catalysis of reactions promoted over zeolite-based catalyst, and to develop and design a new catalyst for production of benzene derivatives, based on cutting-edge techniques. The author wishes that knowledges from this thesis would be guidelines for designing a new zeolite-based catalyst supporting next generation.

Koshiro Nakamura

Koshiro   Nakamura

Department of Chemistry and Biotechnology

Graduate School of Engineering, Tottori University

4-101 Minami, Koyama-cho, Tottori 680-8552, Japan

January 2020

Contents

Chapter 1   General Introduction

1-1 Benzene derivatives

Benzene is the most simple and basic aromatic compound in chemistry. It had

been utilized as an organic solvent until its toxicity was recognized, but even after that,

benzene derivatives have widely been utilized as feedstocks of plastics and fibers which

are very important in our modern life and industry [1-3].

Examples of benzene derivatives and their uses with large demand are

summarized in Figure 1-1. Toluene is converted into *p*-xylene by toluene

disproportionation and then, poly (ethylene terephthalate) (PET) is formed from

terephthalic acid produced via autooxidation of *p*-xylene [4 - 7]. Ethylbenzene is

dehydrogenated into styrene which is the feedstock of polystyrene and other polymers [8-
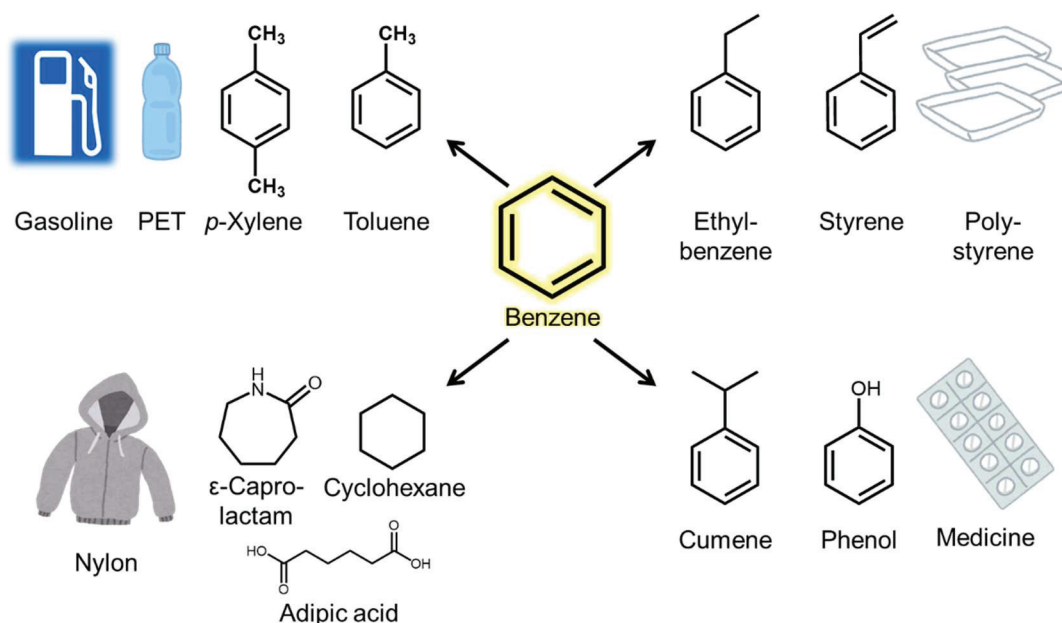

Figure 1-1   Example of utilization in benzene derivatives.

11]. Cumene synthesized from benzene and propylene is an important intermediate of phenol and acetone production [12-16]. Cyclohexane produced from hydrogenation of benzene is also an important intermediate of nylon 6 and nylon 66 [17-19].

Demand of the benzene derivatives is very large all over the world. It leads the demand of benzene in 43.7 million metric tons in 2013, an increase of 2.8% from 2012 [20]. The overall world consumption of PET amounted to about 26 million tons in 2000s [21,22], and 100 million tons in 2016 [23]. Demand for polystyrene was estimated for around 14.9 million tons in 2010, and its market would grow at rate of 5.6% from 2010 to 2020 [24]. Polymethyl-methacrylate (PMMA) produced from methacrylate which often had phenol as functional group was exclusively produced in industry via radical polymerization with annual world production greater than 2 million tons [25]. Adipic acid which is a feedstock was produced 2.6 million tons per year in 2010 and expected to reach 3.3 million tons per year in 2016 [26]. Nylon 6 has been produced over 4 million tons annually [27]. Thus, the demand of benzene derivatives is growing.

Various hydrocarbons have been gained from petroleum with distillation for a long time. However, petroleum is mined very locally at parts of the word, leading that the supply is affected by political conditions. Natural gas has large reserves even within conventional gas sources, and it is recently mined as shale gas in economic scale. In

addition, many unmined resources are still kept as described below. Therefore, development of processes which can convert natural gas into benzene derivatives has been demanded strongly.

1-2 Zeolites

Hydrocarbons are converted from resources into value-added compounds in the petroleum refinery and chemical processes, and in most processes, catalyst are utilized to achieve efficient producibility and selectivity. Reactions related to the benzene derivatives such as ethylation and methylation of benzene, isomerization of cyclohexanone oxime, disproportionation and methylation of toluene, and aromatization of methanol are catalyzed by zeolites. The development of highly efficient zeolite catalysts has supported the modern chemical industries.

Zeolites are microporous crystalline aluminosilicates which are mainly composed with SiO_2. The composition and structure are varied, and it allows zeolites to be utilized as ion exchange reagents, absorbents, catalyst supports, and catalysts, which are necessary for our modern society.

The first zeolite was found as mineral in Northern Sweden by Axel Cronsted who was Swedish mineralogist in 1756, and it was named stillbite afterward [28]. He

surveyed about zeolites and found distinctive properties of them, i.e., when zeolites are heated, bubbles of water vapor emerge from the zeolites.

However, investigation of zeolites had been stopped for about nineteen decades [29]. Then, Richard M. Barrer, a New-Zealand-born chemist, studied adsorption-desorption behavior of zeolites, and he opened a way of zeolite synthesis in 1940s [29-31]. Subsequently, Robert M. Milton developed industrial methods of zeolite synthesis [32]. Since these periods, various zeolites were found and synthesized.

Distinctive properties of zeolites are mainly presented with high surface area, high thermal stability, and ion exchange ability.

The high surface area which is over hundreds m^2 g^{-1} is originated by three-dimensionally regular structure with microporosity. Micropore is defined to have pores with diameter less than 2 nm, and the diameter of the micropores of zeolite is about 0.3-0.8 nm, leading the zeolite categorized into microporous material [33]. Zeolites are

| BEA | MFI | MOR |

Figure 1-2   Examples of different structured zeolites (●: Si, ●: O).

mainly structured with tetrahedral silica (SiO_2), and various structures have been known as examples shown in Figure 1-2. The framework types (framework topology) is shown by the IUPAC framework type code with three alphabetical letters. The name of material, given

Table 1-1   Examples of zeolites and framework type code.

Material name	Framework type code
ZSM-5	MFI
MCM-22	MWW
β	BEA
Y	FAU
Mordenite	MOR
Ferierrite	FER

by the inventor like customary name of compound, is also used as well as the framework type code. Some examples are shown in Table 1-1. Up to now, 248 topologies were registered in International Zeolite Associate database [34].

On the other hand, high thermal stability and ion exchange ability of zeolites are originated by the chemical composition. As explained above, zeolites mainly consist of SiO_2, realizing the high thermal stability against over 800 K. On the other hand, a part of Si^{4+} is isomorphously-substituted with Al^{3+}, generating a negative charge. In order to
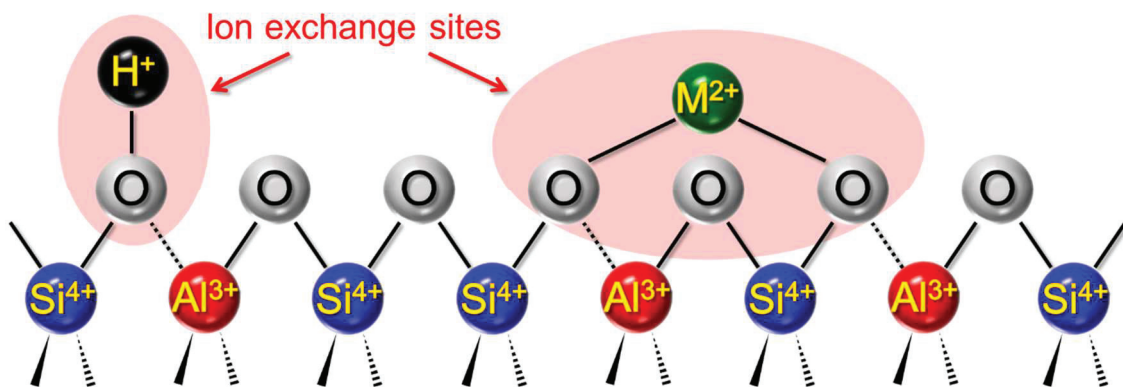

Figure 1-3   A simple model of zeolites.

5

counterbalance the negative charge, zeolites have protons (H^+) and/or metal cations (M^{n+}) near the Al sites, and these cations can be exchanged. The part around of aluminum atoms in zeolites are named as "ion exchange sites" (Figure 1-3). Here, Si^{4+} sites which are possibly exchanged with other atoms like Al^{3+} are called "T sites". IUPAC defines that the zeolite is a tect-silicate with micropores due to the framework topology containing only Si, Al and O in the framework, but Zn^{2+}, B^{3+}, Ga^{3+}, Ge^{3+}, Sn^{4+}. Ti^{4+}, and P^{5+} were reported to be inserted in T sites, and the yielded materials, defined as members of zeotypes, are called metallosilicate molecular sieves [35-41]. Among the zeotypes, aluminosilicate zeolites are preferentially utilized in industrybecause of thermal and chemical stability.

History of utilizing zeolite as a catalyst was started in 1960s [42]. Prior to zeolite, amorphous silica-alumina had been used as a solid acid catalyst in industry. Introduction of zeolite   catalysts was revolution in heterogeneous catalyst processes such as cracking and hydrocracking to produce gasoline, diesel, and fuel. Catalytic activity of a proton type zeolite which had Brønsted acid sites was superior to amorphous silica-alumina. Then, the field related with zeolites has grown quickly. Not only Brønsted acidic but also Lewis acidic zeolites originated by metal species supported on them were developed and applied
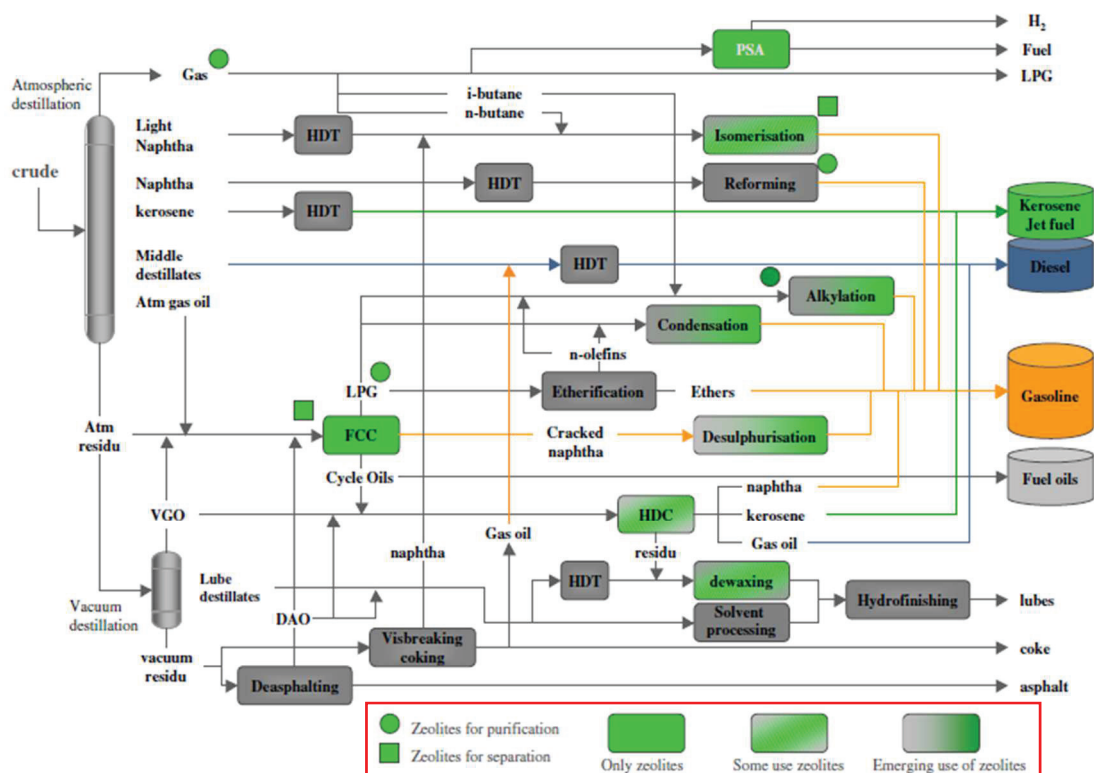
Figure 1-4　Major operations found in modern petroleum refineries [43].

as catalysts in mainly petrochemical field.

Brønsted acidic (proton type) zeolites have been utilized as catalysts for petroleum refinery [43], as shown in Figure 1-4. For example, H-MFI zeolite catalyst has been used for oligomerization [44], toluene alkylation and disproportionation [45,46], cumene hydroperoxide decomposition to phenol and acetone [47], and methanol conversion [48]. H-*BEA zeolite is strongly active catalyst for acylation [49,50]. H-MOR zeolite is often used in the reaction for isomerization of alkane [51]. H-FAU zeolite is a catalyst for fluid catalytic cracking [52].

As mentioned above, zeolites have been utilized very widely, expected to be

found for new structure, and applied as supports, catalysts, ion exchange materials, and

recently membranes. Therefore, studies about application of zeolites and its catalysis have

attracted much interest of many researchers including the author.
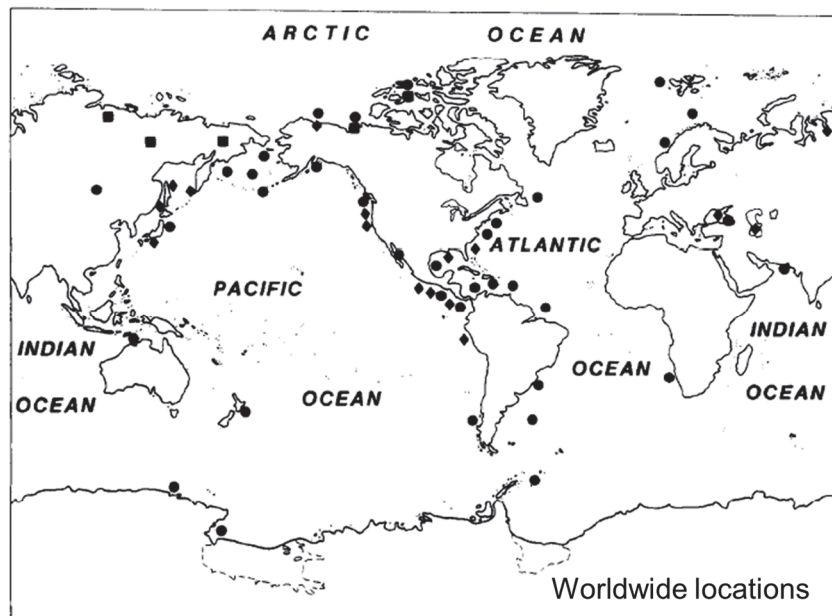

1-3 Natural gas

Figure 1-5   Worldwide locations of known and inferred gas [53].

Natural gas has attracted much interest as an alternative of petroleum, because

natural gas reserves are located in worldwide as shown in Figure 1-5 [53], in contrast to

petroleum. The natural gas is mainly consisting of gaseous hydrocarbons, and practically

composed methane and ethane (Figure 1-6) [54,55]. For a long time, natural gas had been

mined in Russia and Asia [56]. It had been known that that components of natural gas
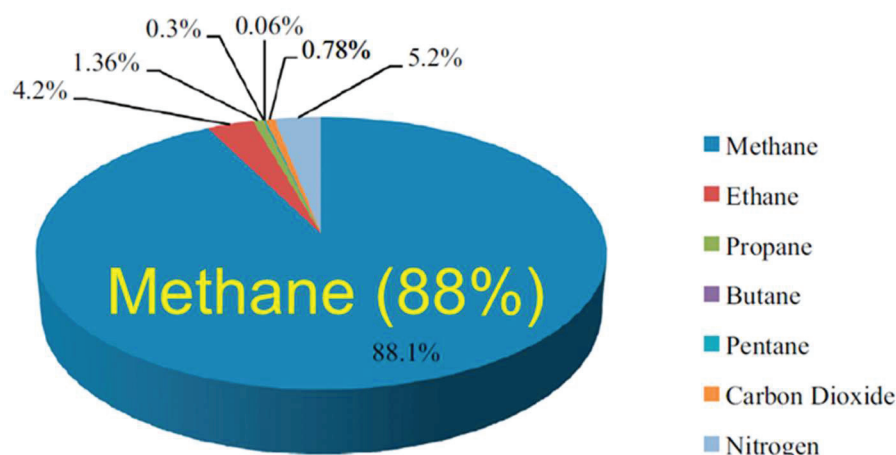
Figure 1-6　　Typical composition of natural gas [55].

existed in shale rocks, but it had been difficult to economically gain them from shale rocks. However, some companies in United States have succeeded to mine the natural gas from shale cost-effectively, and the prices of natural gas and hydrocarbons produced from the gas drastically decreased. It was what we call "shale gas revolution".

After the shale gas revolution, relatively cheap liquid natural gas (LNG) has been exported from US, leading ease of using LNG in place of petroleum. However, the main component of natural gas, methane, is highly stable compound due to the strong C-H bond. On these backgrounds, methane has been utilized mainly by pipeline transportation or liquefying by high pressure (high cost) as an energy source. To make provision against serious lack of petroleum in the future, it is strongly demanded to develop processes which can convert methane into liquid chemicals. For this purpose, improving and designing catalysts is very important.
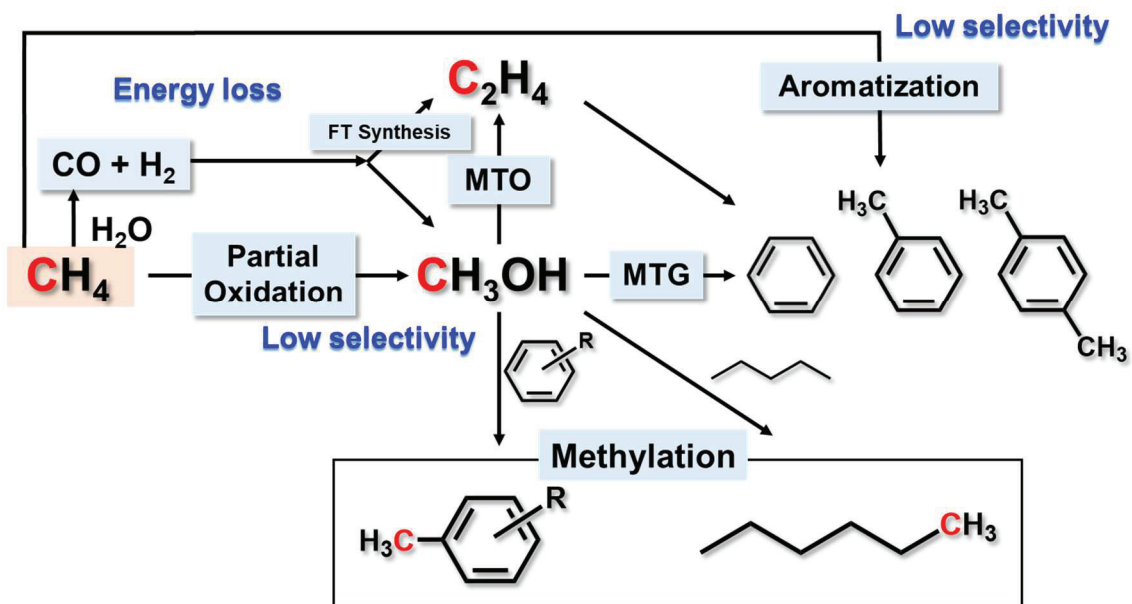
Figure 1-7   Some routes for utilization of methane as a chemical feedstock.

As mentioned above, main component of the natural gas is methane, so that many researchers have challenged developing the process and catalyst (Figure 1-7). In industry, methane is converted into synthesis gas (or called "syngas") by steam reforming [reaction (1)] [57].

$$CH_4 + H_2O \rightarrow CO + 3H_2 \qquad\qquad (1)$$

Then, the syngas is converted into liquid hydrocarbons by Fischer-Tropsch synthesis [reaction (2)],

$$nCO + (2n+1)H_2 \rightarrow C_nH_{2n+2} + H_2O \qquad\qquad (2)$$
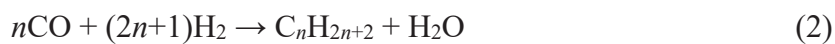
or into methanol by reaction (3).

$$CO + 2H_2 \rightarrow CH_3OH \qquad\qquad\qquad (3)$$

Ways of efficient use of methanol have already been established into synthesis small olefins and gasoline (mixture of hydrocarbons enriched with benzene derivatives), and the two processes are called methanol to olefins [MTO, reaction (4)] and methanol to gasoline [MTG, reaction (5)], respectively, by using zeolites or zeo-type materials as catalysts.

$$CH_3OH \rightarrow Olefins + H_2O \qquad\qquad\qquad (4)$$

$$CH_3OH \rightarrow Gasolines + H_2O \qquad\qquad\qquad (5)$$

It is difficult to describe these reactions by simple reaction formulas, because the processes are complex with some elementary reactions, and many products are formed. Although these processes were attempted in industry, reaction (1) + (2) and (1) + (3) consume much energy due to multistep reactions and endothermal reactions. Therefore, for the next generation, it is necessary to develop other processes.

Alternative process to synthesize methanol has been studied actively in a laboratory scale. It is the direct partial oxidation of methane to methanol [reaction (6)].

$$CH_4 + 1/2O_2 \rightarrow CH_3OH + H_2O \hspace{3cm} (6)$$

This reaction has been considered as a "dream reaction", and therefore attracted many researchers' interest. It has been found that some metals supported on zeolites were active for the reaction [57]. However, in this reaction, still now, the complete oxidation of methane [reaction (7)] as a side reaction has been unavoidable.

$$CH_4 + 2O_2 \rightarrow CO_2 + 2H_2O \hspace{3cm} (7)$$

As a different option, methane dehydroaromatization over Mo supported on MFI-type zeolite has been proposed [reaction (8)] [58].

$$6CH_4 \rightarrow C_6H_6 + 9H_2 \hspace{3cm} (8)$$

In this reaction, it is unavoidable to escape from the complete dehydrogenation of methane producing carbonaceous species which covers active sites of the catalyst,

resulting in quite serious deactivation and short catalyst life. Although it is reported that

addition of methanol in the system improved the problem, selectivity of reaction (8) has

been still low [59].

On the other hand, ethane is also included in the natural gas and converted into

chemical products. In industry, first of all, ethane is dehydrated into ethylene [reaction

(9)].

$$C_2H_6 \rightarrow C_2H_4 + H_2 \qquad\qquad\qquad (9)$$

Ethylene is a kind of olefin, which is easily added to other chemical compounds or

polymerized into polymers. The conversion of ethane is ease compared to the reactions

related to methane from a view of the energy cost and reactivity, so that industrial

achievement has been large in Europe [60]. However, multistep reactions are necessary

to obtain the final products. It is desirable to develop processes which directly convert

ethane into valuable chemicals.

1-4 Ammonia IRMS-TPD

In this section, a technique for the analysis of chemical nature of zeolite-based

catalysts in this thesis is explained.

Measurements of the acidic property are important for designing a fine catalyst. Traditionally, strength of liquid acid was measured with pK_a as an index. The pK_a is defined as equilibrium constant calculated from concentration of proton (H^+) in equilibrium state in a solution, and its measurement is relatively simple and easy. On the contrary, evaluating acidity of solid was difficult in contrast to that of liquid.

To realize it, infrared (IR) and mass spectroscopy (MS) have been utilized with probe gas molecules such as ammonia and pyridine which are adsorbed on an acid site of solid acid. Generally, IR spectra from vibration of adsorbed molecules gives us the information about the type of acid, Brønsted or Lewis, based on difference of wavenumber in the spectra. For example, it has widely been known that deformation band of ammonium cation produced by adsorption of ammonia on a Brøsnsted acid site of a proton-type zeolite is observed around 1450 cm^{-1}, and asymmetry-bending vibration of ammonia on Lewis acid site is observed around 1320 cm^{-1} [61]. On the other hand, the MS tells us amount and strength of the acid. After adsorption of base gas molecule on a solid acid, the sample is heated with constant ramp, and the desorbed molecules are quantified with MS. The amount of desorbed molecules can be regarded as the amount of
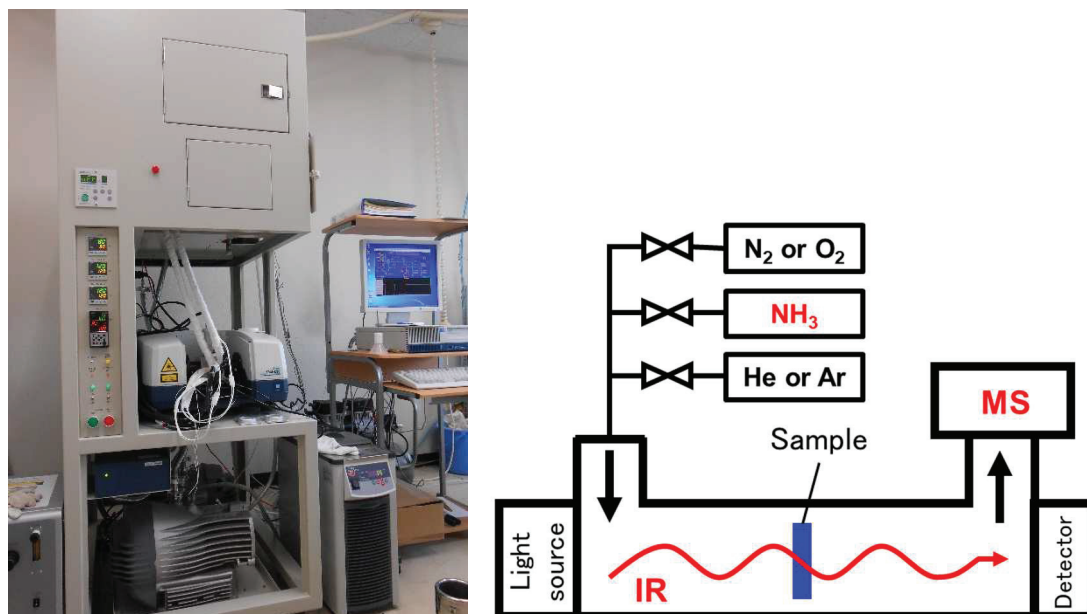
14

Figure 1-8   Ammonia IRMS-TPD in (left) picture of the equipment and (right) the principle.

acid. In addition, acid strength can be calculated based on temperature range of the desorbed molecules. The sequence is called mass spectroscopy/temperature-programmed desorption (MS-TPD). In short, acidity of solid acid indicates 3 means; (i) type of the acid -Brønsted or Lewis (ii) amount of acid sites, and (iii) acid strength, and the former and the two latters can be decided with IR and MS, respectively. This means that totally evaluating the acidity of solid acid is difficult.

Ammonia IRMS-TPD is the best method to solve the difficulty. By combining the IR with MS mechanically as drown in Figure 1-8, we can get the information about the acidity of solid acid in one experiment. Our laboratory has originally developed the method [62]. The sequence of an experiment is mainly composed with 4 steps; (i)

pretreatment, (ii) reference spectra, (iii) ammonia adsorption, and (iv) desorption spectra.

In the step (i), the sample disc is pretreated in oxygen or nitrogen flow at 823 K. In the

step (ii), IR spectra are measured during heating the sample in an inert gas atmosphere

(He or Ar). After the adsorption of ammonia in the step (iii), the sample is heated again

and IR spectra are measured in the step (iv). At the same time, the desorbed ammonia is

quantified with MS.

The analysis of the results in an IRMS-TPD experiment to calculate the acidity

of the sample is introduced in detail in ref. [62]. The first step of the analysis is based on

equilibrium between ammonia molecules in the gas phase and on the zeolite (10) and the

material balance of ammonia (11):

$$K_{\mathrm{p}} = \frac{1-\theta}{\theta} \frac{P_{\mathrm{g}}}{P} = \frac{1-\theta}{\theta} \frac{RT}{P^{\circ}} C_g \qquad (10)$$

$$FC_{\mathrm{g}} = -A_0 W \frac{d\theta}{dt} \qquad (11)$$

where K_{p}, θ, P_{g}, P_0, R, T, C_{g}, F, and W are equilibrium constant, coverage by ammonia,

partial pressure of ammonia in the gas phase, atmospheric pressure, gas constant,

temperature, concentration of ammonia in the gas phase, flow speed of the gas, and

sample weight, respectively. Then, C_{g} is finally derived (12) via some calculations [63]:

16

$$C_{\text{g}} = -\frac{\beta A_0 W}{F}\frac{d\theta}{dT} = \frac{\theta}{1-\theta}\frac{P^{\text{o}}}{RT}\exp\left(-\frac{\Delta H}{RT}\right)\exp\left(\frac{\Delta S}{R}\right) \qquad (12)$$

where T_{m}, θ_{m}, β, ΔH, and ΔS denote temperature and coverage by ammonia at the peak

maximum, ramp rate, change of enthalpy upon desorption of ammonia, and change of

entropy upon desorption of ammonia, respectively.

The IRMS-TPD technique has been applied for evaluating acidities of various

solid acids, such as zeolites, amorphous silica-alumina, silico-alumino phosphate, and

metal oxides [64-86].

1-5 Batch and flow reactor

Because the reactivity of methane is quite low, pioneering works on the methane

utilization usually start from the detection of trace of desired reaction. As stated later, we

studied the reaction of methane and benzene into toluene, and there have been a few

papers reported trace of toluene was detected on the surface of catalytic materials.

However, between the industrial application and such a finding, there is a big gap in the

reaction rate. Throughout the present study, the catalytic reaction were carried out with a

fixed-bad flow method but not a batch method.

Chemical reactions including heterogeneous catalytic reactions are mainly distinguished into 2 types; batch and flow reaction shown in Figure 1-9 [87]. The batch reactor is often used because of some merits following; (i) ease of interpreting the reaction results, (ii) ease of tracing and quantifying the products, (iii) simple device adaptable to small-scale laboratory set-ups. On the other hand, the flow reactor takes advantages following; (i) continuously getting the products without quenching the reaction and (ii) obtaining the reaction kinetics. In industry, the latter, flow reactor, has been applied for most of industrial reactions because of the efficiency. Therefore, the flow reactor should be used for studying and developing new reactions with laboratory scale if possible.
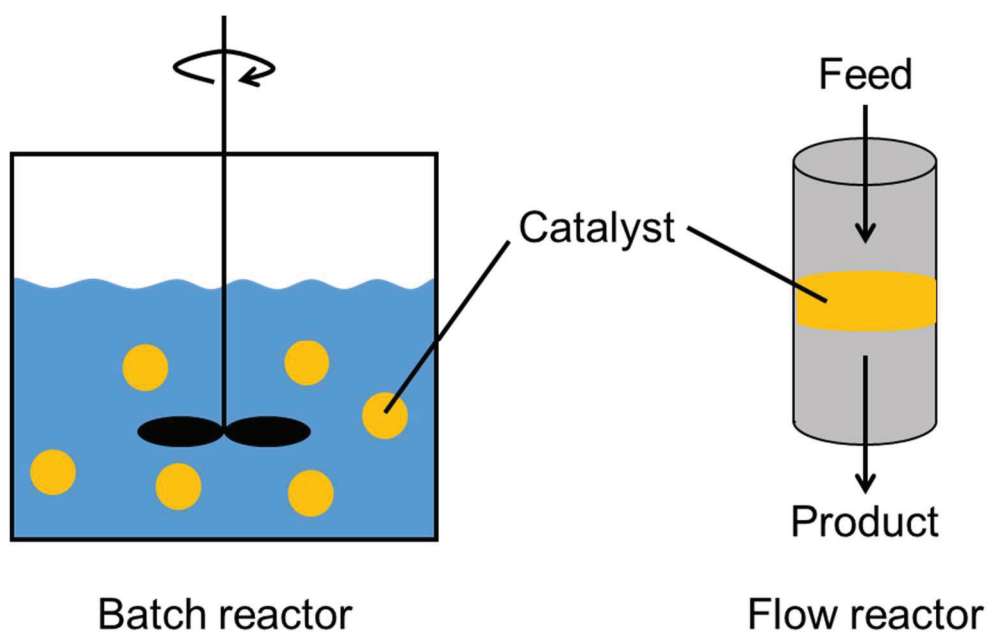

Figure 1-9   Models of batch and flow reactor in heterogeneous catalytic reaction.

1-6 Outline of this study

Based on these backgrounds, the author studied hydrocarbon conversion reactions promoted be zeolite-based catalyst to indicate a new guideline of designing catalysts which are applied for next generation. To realize it, clarifying catalysis on zeolites which is still secret is needed. In addition, developing a new catalyst promoting challenging reactions is important. Therefore, the author kinetically analyzed conversion reactions of aromatic hydrocarbons on zeolite-based catalyst. The author also developed and improved a new catalyst promoting challenging reactions related to natural gas. The purposes of this thesis were mainly composed of 3; (i) kinetically analyzing the catalysis related with aromatic converting reactions, (ii) developing and improving a catalyst promoting direct methylation of benzene with methane, and (iii) searching a catalyst promoting benzene ethylation with ethane. The knowledges in this thesis cultivated cutting-edge fields about analysis and design of zeolite-based catalysts for production of benzene derivatives.

In the Chapter 2, kinetic analysis of reactions related benzene derivatives over solid acid catalysts was described. Benzene derivatives were necessary in modern society and produced via many reactions catalyzed by acid solid catalysts, especially zeolites. Although it has been considered that the acidity determining the catalytic activity, some

19

zeolites were not applied on this rule. We performed toluene disproportionation and cumene cracking over various acid solid catalysts in various temperature. The catalytic activity was normalized by number of acid sites measured with ammonia infrared mass spectrometer / temperature programmed desorption (NH_3-IRMS-TPD). Results of the reactions were kinetically analyzed with Eyring equation to calculate the activation enthalpy ($\Delta H^{*\circ}$) and entropy ($\Delta S^{*\circ}$). Compensation effect between $\Delta H^{*\circ}$ and entropy $\Delta S^{*\circ}$ was observed in both the reaction and compared with results light alkane cracking previously reported by our group. The slopes were in order of [cumene cracking] > [toluene disproportionation] > [C3-8 alkane cracking]. We applied theory of host-guest chemistry to our heterogeneous catalytic system and considered that the difference of slopes was depended on the bulkiness of reactant molecule as cumene > toluene > small alkane. On the other hand, the intercept of $\Delta H^{*\circ}$ in the effect may be index of difficulty for activating a reactant regardless of the degree of freedom.

In the Chapter 3, direct methylation of benzene with methane over Co/MFI catalyst was described. Development of process which can utilize methane as chemical resource is strongly demanded. Various elements supported on zeolites was performed for direct methylation of benzene with methane at 773 K and 101 kPa of total pressure after nitrogen flow at 823 K for 1 h, and cobalt supported on MFI-type zeolite (Co/MFI)

catalyst was found to be distinctly active for the reaction. The catalytic activity was roughly proportionate with concentration of aluminum [Al] of MFI. On the other hand, the activity was negligible at Co/Al = 0 and introducing Co created the activity and showed the maximum at Co/Al = 0.6, and further loading reduced the activity at Co/Al > 0.9. 13C isotope experiments demonstrated that the methyl group and benzene ring of toluene in the reaction products were origin from methane and benzene, respectively. Quantitating the reaction products with mass spectrometer clarified that stoichiometry of the target reaction was correct and dehydrogenation of methane was promoted as a side reaction. Co/MFI was characterized with advanced spectroscopic technique such as NH_3-IRMS-TPD and X-ray absorption spectroscopy to identify the active species. It was clarified that Lewis acidic cobalt (+II) cation mono-atomically dispersed on ion exchange site of MFI zeolite was the active species for the reaction.

In the Chapter 4, reactivity of methane and benzene over metal/MFI zeolite analyzed with temperature-programmed reaction technique was described. Co/MFI showed high catalytic activity for benzene methylation with methane, however, dehydrogenation of methane proceeded as a side reaction and absolute reaction rate was low. Understanding reactivity of methane and benzene over various metal supported on MFI zeolite is important to design new catalyst having higher performance. Methane and

21

benzene were flowed over various elements supported on MFI in 373-843 K after pretreatment in oxygen flow at 823 K for 1 h, and ion currents originated from the reaction products were recorded with mass spectrometer. Based on change of the ion currents, oxidation state of the metal species was speculated to be oxidized or reduced during the reaction, and it was clarified by X-ray absorption near edge structure (XANES) spectra about Co/MFI and Pd/MFI. Oxidation state of cobalt (+II) on ion exchange site was stable even reductive methane + benzene flow at 843 K, whereas some metals represented with noble metal such as Rh, Pd and Pt were reduced into metal(0) species. Toluene and dihydrogen formation rate and methylation selectivity were calculated from the ion currents. Ni, Co, and Nobel metals such as Rh, Pd and Pt showed high toluene formation rate in the metal/MFI catalysts. However, Ni and noble metals were also highly active for the dehydrogenation, resulting in low methylation selectivity. Reason why these noble metals were inactive in chapter 3 was pretreatment with nitrogen. Metal (0) species promoted methane dehydrogenation and was deactivated very quickly, resulting in being inactive. On the other hand, cobalt (+II) was stable as oxidized state during the reaction, and therefore it showed stable catalytic activity.

In the Chapter 5, enhancement of reaction selectivity in benzene emethylation of benzene with methane over Co/MFI catalyst was described. It was mentioned that

Co/MFI promoted methane dehydrogenation as a side reaction, as well as direct methylation of benzene with methane, and that dispersed Co species on ion exchanged site of MFI was active species. There is some possibility that distributions of ion exchange sites are change in MFI zeolites with different Al content [Al]. Therefore, the methane + benzene TPReactions using various Co/MFI catalysts with different composition in [Co] and [Al] were performed to speculate Co species on MFI. From the experiments, it was clarified that Co species on external surface of MFI was reduced into metal Co^0 species and promotes the side reaction, leading rapid deactivation. On the other hand, Co/MFI with $SiO_2/Al_2O_3 = 48$ and Co/Al = 0.6 catalyst showed high selectivity for the methylation. In comparison of Co/MFI with low and high [Al] catalysts in continuous flow reaction at 813 K, the low [Al] one showed long catalytic life.

In the Chapter 6, synthesis of benzene derivatives from reaction of ethane and benzene over Pb/MFI catalyst was described. Ethane is a component of natural gas as well as methane, and should be converted into chemical compounds in one system reaction to avoid big energy loss. By screening meta/MFI catalyst in ethane + benzene reactions, it was found that Zn, Mo, Pt, and Pb/MFI showed high catalytic activity for production of ethylene and its derivatives at 773 K. Among them, Zn, Mo, and Pt/MFI also showed high activity for side reactions such as ethane dehydrogenation and benzene

23

hydrogenolysis, leading production of carbonaceous which causes catalyst deactivation. On the other hand, Pb/MFI showed high selectivity for production of target products, although formation rate of ethylene was high and similar to the other three catalysts. This difference may be caused by Brønsted acidity. From reactions of ethane + benzene over various Pb/MFI catalyst with different [Al] and [Pb] prepared by impregnation and ion exchange method, it was speculated that Pb^{2+} species on ion exchange site of MFI was active species. In addition to that, it was clarified that Pb/MFI with low [Al] showed high selectivity for production of target reactions. Based on results of ethane + benzene reaction with different amount of Pb/MFI, reaction pathways were speculated. On Pb/MFI, ethylbenzene was produced from both direct ethylation of benzene with ethane and ethylene additive reaction into benzene following ethane dehydrogenation of ethane to ethylene.

In the Chapter 7, this study was totally summarized. It totally summaries this study with main results and knowledges.

References

[1] J. C. Gentry, *Asia-Pac. J. Chem. Eng.*, **2**, 272-277 (2007)

[2] J.P. G. Villaluenga, A. Tabe-Mohammadi, *J. Membr. Sci.*, **169**, 159-174 (2000)

[3] K. Othmer, *Encyclopedia of Chemical Technology 3rd Ed.*, Wiley, (1978)

[4] D. Mitsuyoshi, K. Kuroiwa, Y. Kataoka, T. Nakagawa, M. Kosaka, K. Nakamura, S. Suganuma, Y. Araki, N. Katada, *Micropor. Mesopor. Mater.*, **242**, 118-126 (2017)

[5] S. Suganuma, K. Nakamura, A. Okuda, N. Katada, *Mol. Catal.*, **435**, 110-117 (2017)

[6] A. F. T. Ogério, C. M. B. João, F. P. G. João, *Chem. Rev.*, **113**, 7421-7469 (2013)

[7] J. Pang, M. Zheng, R. Sun, A. Wang, X. Wang, T. Zhang, *Green Chem.*, **18**, 342-359 (2016)

[8] N. Mimura, M. Saito, *Catal. Today*, **55**, 173-178 (2000)

[9] G. E. Vrieland, *Appl. Catal.*, **77**, l-8 (1991)

[10] N. Jiang, A. Burri, S.Par, *Chin. J. Catal.*, **37**, 3-15 (2016)

[11] H. Staudinger, E. Geiger, E. Huber, *Chem. Ber.*, **62**, 263-267 (1929)

[12] J. Panming, W. Qiuying, Z. Chao X. Yanhe, *Appl. Catal. A: Gen.*, **91**, 125-129 (1992)

[13] D. H. R. Barton, N. C. Delanghe, *Tetrahedron Lett.*, **38**, 6351-6354 (1997)

[14] C. Ercan, F. M. Dautzenberg, C. Y. Yeh, and H. E. Barner, *Ind. Eng. Chem. Res.*, **37**, 1724-1728 (1998)

[15] R. J. Schmidt, *Appl. Catal. A: Gen.*, **280**, 89-103 (2005)

[16] T. F. Degnan Jr, C. M. Smith, C. R. Venkat, *Appl. Catal. A: Gen.*, **221**, 283-294 (2001)

[17] A. Rahman, M. Mupa1, C. Mahamadi, *Catal. Lett.*, **146**, 788-799 (2016)

[18] C. Gawlig, S. Schindler, S. Becker, Eur. J. Inorg. Chem., 1-6 (2019)

[19] A. Alshammari, A. Köckritz, N. Kalevaru, Bagabas, A. Martin, *Top Catal.*, **58**, 1069-1076 (2015)

[20] R. Nithyanandam, Y. K. Mun, T. S. Fong, T. C. Siew, O. S. Yee, N. Ismail, *J. Eng. Sci. Tech.*, **13**, 4290-4309 (2018)

[21] F. Pöhler, *Kunststoffe Int.*, **6**, 100-103 (2005)

[22] G. P. Karayannidis, D. S Achilias, *Macromol. Mater. Eng.*, **292**, 128-146 (2007)

[23] J. Pang, M. Zheng, R. Sun, A. Wang, X. Wang, T. Zhang, *Green Chem.*, **18**, 342-359 (2016)

[24] M. Rania, W. J. Shima, G. M. Hana, M. Janga, Y. K. Songa, S. H. Honga, *Chemosphere*, **110**, 111-119 (2014)

[25] C. L. Matras, F. Bonnette, E. Mignard, O. Lavastre, *J. Organomet. Chem.*, **693**, 393-398 (2008)

[26] T. Polen,M. Spelberg, M. Bott, *Biotechnol. Bioeng.*, **167**, 75-84 (2013)

[27] S. Liua, A. Sena, R. Parton, *J. Mol. Catal. A: Chem.*, **210**, 69-77 (2004)

[28] C. Colella, A. F. Gualtieri, *Micropor. Mesopor. Mater.*, **105**, 213-221 (2007)

[29] A. F. Masters, T. Maschmeyer, *Micropor. Mesopor. Mater.*, **142**, 423-438 (2011)

[30] R. M. Barrer, B. M. Munday, *J. Chem. Soc.*, (A) 2914 (1971)

[31] R. M. Barrer, Zeolites, **1**, 130-140 (1981)

[32] J. A. Rabo, M. W. Schoonover, *Appl. Catal. A: Gen.*, **222**, 261-275 (2001)

[33] D.H. Everett, *MANUAL OF SYMBOLS AND TERMINOLOGY FüR PHYSICOCHEMICAL QUANTITIES AND UNITS*, IUPAC, p.585 (1971)

[34] International Zeolites Association, https://asia.iza-structure.org/IZA-SC/ftc_table.php

[35] C. Riihrig, H. Gies and B. Marler, *Zeolites*, **14**, 498-503 (1994)

[36] H. Asaoka, *J. Mol. Catal.*, **68**, 301-311 (1991)

[37] K. Suzuki, Y. Kiyozumi, S. Shin, *Zeolites*, **5**, 1-14 (1985)

[38] C. T. G. Knight, R. J. Kirkpatrick, E. Oldfield, *J. Am. Chem. Soc.*, 109, 1632-1635 (1987)

[39] S. D. Kinrade, R. T. Syvitski, K. Marat, C. T. G. Knight, *J. Am. Chem. Soc.*, **118**, 4196-4197 (1996)

[40] B. Sulikowski, J. Klinowski, *Appl. Catal. A: Gen.*, **34**, 141-153 (1992)

[41] H. W. Clark, W. J. Rievert, M. M. Olken, *Micropor. Mesopor. Mater.* **6**, 115-124 (1996)

[42] A. Corma, A. Martinez, *Adv. Mater.*, **7**, 137-144 (1995)

[43] W. Vermeiren, J. P. Gilson, *Top Catal*, **52**, 1131-1161 (2009)

[44] A. G. Popov, V. S. Pavlov, I. I. Ivanova, *J. Catal.*, **335**, 155-164 (2016)

[45] V. P. Shiralkar, P. N. Joshi, M. J. Eapen, B. S. Rao, *Zeolites*, **11**, 511-516 (1991)

[46] X. Cheng, X. Wang, H. Long, *Micropor. Mesopor. Mater.*, **119**, 171-175 (2009)

[47] M P. Padmapriya, G R Rajarajeswari, *J. Chem. Sci.*, **130:36**, 1-7 (2018)

[48] A. A. Rownaghi, Y. Hedlund, *Ind. Eng. Chem. Res.* **50**, 11872-11878 (2011)

[49] R. Srivastava, N. Iwasa, S. Fujita, M. Arai, *Catal. Lett.*, **130**, 655-663 (2009)

[50] N. V. Vlasenko, Y. N. Kochkin, G. M. Telbiz, O. V. Shvets, P. E. Strizhak, *RSC Adv.*, **9**, 35957-35968 (2019)

[51] N. Viswanadham, L. Dixit, J. K. Gupta, M. O. Garg, *J. Mol. Catal. A: Chem.*, **258**, 15-21 (2006)

[52] J. Dwyef, D. J. Rawlence, *Catal. Today*, **18**, 487-507 (1993)

[53] K. A. Kvenvolden, *Org. Geochem.*, **23**, 997-1008 (1995)

[54] Y. Alcheikhhamdon, M. Hoorfar, *J.Nat. Gas. Sci. Eng.*, **34**, 689-701 (2016)

[55] A. H. Kakaee, A. Paykani, M. Ghajar, *Renewable Sustainable Energy Rev.*, **38**, 64-78 (2014)

[56] K. Aruga, *Journal of Unconventional Oil and Gas Resources*, **14**, 1-5 (2016)

[57] P. Gangadharan, K. C. Kanchi, H. H. Lou, *Chemical Engineering Research and Design*, **90**, 1956–1968 (2012)

[58] L. S. Wang, L. X. Tao, M. S. Xie, G. F. Xu, J. S. Huang, Y. D. Xu, *Catal. Lett.*, **21**, 35-41 (1993)

[59] N. Kosinov, A. Parastaev, A. S. G. Wijpkema, I. Vollmer, J. Gascon, F. Kapteijn, E. J. M. Hensen, *ACS Catal.*, **6**, 5366-5370 (2016)

[60] A. Olsen, H. Lütken, J. N. Hegelund, R. Müller, *Hortic Res-England*, **2**, 1-9 (2015)

[61] F. Yin, A. L. Blumenfeld, V. Gruver, J. J. Fripiat, *J. Phys. Chem. B*, 101, 1824-1830 (1997)

[62] M. Niwa, N. Katada, *Chem. Rec.*, **13**, 432-455 (2013)

[63] M. Sawa, M. Niwa, Y. Murakami, *Zeolites*, **10**, 307-309 (1990)

[64] M. Niwa, S. Nishikawa, N. Katada, *Micropor. Mesopor. Mater*. **82**, 105-112 (2005)

[65] K. Suzuki, T. Noda, N. Katada, M. Niwa, *J. Catal.*, **250**, 151-160 (2007)

[66] K. Suzuki, G. Sastre, N. Katada, M. Niwa, *Phys. Chem. Chem. Phys.*, **9**, 5980-5987 (2007)

[67] K. Suzuki, Y. Aoyagi, N. Katada, M. Choi, R. Ryoo, M. Niwa, *Catal. Today*, **132**, 38-45 (2008)

[68] K. Suzuki, G. Sastre, N. Katada, M. Niwa, *Chem. Lett.*, **36**, 1034-1035 (2007)

[69] K. Suzuki, N. Katada, M. Niwa, *J. Phys. Chem. C*, **111**, 894-900 (2007)

[70] N. Katada, T. Tsubaki, M. Niwa, *Appl. Catal. A: Gen.*, **340**, 76-86 (2008)

[71] T. Noda, K. Suzuki, N. Katada, M. Niwa, *J. Catal.*, **259**, 203-210 (2008)

[72] K. Suzuki, G. Sastre, N. Katada, M. Niwa, *Chem. Lett.*, **38**, 354-355 (2009)

[73] N. Katada, K. Suzuki, T. Noda, M. B. Park, H.-K. Min, S. B. Hong, M. Niwa, *Top Catal.*, **53**, 664-671 (2010)

[74] N. Katada, H. Tamagawa, M. Niwa, *Catal. Lett.*, **140**, 134-139 (2010)

[75] K. Okumura, T. Tomiyama, N. Morishita, T. Sanada. K. Kamiguchi, N. Katada, M. Niwa, *Appl. Catal. A: Gen.*, **405**, 8-17 (2011)

[76] K. Suzuki, T. Nishio, N. Katada, G. Sastre, M. Niwa, *Phys. Chem. Chem. Phys.*, **13**, 3311-3318 (2011)

[77] N. Katada, K. Nouno, J. K. Lee, J. Shin, S. B. Hong, M. Niwa, *J. Phys. Chem. C*, **115**, 22505-22513 (2011)

[78] M. Niwa, S. Sota, N. Katada, *Catal. Today*, **185**, 17-24 (2012)

[79] M. Niwa, N. Morishita, H. Tamagawa, N. Katada, *Catal. Today*, **198**, 12-18 (2012)

[80] N. Katada, H. Tamagawa, M. Niwa, *Catal. Today*, **226**, 37-46 (2014)

[81] S. Suganuma, Y. Murakami, J. Ohyama, T. Torikai, K. Okumura, N. Katada, *Catal. Lett.*, **145**, 1904-1912 (2015)

[82] D. Sun, Y. Yamada, S. Sato, S. Suganuma, N. Katada, *Appl. Catal. A: Gen.*, **526**, 164-171 (2016)

[83] K. Nakamura, R. Mizuta, S. Suganuma, E. Tsujia, N. Katada, *Catal. Commun*., **102**, 103-107 (2017)

[84] S. Suganuma, K. Nakamura, A. Okuda, N. Katada, *Mol. Catal*., **435**, 110-117 (2017)

[85] N. Katada, Y. Kawaguchi, K. Takeda, T. Matsuoka, N. Uozumi, K. Kanai, S. Fujiwara, K. Kinugasa, K. Nakamura, S. Suganuma, M. Nanjo, *Appl. Catal. A: Gen*., **530**, 93-101 (2017)

[86] N. Katada, *Mol. Catal.*, **458**, 116-126 (2018)

[87] O. Levenspiel, *Chemical Reaction Engineering 3rd Ed*., Wiley, p39 (1999)

Chapter 2   Kinetic Analysis of Reactions Related Benzene Derivatives over Solid Acid Catalysts

2-1 Introduction

Aluminosilicates including zeolites and amorphous silica-aluminas are important solid acid catalysts [1,2]. Alkane cracking is one of the representative use of the aluminosilicate solid acid catalysts [3-5], whereas various reactions like toluene disproportionation are operated for conversion of mono-cyclic aromatic hydrocarbons [6-8]. Kinetic analysis is a classic method for investigation of these catalysis, but recent advances in analysis of physicochemical properties of solids may give new insights through the kinetic analysis. We have developed a method of ammonia IRMS-TPD (infrared mass spectroscopy temperature-programmed desorption) to quantify the number and strength of Brønsted and Lewis acid sites [9], giving the reaction rate normalized by the number of Brønsted acid site. For small alkane cracking in the mono-molecular mechanism region, we have found a linear relationship between the activation enthalpies (hereafter $\Delta H^{*\circ}$ [J mol^{-1}]) and the enthalpies of ammonia desorption from Brønsted acid sites (ΔH_{NH3} [J mol^{-1}]) on various aluminosilicates [10]. In addition, the activation entropy based on the number of Brønsted acid site ($\Delta S^{*\circ}$ [J K^{-1} mol^{-1}]) showed a linear and compensatory relationship against $\Delta H^{*\circ}$ in which the larger the enthalpy, the larger

the entropy [11].

The compensation effect gives information about the structure of intermediate on the rate determining step. The effect indicates that an active site with lower activation enthalpy holds the intermediate more tightly, losing the freedom of movement of the intermediate and resulting in the low entropy. Thermodynamic analyses in the host-guest complexes with various molecular structures clarified that the slope of the plots of ΔS against ΔH (entropy and enthalpy changes, respectively, of the association of host and guest molecules) shows the extent of complexity of host-guest complex, whereas the intercept on the vertical axis (ΔS at $\Delta H = 0$) shows difference in the freedom between the reactant in solution and the hosted complex [12]. The compensatory relationship between $\Delta S^{*\circ}$ and $\Delta H^{*\circ}$ or pre-exponential factor and activation energy [13] was found in various adsorption [14], non-catalytic and catalytic reactions [15-20]. In the early studies, various speculations and proposals were presented for the origin [17]. However, advances in the host-guest chemistry based on experiments with the molecular structures systematically varied has clearly evidenced that the compensation effect was due to the tendency in which the tightly bounded complex lost the freedom of movement as above [12]. Subsequently to the small alkane cracking [11], in the present study, we measured the kinetic parameters in two reactions of monocyclic aromatic hydrocarbons, i.e., cracking

(dealkylation) of cumene (2-phenylpropane) and disproportionation of toluene. The former has been a typical test reaction of solid Brønsted acid catalyst [21,22], whereas the latter has been applied to the production of para-xylene [23,24]. The relationships between $\Delta S^{*\circ}$ and $\Delta H^{*\circ}$ are related with nature of these important reactions.

2-2 Experimental

Table 2-1 shows the employed catalysts with their acidic properties. Samples of ZSM-5 zeolite (zeolites with MFI framework structure) were prepared by ion exchange of Na-MFI samples commercially available. A sample of Y zeolite (zeolite with FAU structure) was also prepared by ion exchange from Na-Y, and N-USY (ultrastable Y) was prepared by steaming of the above Y zeolite sample followed by NH_4NO_3 treatment [25]. In addition, some samples of mordenite (zeolite with MOR structure), zeolite β (zeolite with *BEA structure) and amorphous silicaalumina were employed as received. The IRMS-TPD method was applied to measure the desorption profile of ammonia from each of Brønsted and Lewis acid sites as already described [9]. The enthalpy of ammonia desorption, ΔH_{NH3} was calculated by a curve-fitting method [26] using a theoretical equation [27]. Toluene disproportionation and cumene cracking were carried out, and the

activation entropy $\Delta S^{*\circ}$ and enthalpy $\Delta H^{*\circ}$ were calculated using Eyring equation [28].

Table 2-1   Employed aluminosilicate catalysts and their acidic properties.

Catalyst	Origin	Structure	Si/Al	Number of acid sites / mol kg^{-1}		Averaged enthalpy of ammonia desorption from Brønsted acid site / kJ mol^{-1}
				Brønsted	Lewis	
MFI (12)^a	Na-MFI from Tosoh Corp. was ion-exchanged into NH$_4$-form.	MFI	12	1.15	0.00	139
MFI (15)^a	Na-MFI from Mizusawa Chemical Industries Co. Ltd. was ion-exchanged into NH$_4$-form.	MFI	15	0.82	0.01	138
FAU^a	Na-Y from Tosoh Corp. was ion-exchanged into NH$_4$-form.	FAU	2.4	0.51	0.00	161
N-USY^a	The above Y was steamed at 823 K and treated with 0.5 mol dm^{-3} NH$_4$NO$_3$ aq. [25]	FAU	2.3	0.52	0.13	134
MOR^b	JRC-Z-HM20^c	MOR	10	0.94	0.00	161
*BEA (13)^b	JRC-Z-HB25 (1)^c	*BEA	13	0.46	0.06	138
*BEA (75)^b	JRC-Z-HB150 (1)^c	*BEA	75	0.13	0.00	145
SAH-1^b	JRC-SAH-1^c	amorphous	2.1	0.32	0.17	113
SAL-2^b	JRC-SAL-2^c	amorphous	5.3	0.20	0.23	116
N631L^b	Supplied from JGC Catalysts and Chemicals Ltd.	amorphous	5.7	0.26	0.02	111

a: Stored as the NH$_4$-form, and converted into the H-form in the pre-treatment of ammonia IRMS-TPD measurements and catalytic tests.

b: Supplied as H-form and used as supplied.

c: Reference catalysts distributed by Catalysis Society of Japan.

2-3 Analysis

2-3-1 *Details in catalytic reactions and kinetic analysis*

Toluene disproportionation and cumene cracking were conducted with fixed bed flow reactors. The amount of catalyst was adjusted to keep the conversion of reactant less than 10%. After pre-treatment in a flow of 0.049 mol h^{-1} of H$_2$ at 823 K under atmospheric pressure for 1 h, the reactions were carried out in a flowing gaseous mixture of 0.049 mol h^{-1} of H$_2$ and 0.015 mol h^{-1} of toluene or 0.011 mol h^{-1} of cumene at 473-823 K with keeping the total pressure at 1 MPa by using a back pressure valve connected to the outlet of reactor. The eluted materials were analyzed by a GC (gas chromatograph) with FID (flame ionization detector). Deactivation was observed in most cases, and therefore, we used a fresh sample of catalyst for every test. The first order kinetics were assumed to obtain the rate constant as follows.

$$-\frac{d\left(\dfrac{P}{P^\circ}\right)}{d\left(\dfrac{W}{F}\right)} = k'\left(\frac{P}{P^\circ}\right)$$

(1)

where P, P°, W, F and k' were the partial pressure of reactant (Pa), the standard pressure (10^5 Pa), the amount of catalyst (kg), the flow rate of reactant (mol s^{-1}) and the rate

35

constant per unit weight of catalyst (mol s^{-1} kg^{-1}), respectively. In addition, the reaction

rate can be assumed to be proportional to the number of active sites.

$$k' = kA_0$$

(2)

where k and A_0 are the rate constant normalized by the number of active site (s^{-1}) and

the number of active site per unit weight of catalyst (mol kg^{-1}), respectively.

From these assumptions, the rate constant was obtained from the

experimentally observed conversion as follows.

$$k = \frac{FP^\circ}{A_0 W P_0} \ln \frac{1}{1-x_0}$$

(3)

where P_0 and x_0 were the partial pressure of reactant at the inlet of the reactor (Pa) and

the conversion of reactant (no dimension) on fresh catalyst which had not been

influenced by deactivation, respectively. Here the number of Brønsted acid sites

measured by ammonia IRMS-TPD method was assumed to be A_0 in this equation.

Then, from the dependence of rate constant on the reaction temperature T (K),

the pre-exponential factor A (s^{-1}), the activation energy E_a (J mol^{-1}), the activation

entropy $\Delta S^{*\circ}$ (exactly the entropy change between the standard state of reactant and the rate-determining step) and enthalpy $\Delta H^{*\circ}$ using Arrhenius (4) and Eyring (5) equations [28].

$$k = Ae^{-\frac{E_a}{RT}} \tag{4}$$

$$\frac{h_p k}{\kappa k_B T} = e^{\frac{\Delta S^{*\circ}}{R}} e^{-\frac{\Delta H^{*\circ}}{RT}} \tag{5}$$

where h_p and k_B are the Planck constant (6.63×10^{-34} J s) and the Boltzmann constant (1.38×10^{23} J K^{-1}), and κ (transmission coefficient, no dimension) is here assumed to be 1.

2-3-2 *Estimation of conversion at time on stream = 0*

As shown in our paper [29], rate of such a reaction as toluene disproportionation in the continuous flow method is influenced by the deactivation of catalyst due to coke formed from alkenes as by-products. The behavior of deactivation is sensitive to property of catalyst such as pore-opening size. The deactivation is weakened by co-feeding of hydrogen [29]. However, even in such conditions, the conversion was gradually decreased with the time on stream (Figure 2-1). This indicates

that deactivation generally proceeded, and the extent of deactivation was observed to be different among the catalysts. The conversion slowly increased with the time on stream on MFI zeolite as an exception, possibly due to some undesired change in structure, e.g., dealumination enhancing the acid strength. In order to analyze the kinetic parameters, these influences should be eliminated. Linear relationships were observed between the logarithm of reaction rate and time on stream (Figure 2-2). Therefore, we assumed the following equation, and the conversion at time on stream = 0 was estimated from the linear plots.

$$x = x_0 e^{-bt_s} \tag{6}$$
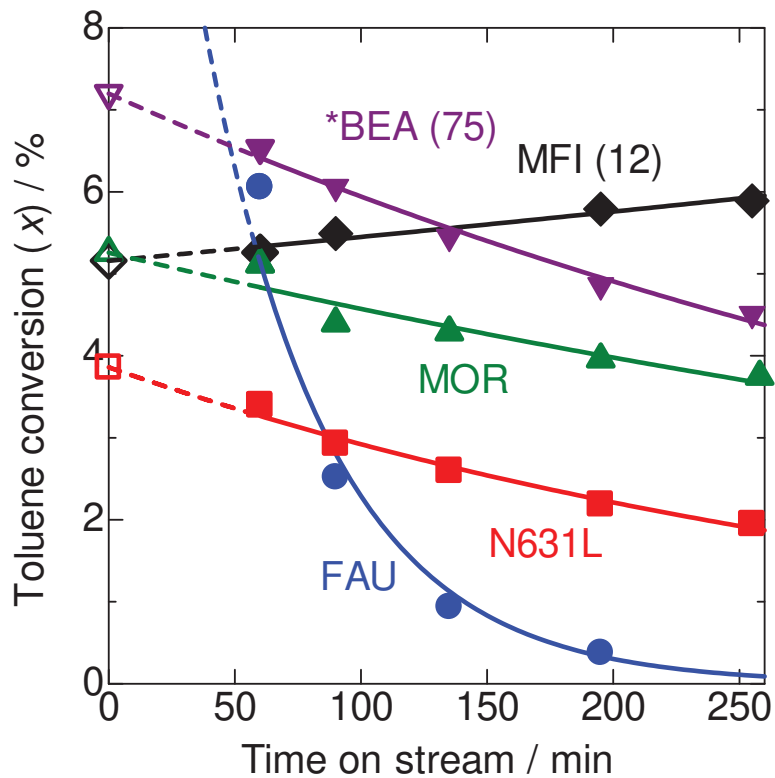
Figure 2-1   Examples of change of toluene conversion with time on stream in toluene disproportionation at 813 K.

where x, b and ts were the conversion at a discussed time on stream, the deactivation

factor (s^{-1}) and the time on stream (s).
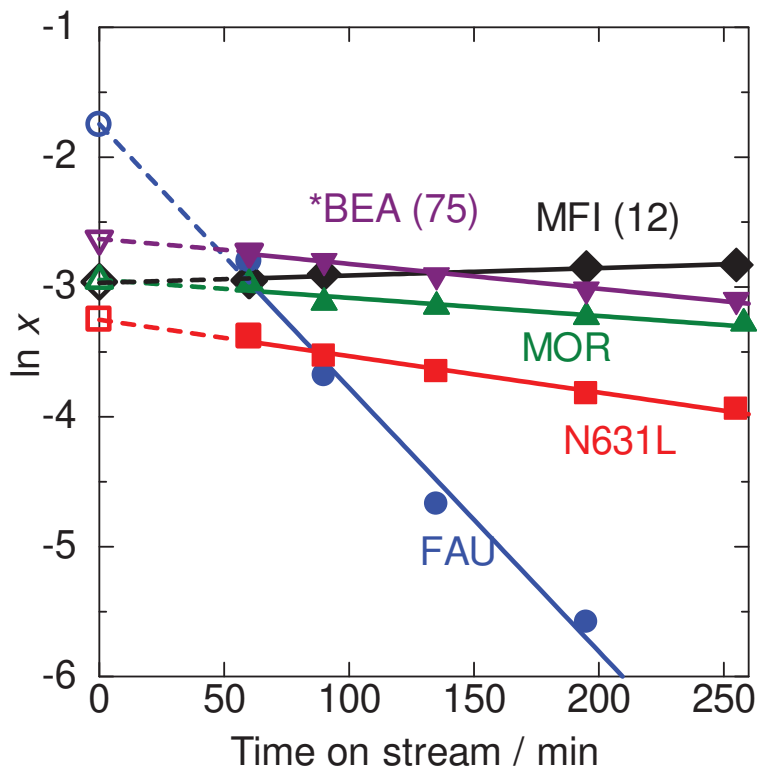
Figure 2-2   Examples of plots of logarithm of toluene conversion taken from Figure 2-1 against time on stream.

2-4 Results and Discussion

As shown in our paper [29], rate of such a reaction as toluene disproportionation in the continuous flow method is influenced by the deactivation of catalyst, even after it is weakened by co-feeding of hydrogen. The conversion at time on stream = 0 was estimated as shown in Supporting information, and kinetic analysis was carried out based on it.

Then, linear relationships were observed between ln (k/T) against T^{-1} in all the cases (Figure 2-3). Values of $\Delta H^{*\circ}$ and $\Delta S^{*\circ}$ are calculated from the slopes and intercepts as shown in Table 2-2.

Figure 2-4 shows the plots of $\Delta H^{*\circ}$ in various reactions against ΔH_{NH3} from Brønsted acid site (shown in Table 1) as an index of Brønsted acid strength. In the case
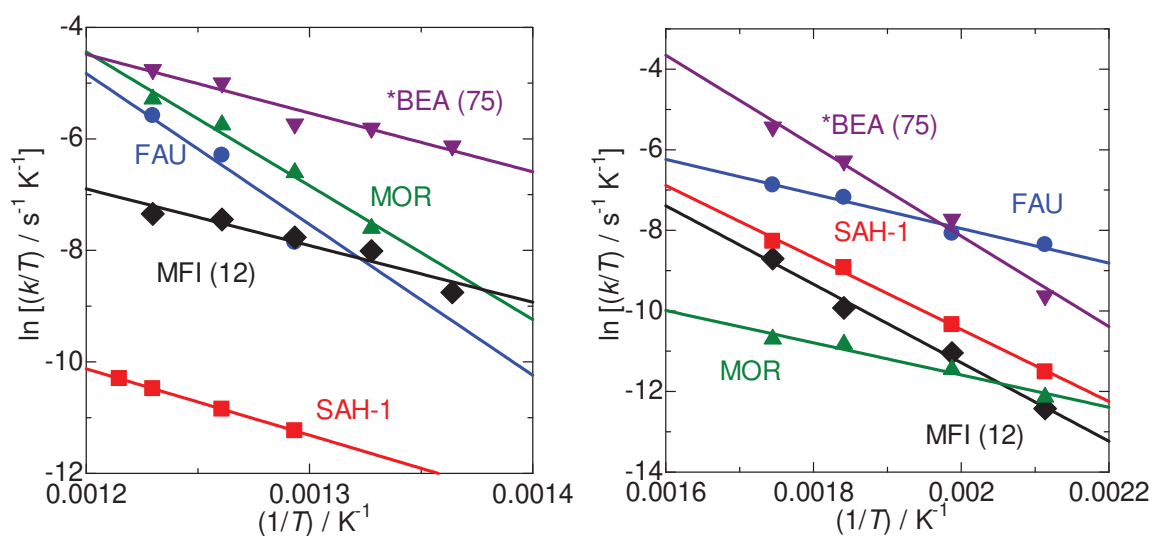
Figure 2-3   Examples of Eyring plots in (A) toluene disproportionation and (B) cumene cracking.

Table 2-2   Kinetic parameters.

Catalyst	Toluene disproportionation				Cumene cracking			
	E_a / kJ mol^{-1}	A / s^{-1}	$\Delta H^{*\circ}$ / kJ mol^{-1}	$\Delta S^{*\circ}$ / J K^{-1} mol^{-1}	E_a / kJ mol^{-1}	A / s^{-1}	$\Delta H^{*\circ}$ / kJ mol^{-1}	$\Delta S^{*\circ}$ / J K^{-1} mol^{-1}
MFI (12)	91	4.2×10^5	84	-154	85	5.1×10^6	81	-129
MFI (15)	181	3.4×10^{11}	172	-44	47	8.4×10^2	62	-167
FAU	231	2.2×10^{15}	225	32	40	2.7×10^3	36	-197
N-MFI	71	4.4×10^4	65	-174				
MOR	206	8.0×10^{13}	200	5	38	39	33	-227
*BEA (13)	94	2.0×10^6	88	-130	98	6.8×10^8	93	-79
*BEA (75)	130	1.8×10^9	124	-94	36	1.8×10^3	36	-200
SAH-1	106	1.4×10^5	99	-163	79	2.3×10^6	74	-136
SAL-2	83	1.7×10^4	77	-180	74	1.4×10^6	70	-140
N631L	28	5.0	21	-248	45	1.3×10^3	41	-199

of alkane cracking, $\Delta H^{*\circ}$ was approximately dependent on the Brønsted acid strength; the higher the ammonia desorption enthalpy ΔH_{NH3}, the lower the activation enthalpy $\Delta H^{*\circ}$. A few exceptional cases (MFI and in some cases of MOR) showed exceptional behaviors, suggesting that very small micropores may disturb the $\Delta H^{*\circ}$-ΔH_{NH3} relationship, but in most cases, simple relationships were observed as the stronger the Brønsted acid sites, the higher the activity [11]. However, $\Delta H^{*\circ}$ in the toluene disproportionation and cumene cracking were not related with ΔH_{NH3}. It is naturally speculated that the reactions of aromatic molecules were more strongly influenced by the steric effects due to the pores of catalysts, especially in the cases of microporous zeolites,
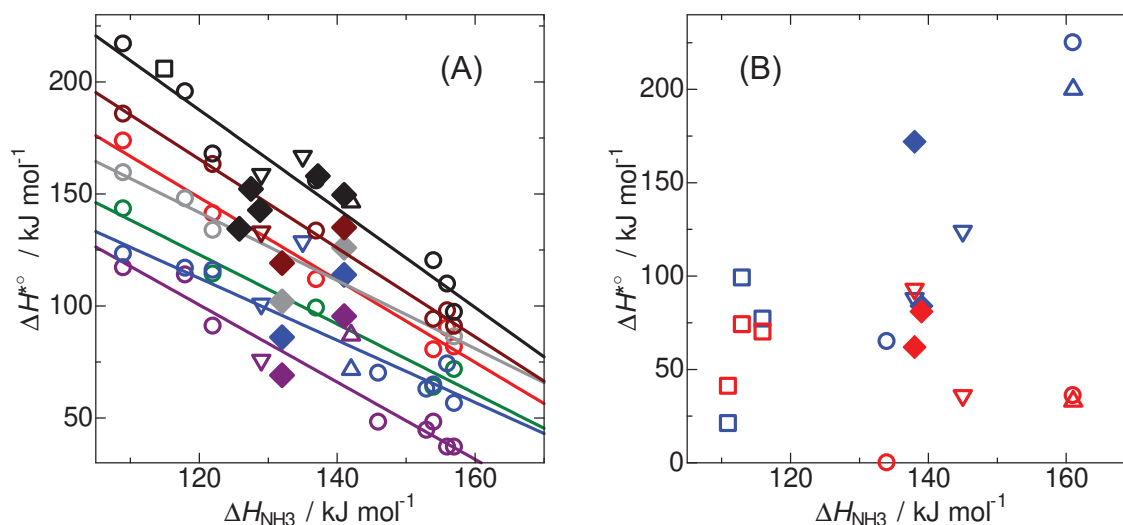
Figure 2-4   Plots of $\Delta H^{*\circ}$ in cracking of (A) propane (black), butane (brown), iso-butane (2-methylpropane, red), pentane (grey), isopentane (2-methylbutane, green), hexane (blue) and octane (purple) [11], (B) toluene disproportionation (blue) and cumene cracking (red) against ΔH_{NH3} from Brønsted acid site over MFI ($\blacklozenge$), MOR ($\triangle$), FAU ($\bigcirc$) and *BEA ($\triangledown$) zeolites, and amorphous silica alumina ($\square$). (For interpretation of the references to colour in this figure legend, the reader is referred to the web version of this article.)

disturbing the influence of Brønsted acid strength.

Figure 2-5 shows the plots of $\Delta S^{*\circ}$ against $\Delta H^{*\circ}$ in the tested reactions. The

linear relationships between them were found in all the reactions. This implies that the

reaction rate was given by some simple principles throughout these reactions.

The slopes in these plots were [cumene cracking] > [toluene disproportionation]

> [C$_{3–8}$ alkane cracking], as shown in Table 2-3. Inoue et al. found that the slope of plots

of ΔS against ΔH in host-guest chemistry showed the degree of complexity of host-guest
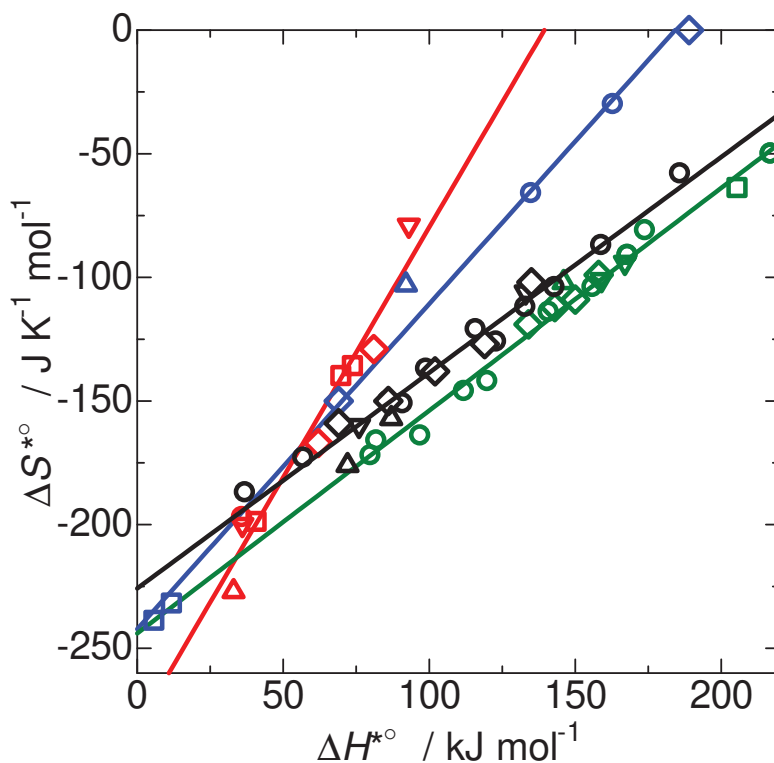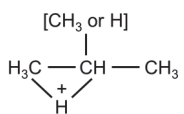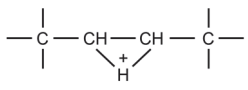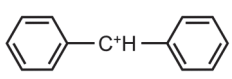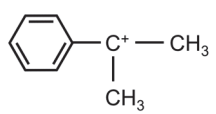
Figure 2-5   Plots of $\Delta S^{*\circ}$ against $\Delta H^{*\circ}$ in cracking of propane and iso-butane (green) [11], cracking of C_4–C_8 linear alkanes and isopentane (black) [11], toluene disproportionation (blue) and cumene cracking (red) over MFI ($\diamond$), MOR ($\triangle$), FAU ($\bigcirc$) and *BEA ($\triangledown$) zeolites and amorphous silica alumina ($\square$). (For interpretation of the references to colour in this figure legend, the reader is referred to the web version of this article.)

complex [12]. Accordingly, the slope in the present study should show the complexity of

transition state on the rate determining step. The complexity of speculated transition states

(Table 2-3) is hence estimated as $4 > 3 > 1 \approx 2$. The order $(4, 3) > 1 \approx 2$ is naturally

understood from the molecular structures, but the order $4 > 3$ needs discussion. It can be

explained as that the rotation around the cation part ($-CH^+-$) of 3 is possible, because

the center carbon has only one hydrogen atom. On the contrary, the cation part in 4

43

Table 2-3　　Speculated key intermediates and parameters in plots of $\Delta S^{*\circ}$ against $\Delta H^{*\circ}$ of tested reactions.

Reaction	Speculated key intermediate	Slope /K^{-1}	Intercept on vertical / J K^{-1} mol^{-1}	Intercept on horizontal / kJ mol^{-1}
Cracking of propane and iso-butane	[CH$_3$ or H] H$_3$C—CH—CH$_3$ (+H)	0.901	-244	270
Cracking of C$_{4-8}$ linear alkanes and iso-pentane	—C—CH—CH—C— (+H)	0.872	-226	255
Toluene disproportionation	⬡—C$^+$H—⬡	1.33	-245	184
Cumene cracking	⬡—C$^+$—CH$_3$ CH$_3$	2.02	-282	136

[$-$C$^+$(CH$_3$)$_2$] is fixed by two methyl groups, as reflected by the slope.

In addition, the slopes of $\Delta S^{*\circ}$-$\Delta H^{*\circ}$ plots in the present catalytic reactions (0.87 to 2.0 K^{-1}) were generally similar or larger than those of ΔS-ΔH plots in the host-guest association (0.51 to 1.07 K^{-1} in [12] and 0.51 to 1.03 K^{-1} in [30]). It is reasonable that a transition state trapped by the solid surface has low freedom of movement compared to a molecule in a solution.

The intercept on the vertical axis of ΔS-ΔH plot has been proposed by Inoue et al. to show the extent of entropy gain by desolvation in the host-guest association [12];

$T\Delta S_0$, where T was 298 K, and ΔS_0 was the intercept on the vertical axis of ΔS-ΔH plot, was 0.0 to 5.0 kcal mol^{-1}[12] and 9.6 to 22.5 kJ mol^{-1} in [30], equivalent to 0 to 70 and 32 to 76 J K^{-1} mol^{-1} of ΔS_0, respectively. The positive values indicate the gain of freedom due to separation from the solvent molecules. On the contrary, the intercept on the vertical axis of $\Delta S^{*\circ}$-$\Delta H^{*\circ}$ plot in this study was -282 to -226 J K^{-1} mol^{-1} (Table 2-3), large negative values, showing loss of freedom of gas molecules by trapping with the solid surface.

We here propose that the intercept on the horizontal axis of $\Delta S^{*\circ}$-$\Delta H^{*\circ}$ plot shows the intrinsic activation barrier, reflecting the chemical nature of the reaction but not influenced by the freedom of movement, because it is $\Delta H^{*\circ}$ at $\Delta S^{*\circ}= 0$ or $\Delta G^{*\circ}$ (activation Gibbs energy defined by $\Delta G^{*\circ}= \Delta H^{*\circ}$-$T\Delta S^{*\circ}$) at T= 0. This parameter was 130 to 270 kJ mol^{-1} in the present catalytic reactions (Table 2-3), reflecting that the activation process is endothermic. On the contrary, the intercept on the horizontal axis of ΔS-ΔH or $T\Delta S$-ΔH plot in the host-guest association was -33 to 0 kJ mol^{-1} in literature [12,30] [calculated using above values by (intercept on horizontal axis) = $-$ (intercept on vertical axis)/(slope)], in agreement with that the reported host-guest association was in most cases spontaneous reaction and hence exothermic.

In addition, the intercept on the horizontal axis of $\Delta S^{*\circ}$-$\Delta H^{*\circ}$ plot was [propane

and isobutane cracking] > [linear C$_{4-8}$ alkanes and isopentane cracking] > [toluene disproportionation] > [cumene cracking], as shown in Table 2-3. From the molecular structures, the difficulty of formation is speculated to be 1 [non-classical carbonium (alkanium) cation associating a primary carbon atom] > 2 (carbonium associating only secondary and/or tertiary carbon atoms) > 3 [carbenium (alkenium) cation at the secondary part] > 4 (carbenium at the tertiary part). This is in good agreement with the observed values.

We still have speculations in the above discussion, and further investigations should be necessary, but the present observations show a possibility of the traditional kinetic study to give a deep insight of the catalytic reactions, especially about what controls the reaction behavior.

2-5 Conclusions

Kinetic analysis based on the reaction rate normalized by the number of Brønsted acid sites on various aluminosilicate solid acid catalysts showed the compensatory relationship between the activation entropy $\Delta S^{*\circ}$ and activation enthalpy $\Delta H^{*\circ}$. The slope of plots of $\Delta S^{*\circ}$ against $\Delta H^{*\circ}$ was in the order of [cumene cracking] > [toluene disproportionation] > [C_{3-8} alkane cracking]. Bulky molecular size and shape of the reactant tended to result in the steep slope. The intercept on the horizontal axis was [C_3 and C_4 monomethyl branched alkane cracking] > [linear C_{4-8} and C_5 monomethyl branched alkane

References

[1] A. Corma, *Chem. Rev*., **95**, 559-614 (1995)

[2] A. Corma, A. Martinez, *Adv. Mater.,* **7**, 137-144 (1995)

[3] V. J. Frilette, W. O. Haag, R. M. Lago, *J.Catal*., **67**, 218-222 (1982)

[4] H. Krannila, W. O. Haag, B. C. Gates, *J. Catal*., **135**, 115-124 (1992)

[5] I. E. Maxwell, W. H. J. Stork, Stud. *Surf. Sci. Catal*., **137**, 747-819 (2001)

[6] S. Al-Khattaf, S. A. Ali, A. M. Aitani, N. Žilková, D. Kubička, J. Čejka, *Catal. Rev. Sci. Eng*., **56**, 333-402 (2014)

[7] C. Perego, P. Ingallina, *Green Chem*., **6**, 274-279 (2004)

[8] J. Čejka, B. Wichterlovă, *Catal. Rev*., **44**, 375-421 (2002)

[9] M. Niwa, K. Suzuki, N. Katada, T. Kanougi, T. Atoguchi, *J. Phys. Chem. B,* **109**, 18749-18757 (2005)

[10] N. Katada, K. Suzuki, T. Noda, W. Miyatani, F. Taniguchi, M. Niwa, *Appl. Catal. A Gen*., **373**, 208-213 (2010)

[11] N. Katada, S. Sota, N. Morishita, K. Okumura, M. Niwa, *Catal. Sci. Technol*., **5**, 1864-1869 (2015)

[12] Y. Inoue, Y. Liu, L.-H. Tong, B.-J. Shen, D.-S. Jin, *J. Am. Chem. Soc*., **115**, 10637-10644 (1993)

[13] G. Lente, *Deterministic Kinetics in Chemistry and Systems Biology*, Springer, Hyderburg (2015)

[14] D. H. Everett, Trans. *Faraday Soc*., **46**, 942-957 (1950)

[15] A. Bhan, R. Gounder, J. Macht, E. Iglesia, *J. Catal*., **253**, 221-224 (2008)

[16] J. E. Leffler, *J. Org. Chem*., **20**, 1202-1231 (1955)

[17] A. K. Galwey, *Adv. Catal.*, **26**, 247-322 (1977)

[18] T.-K. Cheung, F. C. Jentoft, J. L. d'Itri, B. C. Gates, *Chem. Eng. Sci.*, **52**, 4607-4613 (1997)

[19] L. E. Sandoval-Díaz, J. M. Martínez-Gil, C. A. Trujillo, *J. Catal.*, **294**, 89-98(2012)

[20] D. C. Longstaff, *Energy Fuel,* **26**, 801-809 (2012)

[21] A. Corma, B.W. Wojciechowski, *Catal. Rev. Sci. Eng.*, **24**, 1-65 (1982)

[22] A. M. Youssef, A.I. Ahmed, S. E. Samra, *Mater. Lett.*, **10**, 175-180 (1990)

[23] J. S. Beck, D. H. Olson, S. B. McCullen, U. S. Patent 5367099 (1994)

[24] T.-C. Tsai, S.-B. Liu, I. Wang, *Appl. Catal. A: Gen.*, **181**, 355-398 (1999)

[25] K. Okumura, T. Tomiyama, N. Morishita, T. Sanada, K. Kamiguchi, N. Katada, M. Niwa, *Appl. Catal. A: Gen.,* **405**, 8-17 (2011)

[26] N. Katada, H. Igi, J.-H. Kim, Miki Niwa, *J. Phys. Chem. B,* **101**, 5969-5977 (1997)

[27] M. Niwa, N. Katada, M. Sawa, Y. Murakami, *J. Phys. Chem.*, **99**, 8812-8816 (1995)

[28] S. Glasstone, K. J. Leidler, H. Eyring, *Theory of Rate Processes*, McGraw-Hill, New York (1941)

[29] D. Mitsuyoshi, K. Kuroiwa, Y. Kataoka, T. Nakagawa, M. Kosaka, K. Nakamura, S. Suganuma, Y. Araki, N. Katada, *Micro- Mesoporous Mater.*, **242**, 118-126 (2017)

[30] Y. Lin, H. Wang, L.-H. Wang, H.-Y. Zhang, *Thermochim. Acta*, **414**, 65-70 (2014)

Chapter 3　Direct Methylation of Benzene with Methane over Co/MFI Catalyst

3-1 Introduction

　　Methane, the main component of natural gas, has predominantly been consumed as a gaseous fuel for direct combustion or reacted with water to produce hydrogen through steam reforming and water gas shift reaction. However, recently, development of chemical processes for conversion of methane into the value-added organic compounds, i.e. alkenes and mono-cyclic aromatics, has been strongly required [1-4].

　　Considerable efforts have been made in activation of methane [4-14], e.g. partial oxidation of methane into methanol [9-12], and aromatization of methane into valuable aromatic hydrocarbons and hydrogen [14-17]. However , low selectivity of the products are unavoidable problem.

　　Methylation of benzene ring with methane can be an option of effective use of methane, because it can produce such a valued compound as para-xylene. For example, combining the methylation of benzene into toluene (1) and shape selective disproportionation of toluene into para-xylene [18,19] is expected to be a new process for the production of para-xylene from toluene and methane.

$$CH_4 + C_6H_6 \rightarrow H_3C\text{-}C_6H_5 + H_2 \qquad\qquad (1)$$

In very early studies, formation of methylated product from a mixture of aromatic compound and methane was reported [20-23]. However, in the case of production of toluene from benzene and methane, it has been pointed out that toluene was possibly formed by unexpected reactions [24] like hydrogenolysis of benzene [25], where methane acted just as a hydrogen source. Careful experiments using isotope tracers then evidenced that the methylation of benzene with methane (1) was catalyzed on such zeolite-supported transition metal species as Cu/*BEA[26] and Ag/MFI [27].

On the other hand, it was pointed out that equilibrium of the reaction (1) was a problem as follows. The standard enthalpy and entropy are 41.94 kJ mol^{-1} and 4.11 J K^{-1} mol^{-1} (calculated from thermodynamic properties [28,29]), respectively, at 298 K where all the reactants and products are gases, approximately equivalent to the standard Gibbs energy +45.1 kJ mol^{-1} and the equilibrium constant 9×10^{-4} at 773 K, and equilibrium toluene yield calculated from these parameters in some conditions are shown in Figure 3-1. It has been pointed out that the conversion of reaction (1) is limited by the low equilibrium constant [24], suppressing the efficiency under past economic conditions. However, the recent demand for utilization of methane as stated above encourages re-
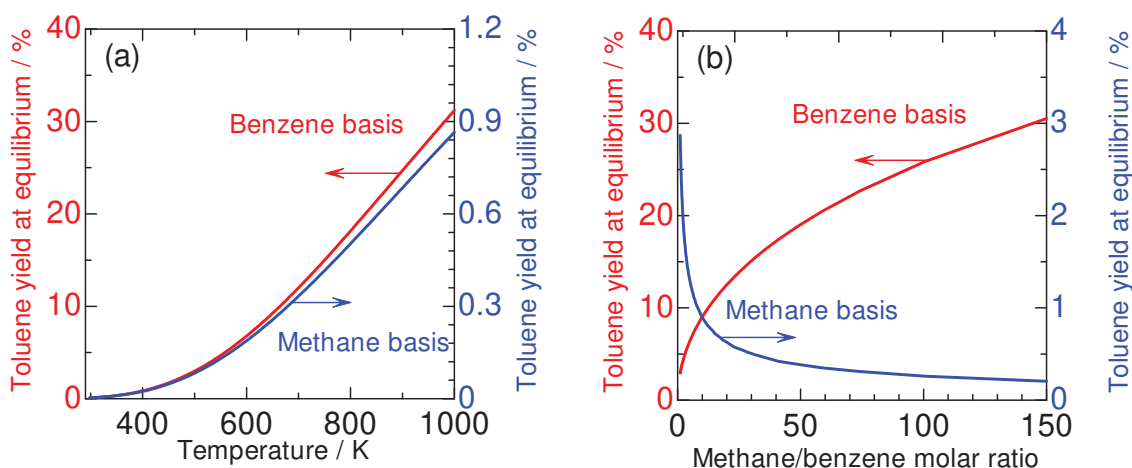
Figure 3-1　　Plots of toluene yield at equilibrium calculated from thermodynamic parameters and normalized by feeds of benzene and methane (a) against temperature with fixing methane/benzene molar ratio at 36.5 and (b) against methane/benzene molar ratio with fixing temperature at 773 K. Because this reaction does not change the number of gaseous molecules, the total pressure does not affect the equilibrium.

investigation of this reaction.

　　As stated above, Cu/*BEA [24] and Ag/MFI [27] were reported to possess the activity for methylation of benzene with methane. The activity was found also on Pt/MFI [30] and In/MFI [31]. In addition, it has been known that a similar reaction, oxidative methylation of benzene (2), was found to proceed on MFI with various counter cations (H, Na, Co, Mn and Cu) [32,33]. Also, for the partial oxidation of methane into methanol, zeolite-supported transition metal species were reported to show the catalytic activity [34-38]. It has been known that zeolite (mainly MFI)-supported metal species are active also for combustion of methane [39], reduction of NOx with methane [40], aromatization of methane [14] and the activation of methane at low temperature [41]. All these studies

suggest that zeolite-supported transition metal species are promising candidates of catalysts for reactions involving the methane activation step.

$$CH_4 + C_6H_6 + 1/2O_2 \rightarrow H_3C\text{-}C_6H_5 + H_2O \qquad (2)$$

Here we mention the difference between the reactions (1) and (2). Comprehensive studies by Adebajo et al. clarified that many kinds of zeolite-supported transition metal species (sometimes typical elements) showed catalytic activity for the reaction (2) [13]. Generally, the rate of (2) is higher than (1) at the same temperature in similar partial pressures of benzene and methane. However, the reaction (2) consumes the hydrogen to form water whereas the reaction (1) forms hydrogen, and complete oxidation of organic materials into CO_2 as a side reaction is probably unavoidable in the presence of oxygen. From these viewpoints, the non-oxidative methylation of benzene with methane (1) should be studied in more detail. Because the rate of (1) is substantially low, the investigation to find an efficient catalyst should be important compared to the case of reaction (2).

As stated above, the preceding literatures reported essential activity of Cu/*BEA [26], Ag/MFI [27], Pt/MFI [30], and In/MFI [31] for the methylation of benzene with

methane, indicating that unique activity was created by the combination of transition metal species and zeolite. In the case of Ag/MFI and In/MFI, Ag^+ and InO^+ species, respectively, held by the ion exchange site of MFI have been identified as the active species [27,31]. It has also been clarified that unique function of the transition metal species concerning the methane activation was induced by the zeolite ion exchange site in other cases [39,41]. We believe that the analysis of structure in atomic dimension and the quantitative analysis of catalytic sites are important in this field for clarifying the role of ion exchange site and unique function of transition metal species on it. X-ray absorption near edge spectroscopy (XANES) and extended X-ray absorption fine structure (EXAFS) were utilized to characterize the oxidation state and structure of active species in atomic scale. Ammonia infrared mass spectrometry-temperature programed desorption (IRMS-TPD), which was recently developed by our group [42], was also applied for the quantitative analysis of Brønsted and Lewis acid sites, showing the quantities of ion exchange sites uncovered and covered by the transition metal species. The analysis of Lewis acidity is also related directly to the activity, because it has been known that Lewis acid strength affects the activity in reactions of methylation reagents [43].

Based on these backgrounds, we investigate the catalytic performances of

various zeolite-supported transition metal species for the methylation of benzene with methane into toluene in non-oxidative conditions. The first purpose is the screening of catalysts with wide variation. Most of the preceding papers [26,27,30,31] reported the catalytic performances for this reaction in batch or closed circular systems, reflecting very slow reaction rate, but a fixed-bed continuous flow method is here employed for practical investigation. The reaction formula and side reactions are analyzed by using isotope tracers and mass spectroscopy (MS). As the second purpose of the study, the physicochemical properties of active species is analyzed using such advanced techniques as XANES, EXAFS and IRMS-TPD. To our knowledge, such a comprehensive study has not been done for the methylation of benzene with methane in non-oxidative conditions. We here report high activity of Co/MFI and the nature of active species.

3-2 Experimental

3-2-1 *Catalyst preparation*

Samples of Na-MFI zeolite with $SiO_2/Al_2O_3 = 24$ (supplied by Tosoh), 30, 48 (Mizusawa), 61 (Zeolyst), and 90 (Craliant) were ion-exchanged into NH_4-form, and in addition, a sample of NH_4-form MFI with $SiO_2/Al_2O_3 = 22$ from Tosoh was also used as the support of transition metal catalysts. Various elements were impregnated from

aqueous solutions of their nitrates (Co, Fe, Ni, Cu, Ag and In), chlorides of ammine complexes (Pt, Pd and Rh) or $(NH_4)_6Mo_7O_{24}$ on NH_4-MFI. Most of the solvent was removed by drying at 343 K with stirring at 400 rpm. The yielded solid was dried again at 383 K overnight in an oven and then stored without further calcination at higher temperatures. Cobalt was also impregnated on NH_4-*BEA (ion exchanged from Na-*BEA, Clariant), NH_4-MOR (as supplied from Tosoh) and NH_4-FAU (ion exchanged from Na-FAU, JGC Catalysts and Chemicals) with SiO_2/Al_2O_3 = 25, 19, and 4.8, respectively. In the case of Co/MFI, an ion exchange method was also examined for the catalyst preparation as follows: NH_4-MFI with SiO_2/Al_2O_3 = 22 was put into an aqueous $Co(NO_3)_2$ solution with desired Co content, and the solution was stirred and heated at 343 K for 4 h. The solid was then filtrated, washed 3 times and dried at 383 K. The Co and Al contents on the ion-exchanged samples were measured by means of inductively coupled plasma emission spectroscopy (ICP-AES, Rigaku ICP CIROS). As a comparison, Co/SiO_2 was prepared by the impregnation of $Co(NO_3)_2$ on a silica gel at [Co] = 0.78 mol kg^{-1}, which is equivalent to the Co content in Co/MFI prepared by the impregnation at Co/Al = 0.6 on the MFI with SiO_2/Al_2O_3 = 22. The thus prepared samples are listed in Table 3-1 with their abbreviations.

Table 3-1 Catalysts employed in this study.

Abbreviation	Transition metal source	Preparation method	Structure of support	[Al] / mol kg^{-1}	[Metal] / mol kg^{-1}	SiO$_2$/Al$_2$O$_3$ in support	Metal / Al molar ratio
H/MFI	-	-	MFI	1.3	0	22	0
IMP-Co-x	Co(NO$_3$)$_2$	Impregnation	MFI	1.3	$1.3 \times x$*	22	x*
IE-Co-x	Co(NO$_3$)$_2$	Ion exchange	MFI	1.3	$1.3 \times x$**	22	x**
Co/MFI (24)	Co(NO$_3$)$_2$	Impregnation	MFI	1.3	0.78*	24	0.60*
Co/MFI (30)	Co(NO$_3$)$_2$	Impregnation	MFI	1.0	0.61*	30	0.60*
Co/MFI (48)	Co(NO$_3$)$_2$	Impregnation	MFI	0.7	0.39*	48	0.60*
Co/MFI (60)	Co(NO$_3$)$_2$	Impregnation	MFI	0.5	0.32*	60	0.60*
Co/BEA	Co(NO$_3$)$_2$	Impregnation	BEA	1.2	0.72*	25	0.60*
Co/MOR	Co(NO$_3$)$_2$	Impregnation	MOR	1.6	0.95*	19	0.60*
Co/FAU	Co(NO$_3$)$_2$	Impregnation	FAU	4.5	2.71*	4.8	0.60*
Co/SiO$_2$	Co(NO$_3$)$_2$	Impregnation	Amorphous (silica gel)	0	0.78*	∞	∞
Fe-0.6	Fe(NO$_3$)$_3$	Impregnation	MFI	1.3	0.81*	22	0.60*
Ni-0.6	Ni(NO$_3$)$_2$	Impregnation	MFI	1.3	0.81*	22	0.60*
Cu-0.6	Cu(NO$_3$)$_2$	Impregnation	MFI	1.3	0.81*	22	0.60*
Zn-0.6	Zn(NO$_3$)$_2$	Impregnation	MFI	1.3	0.81*	22	0.60*
Mo-1.2	(NH$_4$)$_6$ Mo$_7$O$_{24}$	Impregnation	MFI	1.3	1.62*	22	1.20*
Rh-0.6	RhCl$_3$	Impregnation	MFI	1.3	0.81*	22	0.60*
Pd-0.6	PdCl$_2$	Impregnation	MFI	1.3	0.81*	22	0.60*
Ag-0.6	AgNO$_3$	Impregnation	MFI	1.3	0.81*	22	0.60*
In-0.4	In(NO$_3$)$_3$	Impregnation	MFI	1.3	0.54*	22	0.40*
Pt-0.6	H$_2$[PtCl$_6$]	Impregnation	MFI	1.3	0.81*	22	0.60*

*: Based on the amounts of Co in the impregnated solution and Al in the used zeolite.

**: Measured by inductively coupled plasma emission spectroscopy (ICP-AES).

3-2-2 *Reaction tests*

Catalytic tests were performed in a fixed-bed flow reactor. Methane (99.9 % from Iwatani) and benzene (special grade, Wako) were used, and in some cases, methane enriched with ^{13}C (^{13}C 99.9% from Hinomaru Industry, Tottori) was used for the confirmation of reaction path. In standard conditions, powder sample (0.300 g) was placed in a Pyrex tube (i.d.: 10 mm) and pretreated in a flow of nitrogen (1.23 mmol min^{-1}) in the atmospheric pressure at 823 K for 1 h. Then, a mixture of methane and benzene (98.6 and 2.7 kPa, 1.2 and 0.033 mmol min^{-1}, respectively, corresponding to W_{cat} / $F_{benzene}$ = 147 g$_{cat}$ h mol$_{benzene}^{-1}$) was fed to the catalyst bed at 773 K. The outlet materials were trapped by hexane at 273 K with 1,4-diisopropylbenzene as an inner standard material and analyzed with flame ionization detector-gas chromatograph (FID-GC, Shimadzu GC-2010) or were analyzed by using a mass-spectrometer (MS, Pfeiffer Vacuum QMS200) directly connected to the outlet of a reactor. The MS measurements were carried out by means of inner standard method using helium as the standard. The molecular weight of the product of reaction using $_{13}$C-enriched methane was analyzed with a GC-MS (JMS-T100GCV, JEOL). The ^{13}C NMR were recorded on JEOL JNM ECP500 at 11.7 T. Chemical shifts are expressed in ppm downfield from Si(CH$_3$)$_4$.

3-2-3 *Analysis of physicochemical properties*

The acidic property was analyzed by a method of ammonia IRMS-TPD in conditions described elsewhere [42]. Morphology of the catalyst was analyzed with a TEM (HITACHI H800 B) in accelerating voltage 200 kV. Oxidation state and microstructure of the Co species were analyzed by X-ray absorption spectroscopy (XAS or XAFS, i.e., XANES and EXAFS) at BL01B1 in Japan Synchrotron Radiation Research Institute (JASRI, SPring-8) (Proposal No. 2018A1075). After pretreatment of Co/MFI in nitrogen flow of 74 mmol h^{-1} at 101 kPa and 823 K for 1 h, it was mixed with boron nitride (BN), stirred by an agate mortal for 30 min and compressed into a wafer form with 10 mm diameter. A Co-foil and bulk Co oxides (CoO and Co_2O_3) were also measured as the references. The Co K-edge absorption spectra were collected in the quick mode using a Si (111) monochromator. The beam size at the sample position was 5 mm (horizontal) × 1 mm (vertical).

3-3 Results and Discussion

3-3-1 *Catalytic activity*

The continuous flow reaction of benzene and methane was examined at 773 K

on various zeolite-supported transition metal species shown in Table 3-1, and the

formation of toluene was observed on some catalysts. The time course of toluene yield is

shown in Figure 3-2, and Figure 3-3 compares the toluene yield on various elements

(including H) impregnated on MFI zeolite, and Co impregnated on various supports.

Among the employed catalysts covering various elements and zeolite supports, only
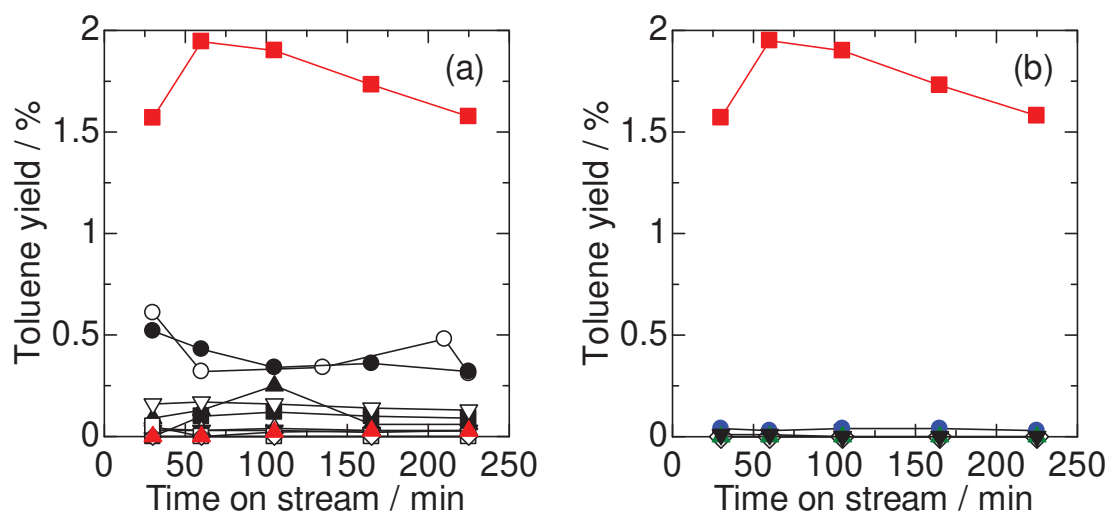
Figure 3-2   Time course of toluene yield at 773 K, P_{CH4} = 98.6 kPa, P_{C6H6} = 2.7 kPa
and W_{cat} / $F_{benzene}$ = 147 g_{cat} h $mol_{benzene}^{-1}$, over (a) Co (■, IMP-Co-0.6), H (▲, H/MFI),
Ni (●, Ni-0.6) , In (○, In-0.4), Mo (▲, Mo-1.2), Cu (■, Cu-0.6), Ag (△, Ag-1.2), Fe (▽,
Fe-0.6), Pt (▼, Pt-0.6), Pd (□, Pd-0.6) and Rh (◇, Rh-0.6) impregnated on MFI
(SiO₂/Al₂O₃ = 22),   where the digits in parentheses show metal / Al and (b) Co
impregnated on MFI (■, IMP-Co-0.6), BEA (●, Co/BEA), MOR (▼, Co/MOR), FAU
(▲, Co/FAU) and silica gel (◇, Co/SiO₂) with keeping Co/Al at 0.6 on zeolites (■, ●,
▼ and ▲) while [Co] was 0.78 mol kg⁻¹ on silica gel (◇).
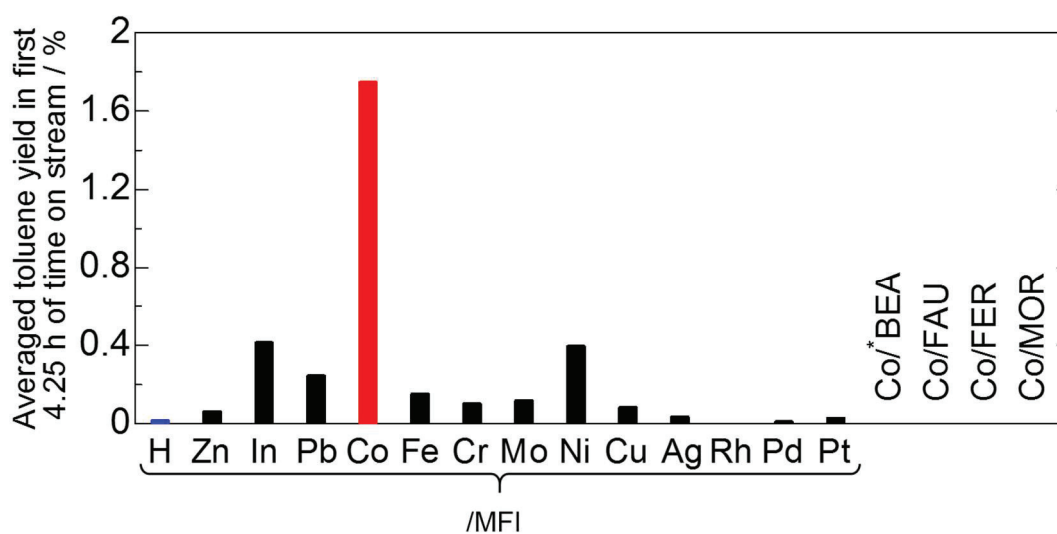
Figure 3-3   Averaged toluene yield for initial 4.25 h in the reaction at 773 K, P_{CH4} = 98.6 kPa, P_{C6H6} = 2.7 kPa and $W_{cat} / F_{benzene}$ = 147 g_{cat} h $mol_{benzene}^{-1}$, over the each zeolite-supported metal species. As Co/MFI, IMP-Co-0.6 (see Table 3-1) was employed; [Al] and Co/Al molar ratio were 1.3 mol kg^{-1} and 0.6, respectively. Compositions and preparation methods of other catalysts are shown in Table 3-1.

Co/MFI showed remarkable activity. Toluene was detected, as well as trace of xylene, while no other organic product was found in the product on Co/MFI. Zeolite (mainly MFI)-supported Ag, In, Cu, Zn, Pt and Mo have been reported to show activities for the present reaction [26-31] or the reactions / activation of methane, i.e., oxidation of methane to methanol [34], combustion of methane [39], selective catalytic reduction of NOx with methane [40], aromatization of methane [14], and the activation of methane at low temperature [41]. Co/MFI showed obviously higher activity for methylation of benzene with methane than those on the other catalysts including the above metals loaded on zeolites. Although Baba et al. reported the activity of Ag^+ species on Ag/MFI for the same

reaction (methylation of benzene) at 673 K [27], the activity of Ag/MFI was obviously

lower than Co/MFI in the present results. On the contrary, Ni/MFI and In/MFI showed

small activities, and the latter is in agreement with Gabrienko et al. [31]; Co/MFI was

found to be more active than all of them. On the other hand, Adebajo et al. reported that

Co/MFI showed the activity for oxidative methylation of benzene with methane (2), but

several other catalysts such as Mn, Cu, and Na-modified MFI also showed the comparable

activity [32,33]. It is noteworthy that the non-oxidative methylation (1) seems to be

substantially difficult and its rate is sensitive to the nature of catalyst compared to (2),
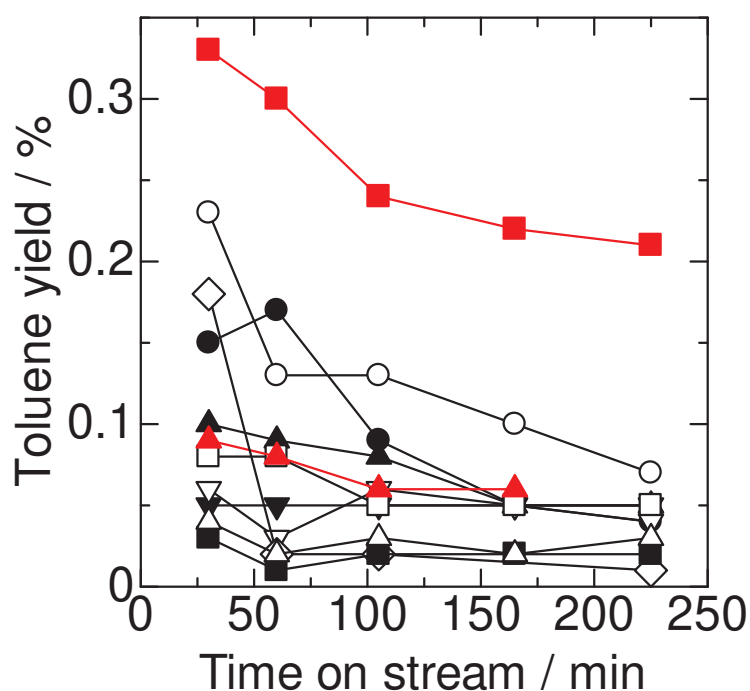
Figure 3-4   Time course of toluene yield under high pressure (P_{CH4} = 1200 kPa and P_{C6H6} = 290 kPa) at 773 K and W_{cat} / $F_{benzene}$ = 5.7 g_{cat} h $mol_{benzene}^{-1}$, over (a) Co (■, IMP-Co-0.6), H (▲, H/MFI), Ni (●, Ni-0.6) , In (○, In-0.4), Mo (▲, Mo-1.2), Cu (■, Cu-0.6), Ag (△, Ag-1.2), Fe (▽, Fe-0.6), Pt (▼, Pt-0.6), Pd (□, Pd-0.6) and Rh (◇, Rh-0.6) impregnated on MFI (SiO₂/Al₂O₃ = 22), where the digits in parentheses show metal / Al.

and therefore only Co/MFI had distinguished activity.

In order to confirm the superiority of Co/MFI for this reaction, the reaction tests were examined also under high pressures of hydrogen and benzene with higher reaction rates. It was demonstrated that Co/MFI always showed high activity compared to the other catalysts (Figure 3-4).

Preceding literature reported that toluene was formed in the co-presence of benzene and methane even on H-MFI without transition metal through the hydrogenolysis of benzene [25], but in the present case, the yield of toluene on H-MFI was negligible as shown in Figure 3-3. The influence of hydrogenolysis is thus believed to be small in the present conditions, as also evidenced by the experiments using isotope tracers shown later.

Figure 3-5 shows the influence of Al content of MFI zeolite as the support with keeping the Co/Al molar ratio at 0.6; the time course is shown in Figure 3-6 (a). The yield increased with the Al content up to $[Al] = 1.3$ mol kg^{-1} corresponding to $SiO_2/Al_2O_3 = 22$, i.e., the highest Al concentration in MFI commercially available.
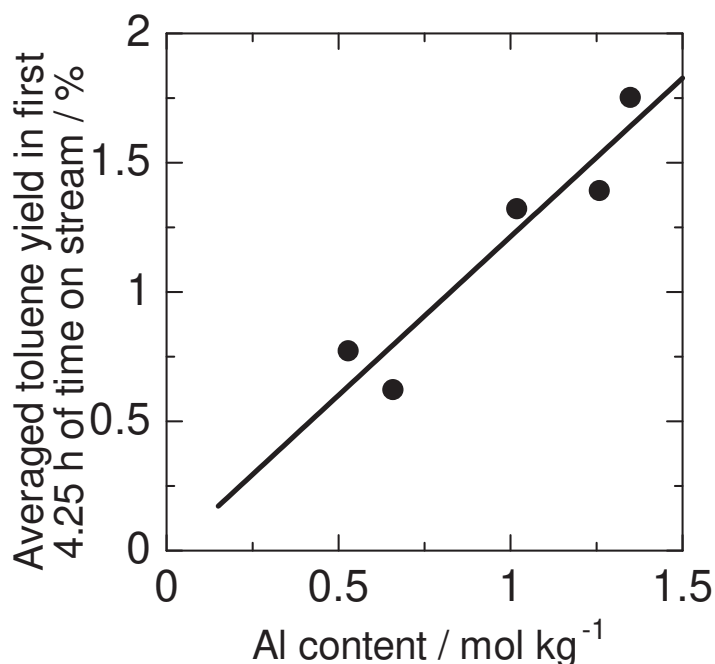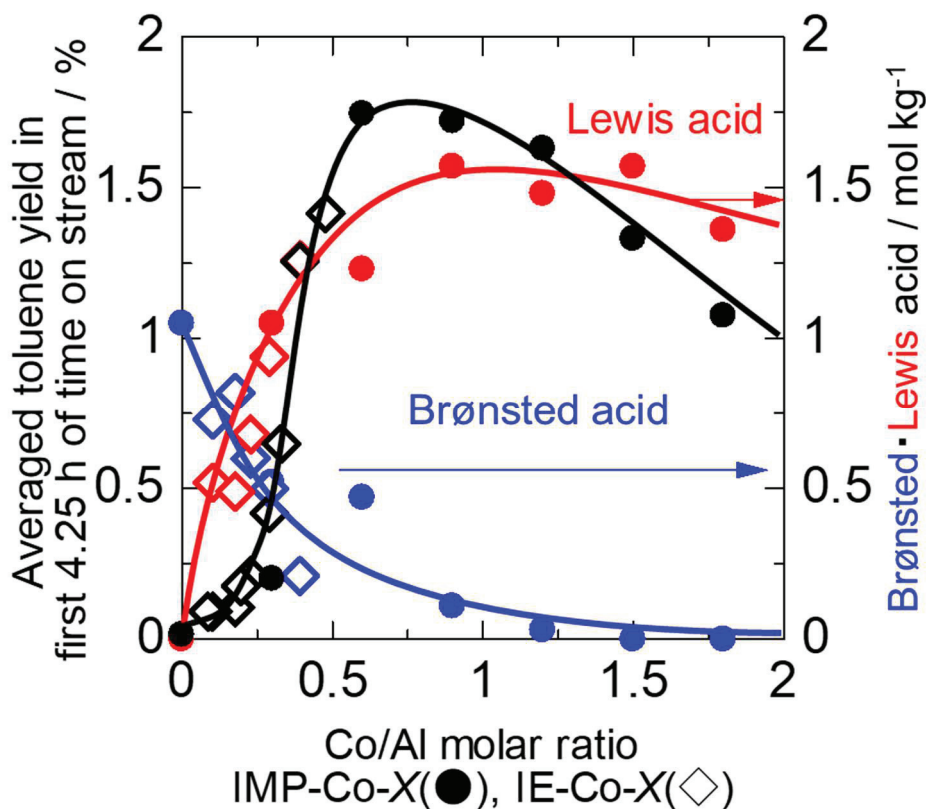
Figure 3-5　Catalytic activity for methylation of benzene with methane at 773 K, P_{CH4} = 98.6 kPa, P_{C6H6} = 2.7 kPa and $W_{cat} / F_{benzene}$ = 147 g_{cat} h $mol_{benzene}^{-1}$ over Co-impregnated on MFI with various Al contents with keeping Co/Al molar ratio at 0.6.
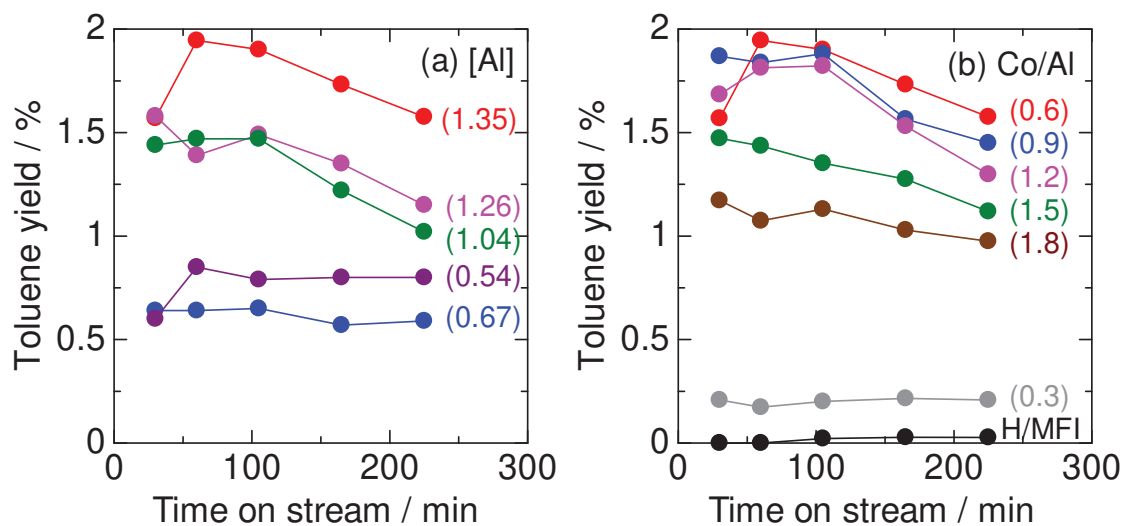
Figure 3-6　Time course of toluene yield over Co impregnated on (a) MFI (SiO_2/Al_2O_3 = 22) with various Co contents (digits in parentheses: Co/Al molar ratio) and (b) MFI with various Al contents with Co/Al = 0.6 (digits in parentheses : [Al] / mol kg^{-1}) at 773 K, P_{CH4} = 98.6 kPa, P_{C6H6} = 2.7 kPa and $W_{cat} / F_{benzene}$ = 147 g_{cat} h $mol_{benzene}^{-1}$.

Figure 3-7 (● and ◇) shows the influence of Co content on MFI with [Al]

fixed at 1.3 mol kg^{-1}; time course is shown in Figure 3-6 (b). Because Co/Al molar ratio

obtained by the ion exchange in the present conditions was < 0.48, further loading of Co

was performed only by the impregnation method, whereas the impregnation (●) and ion

exchange (◇) method gave a common relationship between the activity and Co/Al molar

ratio < 0.48. The activity was negligible at Co/Al = 0 under these conditions, and

Figure 3-7   Catalytic activity for methylation of benzene with methane at 773 K, P_{CH4} =
98.6 kPa, P_{C6H6} = 2.7 kPa and W_{cat} / $F_{benzene}$ = 147 g$_{cat}$ h mol$_{benzene}^{-1}$ (● and ◇), and amounts
of Brønsted (● and ◇) and Lewis (● and ◇) acid sites on Co/MFI prepared by
impregnation (●) and ion exchange (◇) methods using MFI with SiO$_2$/Al$_2$O$_3$ = 22 ([Al] =
1.3 mol kg^{-1}) plotted against Co/Al molar ratio.

introducing Co created the activity. The toluene yield showed the maximum at Co/Al =

0.6, and further loading reduced the activity at Co/Al > 0.9.

3-3-2 *Confirmation of reaction formula*

Experiments using isotope tracer were carried out on IMP-Co-0.6 to confirm that

the toluene formation was ascribed to the reaction (1) but not due to the benzene

hydrogenolysis [25]. Methane enriched with ^{13}C (hereafter $^{13}CH_4$) and ordinal benzene

(hereafter shown as $^{12}C_6H_6$, but containing naturally abundant ^{13}C) were used as the

reactant s, and the products were analyzed with a gas chromatography-mass spectrometer

(GC-MS) and ^{13}C nuclear magnetic resonance (NMR). Results of the GC-MS analysis

are shown in Figure 3-8 and indicate that the *m/e* ratios of major peaks of toluene
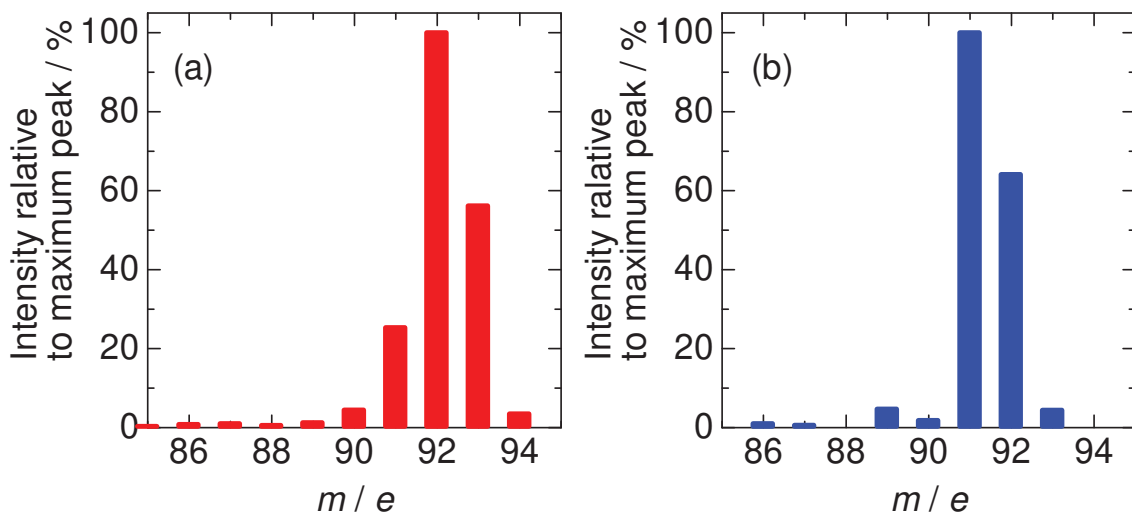
Figure 3-8   Intensity of peaks in GC-MS spectra of the outlet liquid after (a) $^{13}CH_4$ (^{13}C-enriched methane) + benzene and (b) $^{12}CH_4$ + benzene reactions on IMP-Co-0.6 at W_{cat} / $F_{benzene}$ = 147 g_{cat} h $mol_{benzene}^{-1}$ at 773 K, P_{CH4} = 98.6 kPa, P_{C6H6} = 2.7 kPa.

produced by the reaction of $^{13}CH_4 + {}^{12}C_6H_6$ were 92 and 93, consistent with the molecular weight 93 of $^{13}C^{12}C_6H_8$, whereas the reaction of $^{12}CH_4$ (ordinal methane) + $^{12}C_6H_6$ gave the *m/e* ratios of toluene 91 and 92, showing the molecular weight 92 of $^{12}C_7H_8$.

Figure 3-9 shows ^{13}C NMR spectra. The naturally abundant ^{13}C was found in a mixture of benzene, the solvent (hexane) and the inner standard material (1,4-diisopropylbenzene) [(i) and (ii)]. In addition to these peaks, a signal at 21.4 ppm assigned to the methyl group of toluene [44] was observed in the product of $^{13}CH_4 + {}_{12}C_6H_6$ (iii) but not in the product of $^{12}CH_4 + {}^{12}C_6H_6$ (ii) [Figure 3-9 (a)]. On the other hand, the product of $^{13}CH_4 + {}^{12}C_6H_6$ (iii) showed no peaks at 125.3, 128.3, 129.1 nor 137.8 ppm where carbons in the benzene ring of toluene might show resonances [44] [Figure 3-9 (b)]. It has thus been evidenced that most of toluene was formed from a pair of methane and benzene molecules, and the carbon atom in the methyl group of toluene came from methane, whereas the carbon atoms in the benzene ring came from benzene.
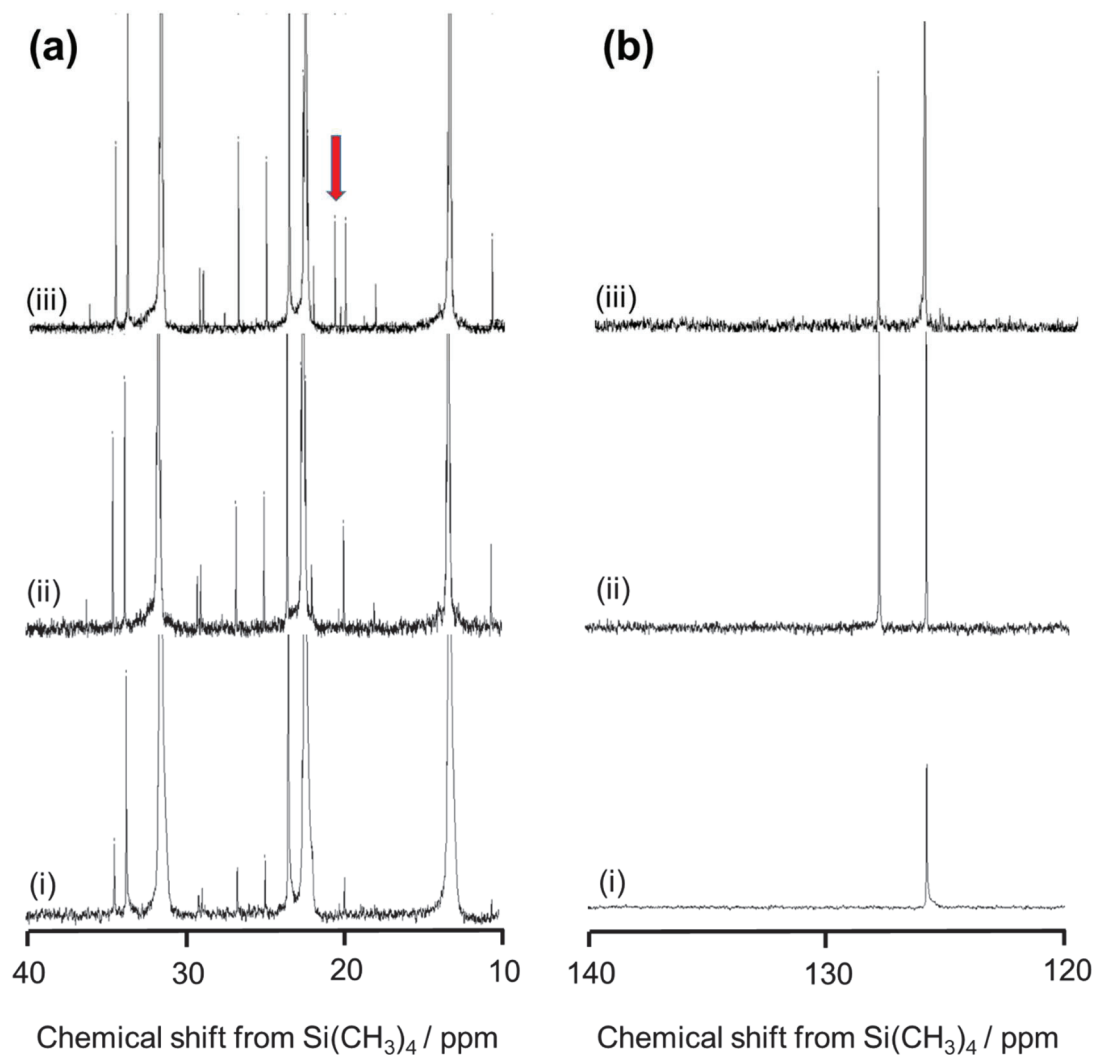
Figure 3-9　(a) 10-40 ppm and (b) 120 - 140 ppm regions of ^{13}C NMR spectra of (i) blank solution of hexane (solvent) and 1,4-diisopropylbenzene (inner standard material), (ii) outlet materials of reaction of [^{12}CH$_4$ + ^{12}C$_6$H$_6$ (benzene)], and (iii) outlet materials of reaction of [^{13}CH$_4$ + ^{12}C$_6$H$_6$] on IMP-Co-0.6 at 773 K, W_{cat} / $F_{benzene}$ = 147 g$_{cat}$ h mol$_{benzene}^{-1}$ in 98.6 and 2.7 kPa of methane and benzene, respectively.

The MS analysis of the outlet gas detected only dihydrogen (H_2), toluene and trace of xylene as the products of the reaction of $^{12}CH_4 + {}^{12}C_6H_6$ on Co/MFI, whereas no other hydrocarbon was found at $m/e < 100$. This is consistent with that the hydrogenolysis of benzene did not occur. Figure 3-10 shows the rates of formation of toluene and
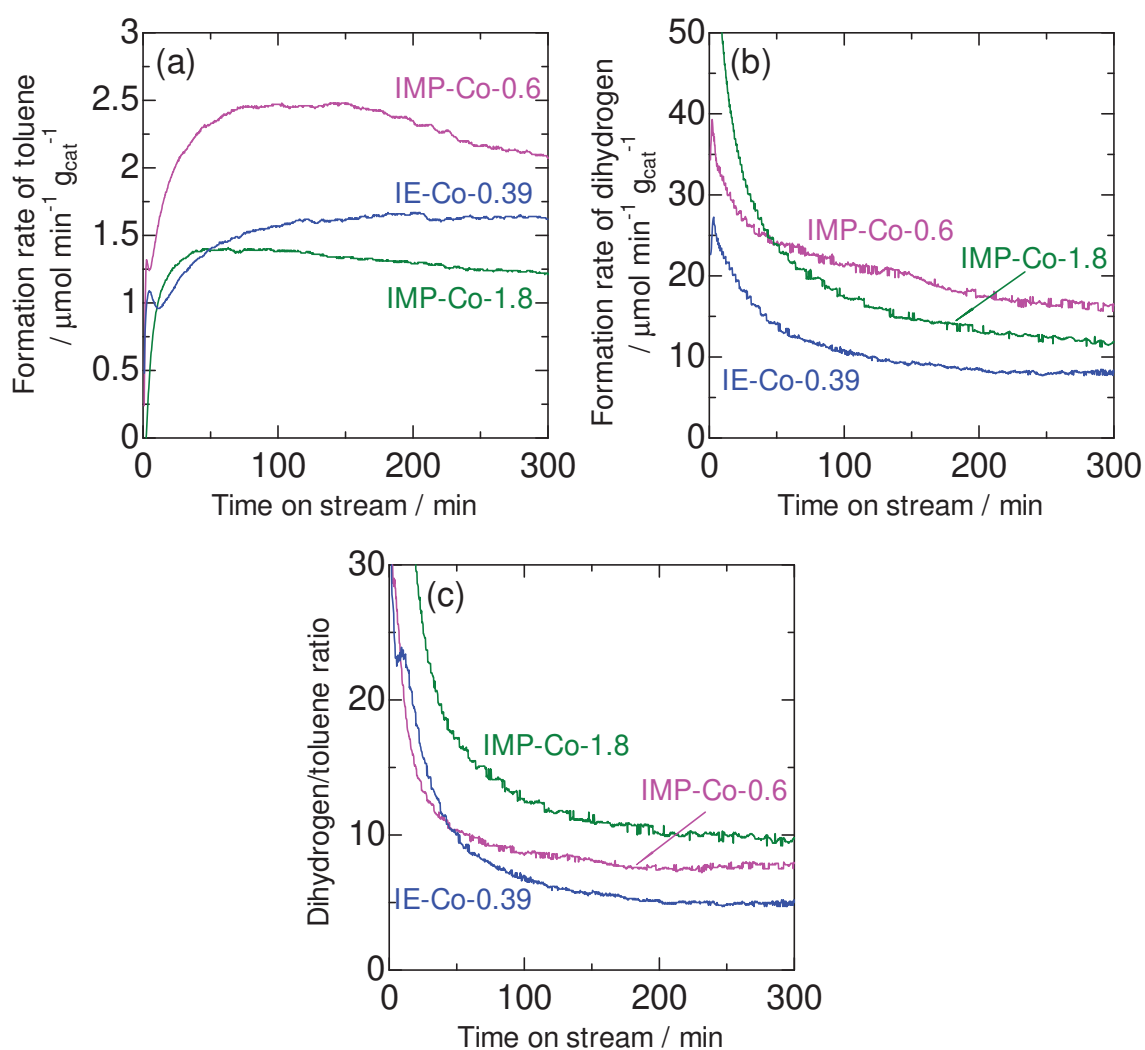
Figure 3-10   Changes in formation rate of (a) toluene and (b) dihydrogen, and (c) dihydrogen/toluene molar ratio with time on stream in the methylation of benzene with methane at 773 K, P_{CH4}, P_{He} and P_{C6H6} = 91.4, 6.8 and 3.2 kPa, respectively, and W_{cat} / $F_{benzene}$ = 125 g_{cat} h $mol_{benzene}^{-1}$ on Co/MFI. The pretreatment of catalysts for these experiments were carried out at 823 K in nitrogen flow for 2 h.

dihydrogen and their time course on IE-Co-0.39, IMP-Co-0.6 and IMP-Co-1.8 as the

catalysts; the toluene formation rate was consistent with the experiments shown in Figure

3-10 (a). The formation of dihydrogen was significant at the initial stage of flow reaction

(< 50 min) [Figure 3-10 (b)]. This suggests that the dehydrogenation of methane (3)

proceeded on these catalysts. The formation rate of dihydrogen decreased quickly,

especially for IMP-Co-1.8. Probably the carbonaceous formed due to the reaction (3)

blocked the active sites for the dehydrogenation. After this initial deactivation, the

formation of dihydrogen has continued. The molar ratio of dihydrogen/toluene was

generally higher than unity even after the initial deactivation, as shown in Figure 3-10 (c).

This ratio should be unity if only the reaction (1) proceeds. The value higher than unity

indicates the dehydrogenation (3) taking place as a side reaction. The ratio was in the

order of IMP-Co-1.8 > IMP-Co-0.6 > IE-Co-0.39, indicating that excess of Co forming

the aggregates resulted in the significant side reaction.

$$CH_4 \rightarrow C + 2H_2 \tag{3}$$

These findings indicate that the direct methylation of benzene with methane into

toluene and dihydrogen (1) proceeded on Co/MFI in the employed reaction conditions,

accompanied with dehydrogenation of methane into carbonaceous material and dihydrogen as a side reaction; its extent was dependent on the loading of Co. Simultaneously undesired reactions such as hydrogenolysis of benzene was not observed.

3-3-3 *Investigation of active species*

The acidic property was analyzed by means of ammonia IRMS-TPD method [42]. Figure 3-7 also shows the amount of the Brønsted and Lewis acid sites as overlapped on the catalytic activity. Similarly to the activity, the impregnation and ion exchange methods gave no remarkable difference in the relationship between the acid amounts and Co/Al ratio. On the parent H-MFI (Co/Al = 0), a considerable amount of Brønsted acid sites were detected, and the loading of Co decreased the Brønsted acid sites. This indicates that the Co species were bound to the ion exchange sites. The Lewis acid sites were generated by the Co loading, showed the maximum at Co/Al = ca. 0.9, and then gradually decreased. Generation of Lewis acid sites by introduction of transition metal species on the ion exchange site of zeolite has been found.[45,46] As stated in the previous paragraph, the catalytic activity for methylation of benzene with methane was also created by the Co loading, showed the maximum and decreased with further loading. The similar trend suggests that the active site was Lewis acidic Co species held by the ion exchange site.
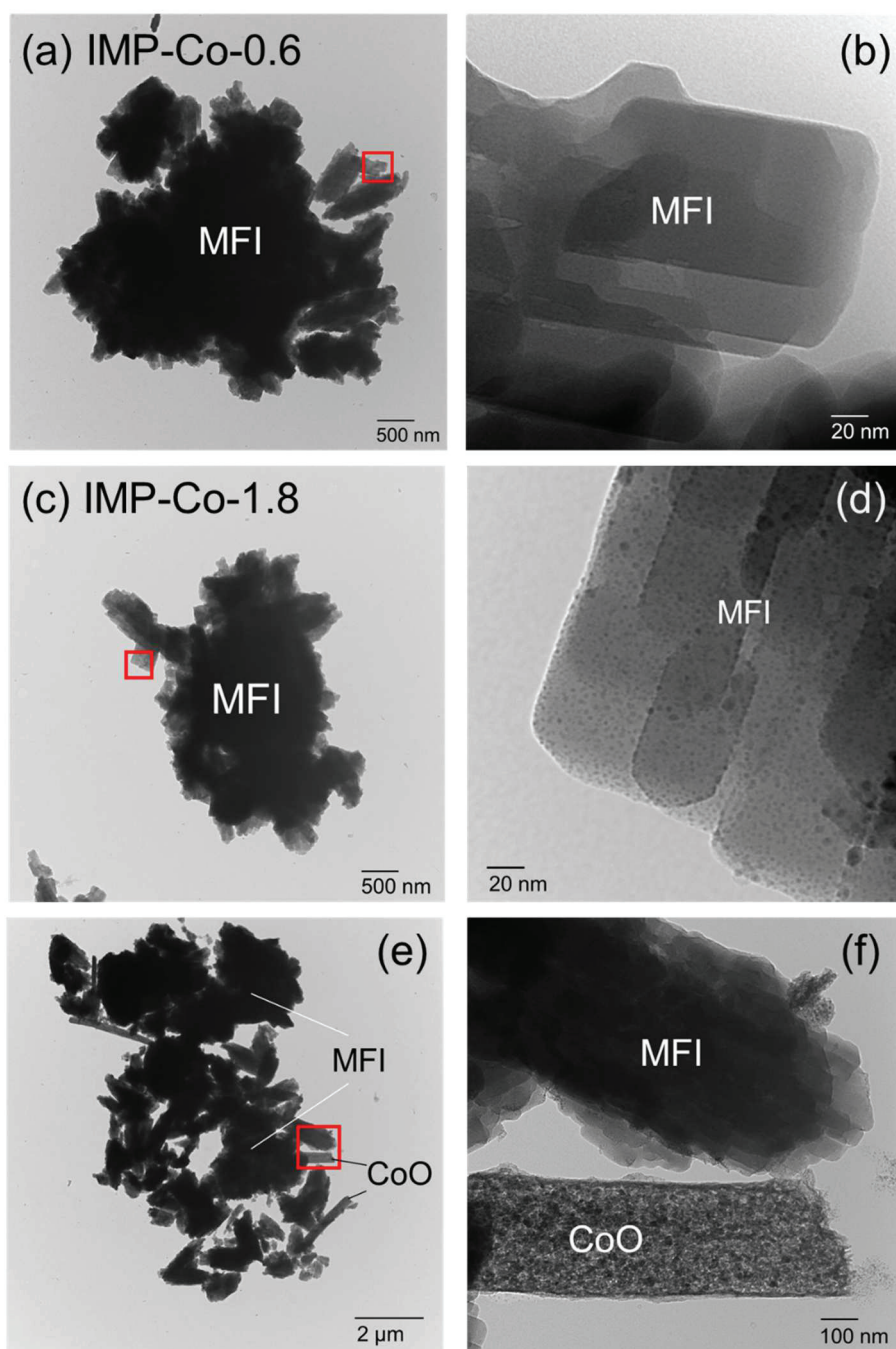
Figure 3-11   TEM images of (a), (b) IMP-Co-0.6 and (c)-(f) IMP-Co-1.8.

Figure 3-11 shows transmission electron microscope (TEM) images of IMP-Co-0.6 and IMP-Co-1.8. Both had coffin-shaped particles, i.e., typical crystallites of MFI type zeolite. Aggregates were scarcely observed on IMP-Co-0.6 [Figure 3-11 (b)],
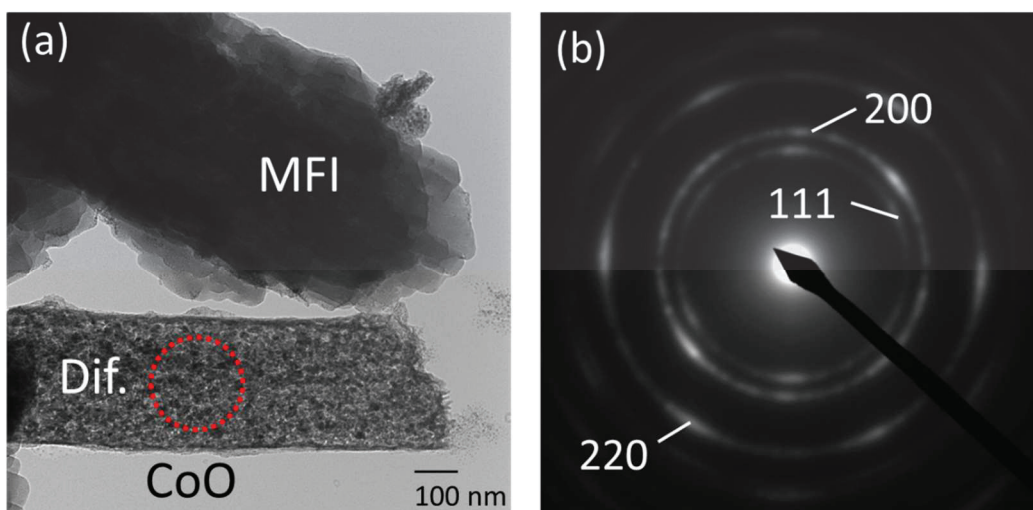
Figure 3-12   (a) TEM image of IMP-Co-1.8, and (b) electron diffraction pattern at point shown by red circle in Figure 3-12(a).

implying that Co species was highly dispersed in the micropores of MFI, because the solution of TEM was ca. 1 nm. On the contrary, IMP-Co-1.8 had aggregates on it [Figure 3-11 (d)], as well as rod-shaped structures [Figure 3-11 (f)]. They were identified to fcc-CoO from the electron diffraction pattern (Figure 3-12). Figure 3-13 (a) shows the XANES (X-ray absorption near edge structure) spectra after the pretreatment in the same conditions to those of reaction (in N_2 flow at 823 K for 1 h). The spectra of all the Co/MFI samples employed here had similar positions and shapes to those of bulk CoO, indicating that the oxidation state of Co supported on MFI was insensitive to the loading amount and around +II in the experimental region of Co loading even after pretreatment in reducing atmosphere. It may be reason for the fact that Co/MFI showed specific activity for this reaction, because oxidized state is important for dehydration from methane.
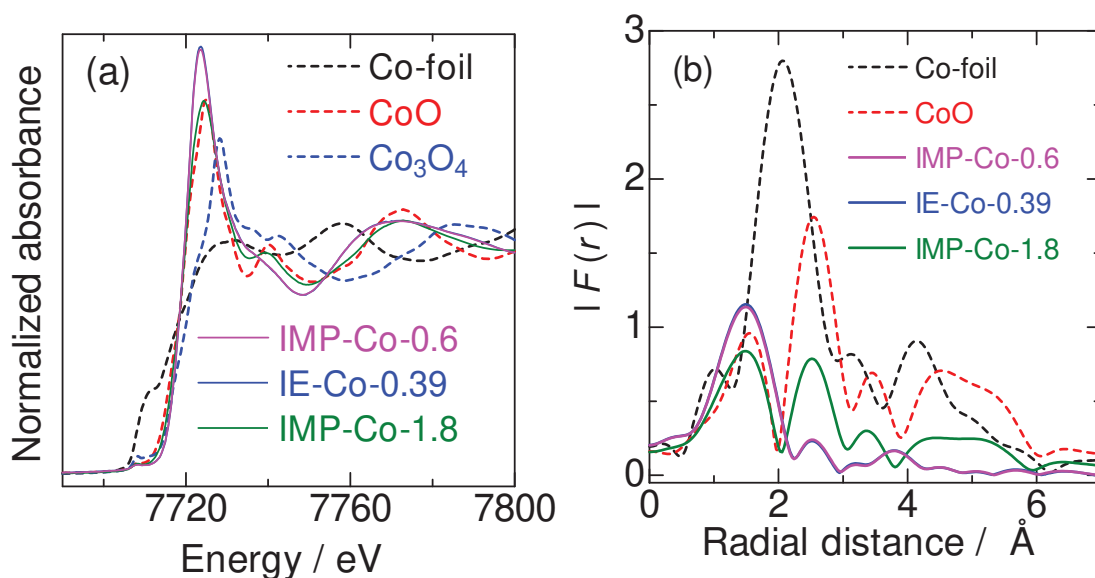
Figure 3-13　　(a) XANES spectra of Co/MFI pretreated in same conditions to those of reaction (in nitrogen flow at 823 K for 1 h) and reference samples, and (b) Radial distribution function of Co K-edge EXAFS of Co/MFI pretreated in same conditions to those of reaction (in nitrogen flow at 823 K for 1 h) and reference samples.

Figure 3-13 (b) shows the radial distribution function of Co K-edge EXAFS (extended X-ray absorption fine structure). The Co/MFI samples with small Co loadings (IMP-Co-0.6 obtained by impregnation and IE-Co-0.39 obtained by ion exchange) showed a distribution peak at 0.15 nm, attributed to Co-O, whereas the sample with excess of Co (IMP-Co-1.8) had an additional peak at 0.25 nm, attributed to Co-O-Co, similarly to the bulk oxides. These indicate that Co species were mono-atomically dispersed at Co/Al < 0.6, whereas a fraction of Co species were oligomerized or aggregated with further loading.

　　　　The TEM and EXAFS thus demonstrated that the Co species was mono-

atomically dispersed on the ion exchange site of MFI, the XANES showed the oxidation

state +II, and the ammonia IRMS-TPD pointed out the Lewis acidity in the region of

Co/Al < 0.6. Excess Co formed aggregates of CoO. From the reaction tests, the

methylation of benzene with methane (1) proceeded on Co/MFI with Co/Al < 0.6. The

further loading decreased activity for the desired reaction (1) and kept increasing the

activity of side reaction (3). These facts derive a conclusion that divalent (oxidation state

+II) cobalt species with Lewis acidity mono-atomically dispersed on the ion exchange

site of MFI zeolite was the active site for the methylation of benzene with methane.

3-4 Conclusions

Benzene was methylated with methane in non-oxidative conditions at 773 K on Co/MFI zeolite as the catalyst. The activity was created by loading of Co on MFI, and the maximum activity was observed with appropriate Co/Al molar ratio 0.6. High concentration of Al, when Co/Al ratio was fixed at 0.6, resulted in the high activity. The isotope and MS experiments evidenced the reaction formula. The ammonia IRMS-TPD indicated that the loaded Co species were Lewis acidic and mainly held by the ion exchange sites of MFI zeolite. The TEM and EXAFS showed that Co species were mono-atomically dispersed at Co/Al < 0.6. The XANES showed the oxidation state of Co to be +II. The active site for the methylation of benzene with methane is suggested to be the Co (+II) species with Lewis acidity mono-atomically dispersed on the ion exchange site of MFI zeolite.

Acknowledgements

References

[1] R. H. Crabtree, *Stud. Surf. Sci. Catal.,* **81**, 85-92 (1994)

[2] B. A. Arndtsen, R.G. Bergman, T. A. Mobley, T.H. Peterson, *Acc. Chem. Res*., **28**, 154-162 (1995)

[3] R. G. Bergman, *Nature*, **446**, 391-393 (2007)

[4] A. I. Olivos-Suaraz, À. Szécsényi, E. J. M. Hensen, J. Ruiz-Martinez, E. A. Pidko, J. Gascon, *ACS Catal*., **6**, 2965-2981 (2016)

[5] H. Schwarz, *Angew. Chem. Int. Ed*., **50**, 10096-10115 (2011)

[6] G. Kumar, S. L. J. Lau, M.D. Krcha, M. J. Janik, *ACS Catal*., **6**, 1812-1821 (2016)

[7] K. Aasberg-Petersen, I. Dybkjaer, C. V. Ovesen, N. C. Schjodt, J. Sehested, S. G. Thomsen, *J. Nat. Gas Sci. Eng.*, **3,** 423-459 (2011)

[8] C. K. Rofer-DePoorter, *Chem. Rev*., **81**, 447-474 (1981)

[9] N. V. Beznis, B. M. Weckhuysen, J. H. Bitter, *Catal. Lett*., **136**, 52-56 (2010)

[10] C. Hammond, M. M. Forde, M. H. Ab Rahim, A. Thetford, Q. He, R. L. Jenkins, N. Dimitratos, J. A. Lopez-Sanchez, N. F. Dummer, D. M. Murphy, A. F. Carley, S. H. Taylor, D.J. Willock, E. E. Stangland, J. Kang, H. Hagen, C.J. Kiely, G.J. Hutchings, *Angew. Chem. Int. Ed*., **51**, 5129-5133 (2012)

[11] S. I. Chan, Y.-J. Lu, P. Nagababu, S. Maji, M.-C. Hung, M. M. Lee, I.-J. Hsu, P. D. Minh, J. C.-H. Lai, K. Y. Ng, S. Ramalingam, S. S.-F. Yu, M. K. Chan, *Angew. Chem. Int. Ed*., **52**, 3731-3735 (2013)

[12] E. M. C. Alayon, M. Nachtegaal, A. Bodi, J. A. V. Bokhoven, *ACS Catal*., **4**, 16-22 (2014)

[13] M. O. Adebajo, *Green Chem.*, **9**, 526-539 (2007)

[14] L. S. Wang, L. X. Tao, M. S. Xie, G. F. Xu, J. S. Huang, Y. D. Xu, *Catal. Lett.*, **21**, 35-41 (1993)

[15] S. Ma, X. Guo, L. Zhao, S. Scott, X. Bao, *J. Energy Chem.*, **22**, 1-20 (2013)

[16] B. Liu, Y. Yang, A. Sayari, *Appl. Catal. A*, **214**, 95-102 (2001)

[17] P. Tan, *J. Catal.*, **338**, 21-29 (2016)

[18] J. S. Beck, D. H. Olson, S. B. McCullen, U. S. Patent 5 367 099 (1994)

[19] D. Mitsuyoshi, K. Kuroiwa, Y. Kataoka, T. Nakagawa, M. Kosaka, K. Nakamura, S. Suganuma, Y. Araki, N. Katada, *Micro- Mesopor. Mater.*, **242**, 118-126 (2017)

[20] Y. Osada, N. Okino, S. Ogasawara, T. Fukushima, T. Shikada, T. Ikariya, *Chem. Lett.*, **19**, 281-282 (1990)

[21] T. Suzuki, K. Wada, Y. Watanabe, *Ind. Eng. Chem. Res.*, **30**, 1719-1725 (1991)

[22] H. Kim, H. M. Sub, H. Paik, *Appl. Catal. A*, **87**, 115-127 (1992)

[23] S. J. X. He, M. A. Long, M. I. Attalla, M. A. Wilson, *Energy Fuels*, **6**, 498-502 (1992)

[24] E. M. Kennedy, F. Lonyi, T. H. Ballinger, M. P. Rosynek, J. H. Lunsford, *Energy Fuels*, **8**, 846-850 (1994)

[25] T. Sano, K. Okabe, H. Hagiwara, H. Takaya, H. Shoji, K. Matsuzaki, *J. Mol. Catal.*, **40**, 113-117 (1987)

[26] S. J. X. He, M. A. Long, M. A. Wilson, M. L. Gorbaty, P.S. Maa, *Energy Fuels*, **9**, 616-619 (1995)

[27] T. Baba, H. Sawada, *Phys. Chem. Chem. Phys.*, **4**, 3919-3923 (2002)

[28] G. M. Barrow, *Physical Chemistry fifth ed.* McGraw-Hill, New York (1988)

[29] D. R. Lide in *Handbook of Chemistry and Physics seventy-third ed.* (Eds.: M. Bass, B. L. Karger, L. Brewer, W. C. Lineberger, F. J. DiSalvo, D. A. Palmer, R. J. Donnelly, D. Seyferth, H. P. R. Frederikse, J. H. Westbrook), CRC Press, Florida, pp. section5 54 (1992)

[30] D. B. Lukyanov, T. Vazhnova, *J. Mol. Catal. A*, **305**, 95-99 (2009)

[31] A. A. Gabrienko, S. S. Arzumanov, I. B. Moroz, I. P. Prosvirin, A. V. Toktarev, W. Wang, A. G. Stepanov, *J. Phys. Chem. C*, **118**, 8034-8043 (2014)

[32] M. O. Adebajo, M. A. Long, R. F. Howe, *Res. Chem. Intermed.*, **26**, 185-191 (2000)

[33] M. O. Adebajo, M. A. Long, R. L. Frost, *Catal. Commun.*, **5**, 125-131 (2004)

[34] G. I. Pannov, V. I. Sobolev, A. S. Kharitonov, *J. Mol. Catal.*, **61**, 85-97 (1990)

[35] M. H. Groothaert, P. J. Smeets, B. F. Sels, P. A. Jacobs, R. A. Schoonheydt, *J. Am. Chem. Soc.*, **127**, 1394-1395 (2005)

[36] P. Vanelderen, R. G. Hadt, P. J. Smeets, E. I. Solomon, R. A. Schoonheydt, B. F. Sels, *J. Catal.*, **284**, 157-164 (2011)

[37] S. Grundner, M. A. C. Markovits, G. Li, M. Tromp, E. A. Pidko, E. J. M. Hensen, A. Jentys, M. Sanchez-Sanchez, J. A. Lercher, *Nat. Commun.*, **6**, 7546-7546 (2015)

[38] V. L. Sushkevich, D. Palagin, M. Ranocchiari, J. A. van Bokhoven, *Science*, **356**, 523-527 (2017)

[39] K. Okumura, S. Matsumoto, N. Nishiaki, M. Niwa, *Appl. Catal. B*, **40**, 151-159 (2003)

[40] F. Lónyi, H. E. Solt, J. Valyon, A. Boix, L. B. Gutierrez, *Appl. Catal. B*, **117**, 212-223 (2012)

[41] A. Oda, H. Torigoe, A. Itadani, T. Ohkubo, T. Yumura, H. Kobayashi, Y. Kuroda, *J. Phys. Chem. C*, **117**, 19525-19534 (2013)

[42] M. Niwa, N. Katada, *Chem. Rec.*, **13**, 432-455 (2013)

[43] D. K. Murray, T. Howard, P. W. Goguern, T. R. Krawietz, J. F. Haw, *J. Am. Chem. Soc.*, **116**, 6354-6360 (1994)

[44] National Institute of Advanced Industrial Science and Technology, SDBS Web. http://sdbs.db.aist.go.jp/, 2017 (accessed 2 November 2017)

[45] M. D. Kadgaonkar, S. C. Laha, R. K. Pandey, P. Kumar, S. P. Mirajkar, R. Kumar, *Catal. Today*, **97**, 225-231 (2004)

[46] S. Suganuma, K. Nakamura, A. Okuda, N. Katada, *J. Mol. Catal.*, **435**, 110-117 (2017)

Chapter 4 Reactivity of Methane and Benzene over Metal/MFI Zeolite Analyzed with Temperature-Programmed Reaction Technique

4-1 Introduction

Methane is the largest component in natural gas, whose recovery resources is believed to be large, especially after the commercialization of shale gas mining. Development of chemical processes which can convert the methane into valued chemical products has been demanded, and most of the research targets require the development of new catalysts [1-4]. Conversion of methane into syngas has been industrially operated [5], but the large energy loss due to high reaction temperature limits the application field [6]. Partial oxidation of methane into methanol [7-10], and dehydroaromatization of methane into aromatics [11-13] have been actively studied. However, up to now, they have still unavoidable disadvantages such as low selectivity and/or poor catalyst life [6].

Baba et al. [14] and Gabrienko et al. [15] reported that indium oxide on MFI zeolite catalyzed the direct methylation of benzene with methane in non-oxidative conditions (1). We have recently found that Co supported by MFI type zeolite, hereafter Co/MFI, had distinct catalytic activity for the methylation of benzene with methane at 773 K [16].

$$CH_4 + C_6H_6 \rightarrow C_6H_5\text{-}CH_3 + H_2 \quad (1)$$

The catalytic activity for (1) was found to be negligible on various kinds of elements loaded on MFI zeolite, while only Co showed high activity [16]. It should be noteworthy that little activities were found on Ni, which generally shows chemical nature to Co, and noble metals, which are generally active for hydrogenation/dehydrogenation type reactions (Ni is also active), although the reaction (1) is one kind of dehydrogenation. In this study, we aimed to analyze the chemical reactivities of various elements loaded on MFI zeolite to find the character of Co suitable for generation of catalysis.

A side reaction, dehydrogenation of methane (2), was also found accompanying to the target reaction (1).

$$CH_4 \rightarrow C + 2H_2 \quad (2)$$

It is therefore considered that the high catalytic performance requires high selectivity and long catalyst life [durability against the coverage of active site with carbonaceous formed by (2)], as well as the high ability for activation of methane, which

has been known to be a chemically stable molecule. The activity, selectivity and life should be complicatedly dependent on the reaction temperature, although our previous study was carried out at a limited temperature, 773 K [16]. Therefore, the analysis was here carried out over a wide range of reaction temperature.

Many researchers have reported that ability for activation of methane on metal species whose structure were controlled by the ion exchange sites on zeolites. For example, it was reported that copper (+II) species on ion exchange site of MFI converted methane into methanol [17,18]. Rh_1O_5 species on MFI zeolite promoted methane partial oxidation [19]. In addition those, it has been reported that metal species on zeolite (mainly MFI) had quite unique activities for methane-related reactions, i.e., aromatization of methane [20], combustion of methane [21], selective catalytic reduction of NOx with methane [22], and methane activation at low temperature [23]. Therefore, metal species supported on zeolite (or MFI zeolite) possibly have the ability for methane activation. The behaviors of metal/MFI with regard to the activation of methane and catalytic performance in the reaction atmosphere over a wide temperature range might give us insights about what is necessary for the generation of catalytic activity for the methylation of benzene with methane.

Based on these backgrounds, in this study, we applied a temperature-

programmed reaction (hereafter TPR) method to metal/MFI catalysts. Mass spectroscopy was used for measurements of reactivity of catalytic system and investigation of oxidation state of metal species over a wide range of temperature, as provided [24-26]. Various metal/MFI catalysts were tested by TPR with a flow of methane-benzene mixture. The mass spectrometer contributed to estimate the rates of desired (1) and side (2) reactions and then the selectivity. The oxidation state speculated from TPR was, in some cases, confirmed by X-ray absorbed near edge structure (XANES). Relationship between the activity and selectivity is discussed to find out the nature of Co/MFI generating the high activity.

4-2 Experimental

4-2-1 *Catalyst preparation*

Various metal elements were impregnated from aqueous solutions of their nitrates (Cr, Mn, Fe, Co, Ni, Cu, Zn, Ga, Ag, In, and Pb), chlorides (Rh and Ru), chlorides of ammine complexes (Pd and Pt), or $(NH_4)_6Mo_7O_{24}$ on a NH_4-MFI zeolite powder (Tosoh Corp., [Al] = 1.3 mol kg^{-1}, SiO_2/Al_2O_3 molar ratio = 22.1) as described in our previous paper [16]. The zeolite powder was put into the solution and heated at 343 K with stirring at 400 rpm up to most of the solvent (water) was removed by vaporization. The yielded solid was further dried again at 383 K for 3 hours and then stored without

further calcination at higher temperatures. The prepared samples are listed in Table 4-1

with the abbreviations.

Table 4-1   List of metal/MFI samples prepared by impregnation of metal salts on MFI
zeolite with [Al] = 1.3 mol kg^{-1}.

Sample name	Precursor of metal element	[Metal] / mol kg^{-1}	Metal / Al molar ratio*
NH$_4$-MFI	-	0	0
Mg-0.6	Mg(NO$_3$)$_2$	0.78	0.6
Ca-0.6	Ca(NO$_3$)$_2$	0.78	0.6
Cr-0.4	Cr(NO$_3$)$_3$	0.52	0.4
Mn-0.4	Mn(NO$_3$)$_2$	0.78	0.6
Fe-0.4	Fe(NO$_3$)$_3$	0.52	0.4
Co-0.6	Co(NO$_3$)$_2$	0.78	0.6
Ni-0.6	Ni(NO$_3$)$_2$	0.78	0.6
Cu-0.6	Cu(NO$_3$)$_2$	0.78	0.6
Zn-0.6	Zn(NO$_3$)$_2$	0.78	0.6
Ga-0.4	Ga(NO$_3$)$_3$	0.52	0.4
Ag-1.2	AgNO$_3$	1.56	1.2
In-0.4	In(NO$_3$)$_3$	0.52	0.4
Pb-0.6	Pb(NO$_3$)$_2$	0.78	0.6
Mo-0.6	(NH$_4$)$_6$Mo$_7$O$_{24}$	0.78	0.6
Ru-0.4	RuCl$_3$	0.52	0.4
Rh-0.4	RhCl$_3$	0.52	0.4
Pd-0.6	(NH$_4$)$_2$[PdCl$_4$]	0.78	0.6
Pt-0.3	H$_2$[PtCl$_6$]	0.39	0.3

*: [Al] is here assumed to be kept at 1.3 mol kg^{-1} during the preparation procedure.

4-2-2 *X-ray absorption near edge structure (XANES)*

Oxidation states of Co-0.6, Pd-0.6, and Pt-0.3 were analyzed by X-ray absorption near edge structure (XANES) before and after the catalytic tests. The metal/zeolite sample was molded into a wafer with 10 mm of the diameter by compression. Cobalt foil, CoO, Co_3O_4, palladium foil, PdO, and Pt-foil were also measured as the references. The Co, Pd K-edge and Pt L_3-edge absorption spectra were collected in the quick mode using a Si (111) monochromator at BL01B1 with the approval of the Japan Synchrotron Radiation Research Institute (JASRI, SPring-8, Proposal number 2018B1146, 2019B1325). The beam size at the sample position was 5 mm (horizontal) × 1 mm (vertical).

4-2-3 *Temperature-programmed reaction (TPR)*

Catalytic activity and selectivity of metal/MFI over a wide range of temperature were studied with TPR in a glass fixed-bed flow reactor (i.d. = 10 mm). Metal/MFI (0.300 g) was pretreated in an oxygen (99.9% from Hinomaru Industry) flow with 1.23 mmol min^{-1} of the flow rate in atmospheric pressure at 823 K for 1 hour, and then catalyst bed was cooled to 373 K. A mixture of methane (99.9% from Iwatani), benzene (special grade from Wako), and helium (as internal standard, 99.9% from Taiyo Nippon Sanyo) with 1.14×10^3, 4.46 and 81.7 µmol min^{-1}, respectively, was fed with recording the mass

spectra continuously by using a mass spectrometer (Pfeiffer Vacuum, QMG220) connected to the outlet of reactor. After the ion currents were stabilized, the catalyst bed was heated again to 843 K at a ramp rate of 10 K min^{-1}. Benzene, toluene, and dihydrogen were quantitated from their ion currents, as well as other mass spectral signals within m/z (mass / charge ratio) = 1 to 200.

The TPR in methane without benzene was performed with a mixed flow of methane and helium with 1.14×10^3 and 87.2 µmol min^{-1}, respectively, in place of the methane-benzene-helium mixture as above.

4-2-4 *Steady state reaction*

Reactions at a fixed temperature (ordinal fixed-bed continuous flow reactions) were performed with same procedure to the TPR until the MS stabilization step. Then, temperature of the catalyst bed was elevated to 773 K at a ramp rate of 10 K min^{-1}, and then fixed at 773 K. The mass spectra were continuously recorded throughout the temperature elevation and steady temperature steps, but the results will be shown from the time when the temperature became 773 K as time on stream = 0. Benzene, toluene, and dihydrogen were quantitated from their ion currents.

4-3 Results

4-3-1 *Changes found in TPR*

Figure 4-1 shows TPR profiles, namely, the plots of ion currents against the temperature at *m/z* which will be the subjects of below discussion, on NH_4-MFI, Co-0.6, Pd-0.6 and Pt-0.3. In all the profiles, ion current at *m/z* = 4, attributed to helium, was stable during the measurements, indicating that the total gas flow was stable during the experiments, and the following changes of ion current showed the formation and consumption of gaseous compounds. The current at *m/z* = 16, attributed to the parent signal of methane, respectively, was also approximately stable during the measurements; as stated below, methane was consumed by the reactions, but the conversion was small, and therefore the decrease of methane was not apparent here. The ion current at *m/z* = 18 mainly due to water (H_2O) showed a desorption peak around 473 K on all the samples shown here, indicating that some water (mainly as an impurity in benzene difficult to completely remove) had been adsorbed on the zeolite during the MS stabilization step and desorbed in the TPR measurements.

On Co-0.6 [Figure 4-1 (b)], the ion current at *m/z* = 78, the parent signal of benzene, showed decrease of intensity at > 800 K. The formation of toluene (*m/z* = 91) was apparent at > 673 K. The parent peak with *m/z* = 92 assigned to $C_7H_8^+$ was also observed, and here the largest signal at *m/z* = 91 is shown. The signal at *m/z* = 91 is
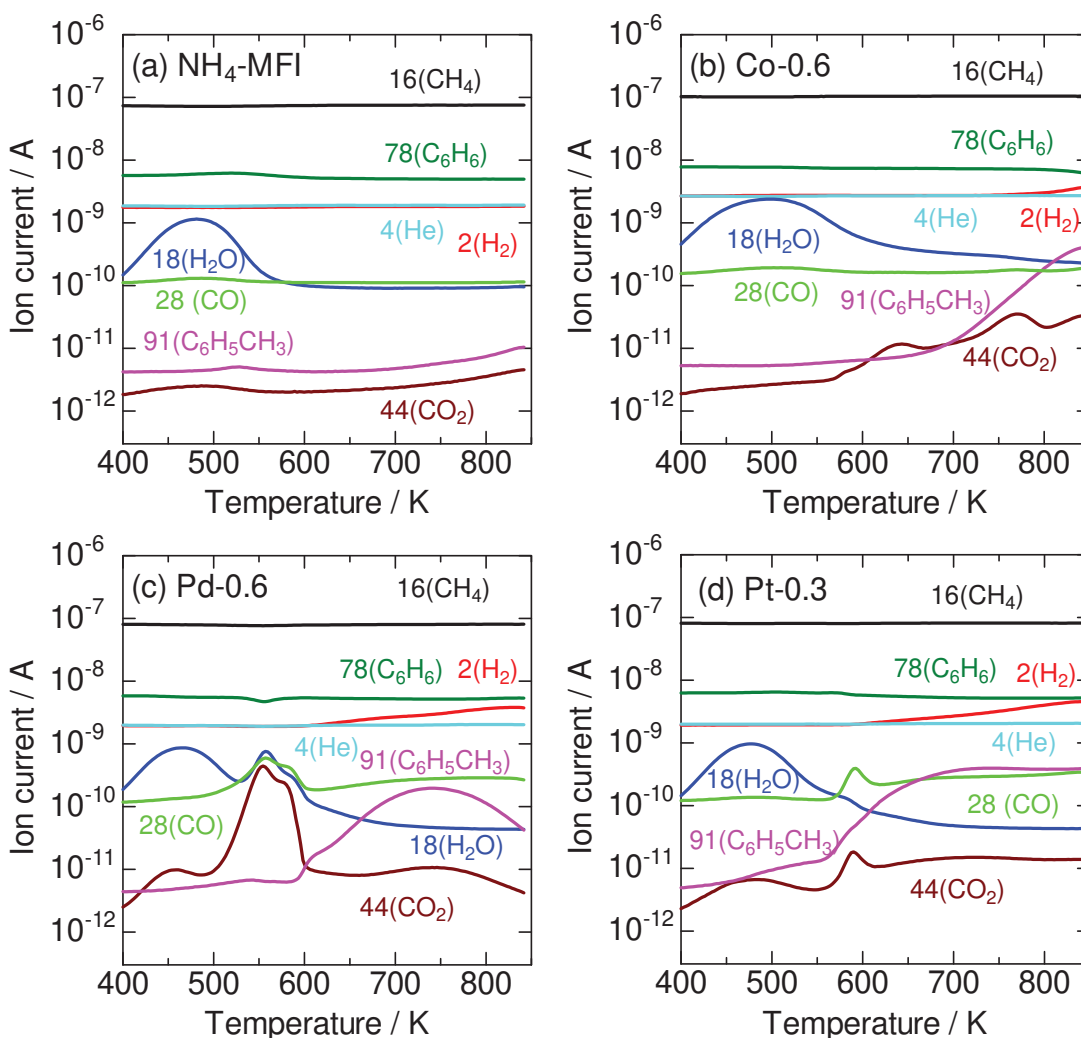
90

Figure 4-1　Profiles of TPR using methane (94 kPa)-benzene (0.37 kPa) in 373-843 K over (a) NH$_4$-MFI, (b) Co-0.6, (c) Pd-0.6, and (d) Pt-0.3.

ascribed to the fragment C$_7$H$_7^+$ formed in the mass spectrometer mainly from toluene as already detailed in our previous paper [16]. The formation of toluene and its reaction rate have been confirmed using a gas chromatograph (GC) [16]. The signal at $m/z = 91$ (C$_7$H$_7^+$) directly shows the presence of tropylium ion, which can be formed from xylene and other methyl derivatives of benzenes. In these conditions, it has been clarified and reported that toluene was mainly detected as a product by the GC with trace of xylene, in agreement

with the low intensity of signal at m/z = 106 below 1×10^{-12} A at the maximum in the

present measurements (data not shown). Thus, the formation rate of toluene will be

analyzed based on the ion current at m/z = 91 hereafter. The ion current at m/z = 2, whose

change was mainly attributed to the formation of dihydrogen (H_2), increased its intensity

> ca. 700 K, evidencing the methylation of benzene with methane into toluene and

dihydrogen (1) on Co/MFI.

On NH_4-MFI [Figure 4-1 (a), exactly H-MFI in the experimental conditions,

because it had been pretreated at a high temperature], the ion current at m/z = 91 slightly

increased its intensity from the background at > 700 K. This shows the formation of

toluene even on H-MFI, but the intensity was far smaller than that on Co/MFI. The ion

current at m/z = 44 showed the similar temperature dependence to that of toluene. These

suggest dehydrogenation of methane and hydrogenolysis of benzene [27,28], because the

hydrogenolysis of benzene produces toluene and light hydrocarbon molecules with

carbon atoms less than five. The signal at m/z = 44 is attributable to C_3H_8 here on H-MFI,

because C_3H_8 is speculated to be included in the light hydrocarbons produced by the

hydrogenolysis of benzene. We can summarize that the methylation of benzene with

methane (1) proceeded on Co/MFI, whereas a tiny amount of toluene was formed by

hydrogenoloysis of benzene on H-MFI.

On Pd-0.6 [Figure 4-1 (c)], the ion current at $m/z = 44$ showed a different thermal behavior from that of toluene, and therefore it is not attributed to the light hydrocarbons formed by the hydrogenolysis of benzene. It was presumably ascribed to CO_2, and showed a sharp peak at 580 K, indicating the reduction of Pd species into metallic species (Pd^0) by the methane (e.g., $4PdO + CH_4 \rightarrow 4Pd + CO_2 + 2H_2O$). Co/MFI (Co-0.6) also showed small peaks ascribed to the formation of CO_2 around 600 - 800 K. The reduction of Co species by methane (e.g., $3CoO + CH_4 \rightarrow 3Co + CO_2 + H_2 + H_2O$ [29,30]) is thus speculated, but as stated later, this occurred on a small fraction of Co. On Pd/MFI, at the high temperature after the reduction of Pd occurred (> 600 K), toluene was observed to increase. This indicates that toluene was formed over Pd^0 species. However, the ion current due to toluene decreased over 733 K. On the other hand, the current at $m/z = 2$ (H_2) monotonously increased over 600 K. It means that simple dehydrogenation of methane (2) proceeded continuously [31,32]. On the contrary, the high formation rate of toluene on Co/MFI was not lost at the high temperature within the experimental range.

Figure 4-1 (d) shows the TPR profile on Pt-0.3. Similarly to Pd/MFI, the Pt/MFI showed the sharp peak of CO_2 at ca. 590 K. At higher temperatures, the formation of toluene was detected, and it continued over a wide temperature range compared to Pd/MFI.

93

It is concluded that the TPR demonstrated the rates and features of reactions (1) and (2), the methylation of benzene with methane and dehydrogenation of methane, respectively, on the transition metal species on MFI, as well as the reduction behavior of the metal species over a wide range of temperature.

TPR experiments without benzene were performed in methane and helium flow to identify influence of the existence of benzene (Figure 4-2). On Co-0.6, formation of benzene, toluene, nor any aromatic compounds from methane were not observed in the experimental range of temperature. Formation of CO_2 was observed, and the ion current at $m/z = 2$ (H_2) was obviously stable, corresponding to the low dihydrogen formation rate, compared to that in the methane + benzene TPR where the formation of dihydrogen was observed at > 700 K as stated above. These indicate that existence of benzene changed
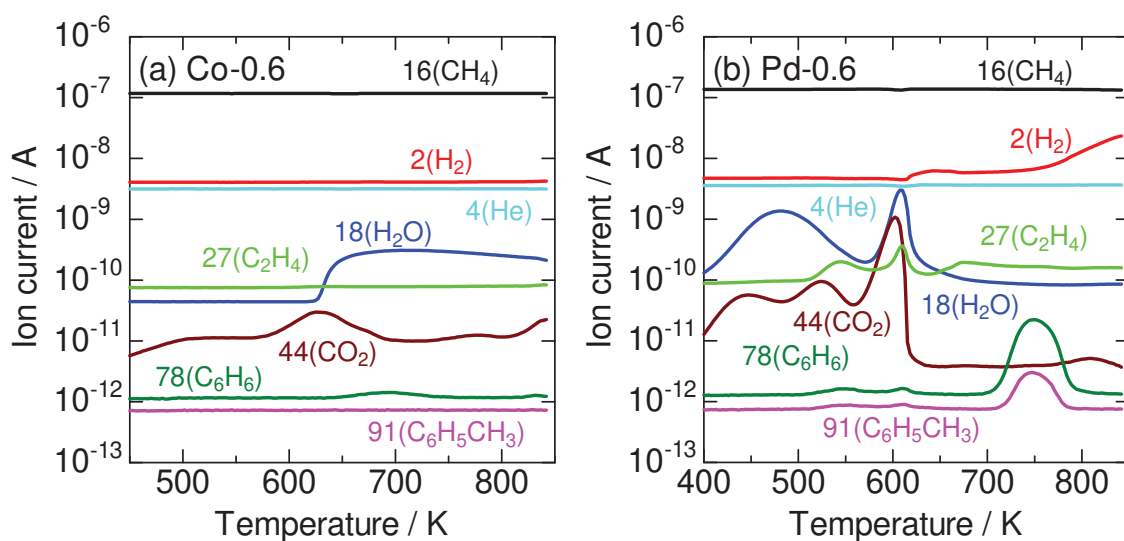
Figure 4-2   Profiles of TPR using methane (95 kPa) in 373-843 K over (a) Co-0.6 and (b) Pd-0.6.

94

the chemical reactivity of Co species with methane. On the other hand, Pd-0.6 [Figure 4-2 (b)] showed some reduction peaks similar to Figure 4-1 (c) under 600 K. In addition, benzene and toluene formation due to aromatization of methane was observed around 750 K. The ion current of dihydrogen stepwisely increased. The first step was found at 600-700 K, and the second one was observed above 700 K. On the first step, the ion current at m/z = 27 (attributable to ethene) accompanied, indicating that ethene was formed by dehydrocoupling of methane [33]. On the second step, in place of ethene, aromatic compounds were observed, and decomposition of methane into carbon and dihydrogen was predominant at the higher temperature. In the TPR with methane and benzene flow, the formation rate of toluene was much higher and that of dihydrogen was lower than those in the TPR with only methane flow. Thus, the TPR with methane and benzene on Co/MFI and Pd/MFI demonstrated the catalytic performances of these catalysts obviously different from the nature in pure methane flow.

4-3-2 *Comparison of TPR on various metals*

Figure 4-3 shows formation rates of toluene and dihydrogen calculated from the ion currents in TPR on various metal/MFI catalysts. Relatively high toluene formation rate was observed on Pt, Rh, Co, Pd, Ni, In, Fe, Mo, Cr and Mn. The activity of In and Pt

has been reported by Baba [14] and Lukyanov [34], respectively. This study indicates the remarkable high activity on Pt, Rh, Co, Pd and Ni. Sharp CO_2 formation peaks were found on some of the catalysts (Cr, Mn, Fe, Cu, In, Ru, Rh, Pd and Pt) at the temperatures shown by ● in Figure 4-3, indicating the reduction of these elements at the shown temperatures. The solid lines show the reaction rates in the oxidized state, whereas the broken lines show the rates in the reduced state. Figure 4-3 (a) and (c) show the total drawings, whereas
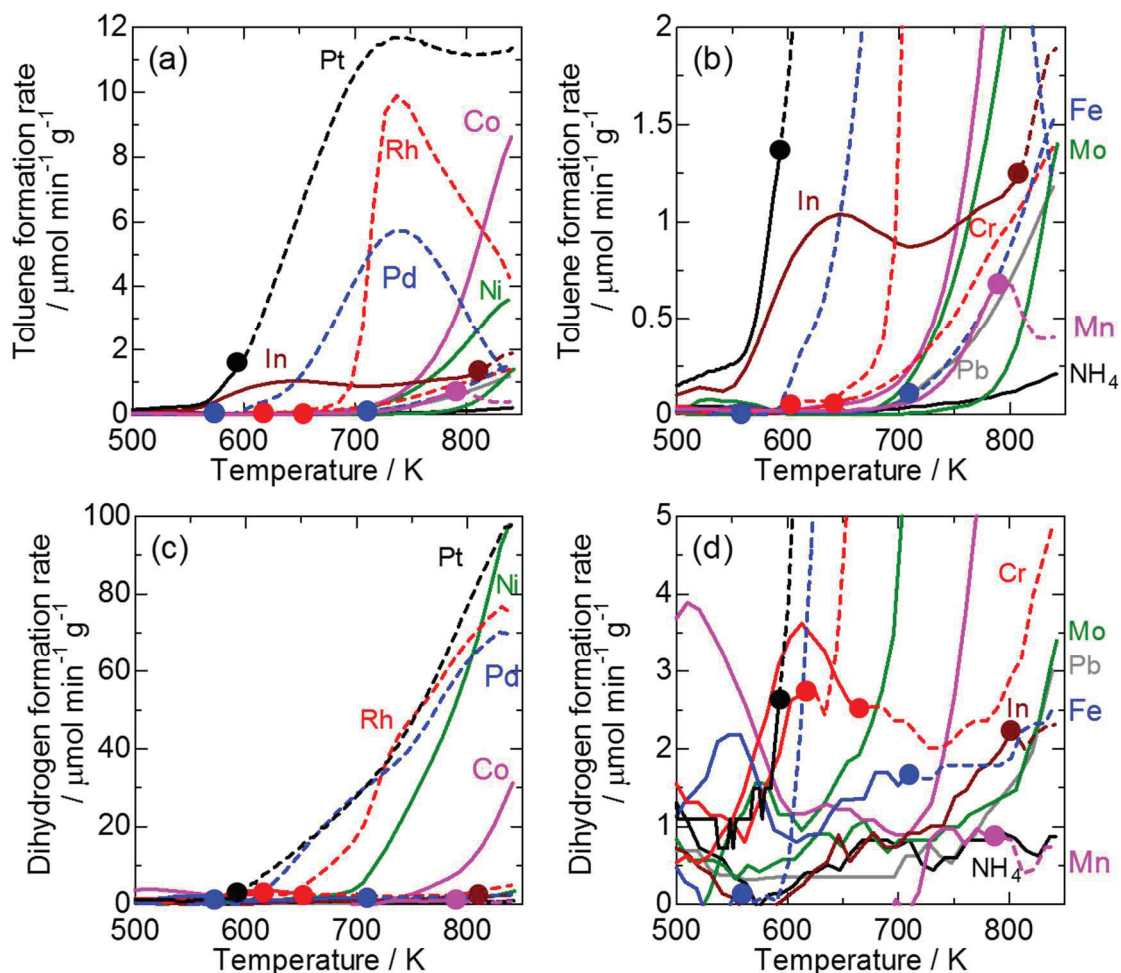
Figure 4-3   Formation rates of [(a) and (b)] toluene and [(c) and (d)] dihydrogen in TPR using methane (94 kPa)-benzene (0.37 kPa) over NH_4-MFI, and oxidized (solid line) or reduced (broken line) metal/MFI.

(b) and (d) show the enlarged portions of low reaction rate. The toluene formation rates on NH_4, Mg, Ca, Cu, Ga, Ag, and Ru/MFI were negligible, less than 0.5 μmol g^{-1} min^{-1} even at the maximum, and therefore the drawings are omitted in Figure 4-3 except for NH_4-MFI.

As shown in Figure 4-3 (a), Co and Ni/MFI, which had little been reduced in the TPR experiments, showed monotonous increase of the toluene formation rate with elevation of the temperature. In contrast, most of the elements which were reduced during the TPR experiments (Pt, Rh, Pd, In, and Mn) showed non-monotonous change of the toluene formation rate against the temperature. Pt/MFI in the reduced state showed high activity for the reaction, and showed the maximum at 734 K. Other noble metals, Pd and Rh in the reduced states, were also relatively active for this reaction, and showed the maximum rate at around 740 K. In/MFI showed unique behavior. Toluene formation started from 550 K in the oxidation state. After In species was reduced at ca. 800 K, the activity started to increase again. The observation tells us that the oxidation state and reduced state of an element have different behaviors in the reaction of methane and benzene.

On the other hand, behaviors of the dihydrogen formation rates increased monotonously against the temperature on most of the employed catalysts [Figure 4-3 (c),

(d)].

The temperature where reduction observed, and the formation rates of toluene and dihydrogen and the standard reduction potentials in aqueous solutions [35] are summarized in Table 4-2.

The selectivity of methylation of benzene with methane was calculated by the following equation.

$$S_{\mathrm{Methyl}}\ (\%)= \frac{r_{\mathrm{Toluene}}}{r_{\mathrm{Toluene}}+\dfrac{r_{\mathrm{Dihydrogen}}-r_{\mathrm{Toluene}}}{2}} \times 100 \quad \cdot\ \cdot\ \cdot\ (3)$$

where, S_{Methyl}, r_{Toluene}, $r_{\mathrm{Dihydrogen}}$ are methylation selectivity, toluene formation rate, and dihydrogen formation rate, respectively. Here it is assumed that only the reactions (1) and (2) occurred. Figure 4-5 (a) shows relationship between temperature and methylation selectivity in the region with the total reaction rate ($r_{\mathrm{Toluene}}+$ $\dfrac{r_{\mathrm{Dihydrogen}}-r_{\mathrm{Toluene}}}{2}$) > 1.0 µmol g^{-1} min^{-1}; the selectivity calculated in low reaction rate region is disturbed by large experimental errors due to small values.

Mn, In, Fe, Mo, and Pb showed relatively high selectivity but with low toluene formation rate. Among the remarkably active catalysts (Pt, Co, Rh, Pd and Ni), high selectivity was found only on Pt and Co. The Co/MFI showed relatively high selectivity

98

Table 4-2   Reduction behavior and reaction rates observed in methane + benzene TPR over metal/MFI.

Sample name	Temperature of reduction	E° [a]	Maximum of $r_{Toluene}$	Temperature where maximum $r_{Toluene}$ was recorded	Maximum of $r_{Dihydrogen}$	Temperature where maximum $r_{Dihydrogen}$ was recorded
	K	V	$\mu mol\ g_{cat}^{-1}\ min^{-1}$	K	$\mu mol\ g_{cat}^{-1}\ min^{-1}$	K
NH$_4$-MFI	-	-	0.21	843	1.41	478
Mg-0.6	-	-2.37[b]	0.20	805	1.35	695
Ca-0.6	-	-2.86[b]	0.22	826	1.77	743
Cr-0.4	610	-0.74[c]	1.40	843	5.06	843
Mn-0.4	779	-1.18[b]	0.72	791	0.97	814
Fe-0.4	707	-0.03[c]	1.55	843	2.67	843
Co-0.6	-	-0.28[b]	8.70	843	31.81	843
Ni-0.6	-	-0.25[b]	3.65	843	98.63	843
Cu-0.6	662	0.34[b]	0.43	843	8.64	843
Zn-0.6	-	-0.76[b]	0.49	843	3.60	843
Ga-0.4	-	-0.54[c]	0.34	843	7.12	843
Ag-1.2	-	0.79[d]	0.06	636	1.45	811
In-0.4	797	-0.33[c]	1.89	843	2.31	843
Pb-0.6	-	-0.12[b]	1.20	843	2.97	843
Mo-0.6	-	-	1.40	843	3.40	843
Ru-0.4	596	0.45[b]	0.03	843	5.86	835
Rh-0.4	592	0.75[c]	9.93	735	77.55	834
Pd-0.6	578	0.95[b]	5.77	738	70.92	831
Pt-0.3	592	1.18[b]	11.68	734	98.58	843

[a] Standard reduction potential in solution at 298 K and 101 kPa from ref. [35].

[b] Value in a reaction of $M^{2+} + 2e^- \rightarrow M^0$.

[c] Value in a reaction of $M^{3+} + 3e^- \rightarrow M^0$.

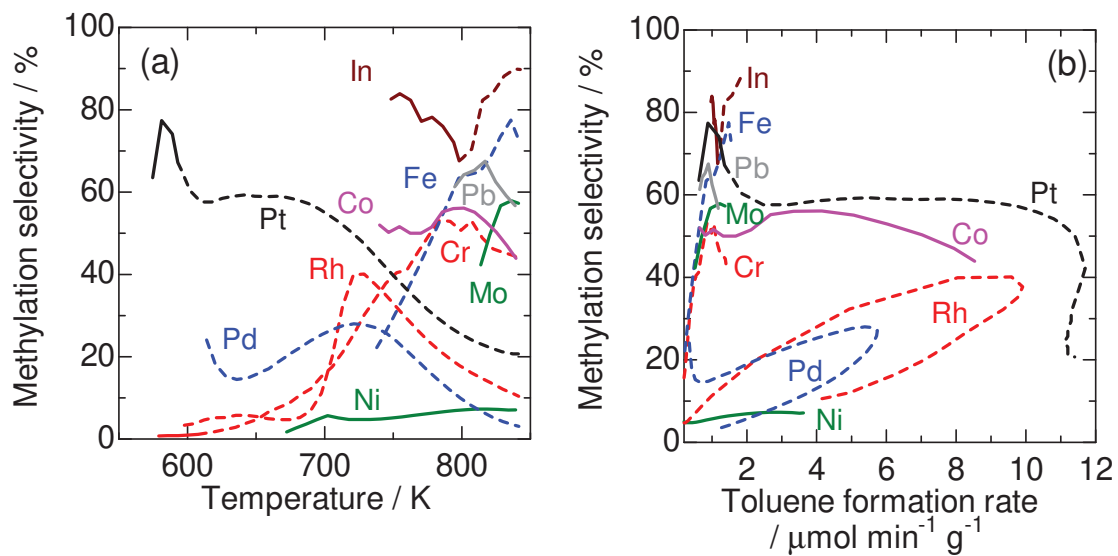[d] Value in a reaction of $Ag^+ + e^- \rightarrow Ag^0$.

Figure 4-4   Methylation selectivity plotted against (a) temperature and (b) toluene formation rate in TPR using methane (94 kPa)-benzene (0.37 kPa) 373-843 K over oxidized (solid line) or reduced (broken line) metal/MFI.

(ca. 50 %) over a wide temperature range, i.e., over a wide reaction rate range, whereas

the selectivity on Pt/MFI dropped above 700 K, i.e., at very high reaction rate.

4-3-3 *Steady temperature reaction*

Figure 4-5 shows the time course of catalytic activity in the continuous flow reaction at a fixed temperature. The toluene formation rate on Pt/MFI was high at the initial stage of time on stream, but soon decreased down, while Co/MFI showed stable activity at 773 K.
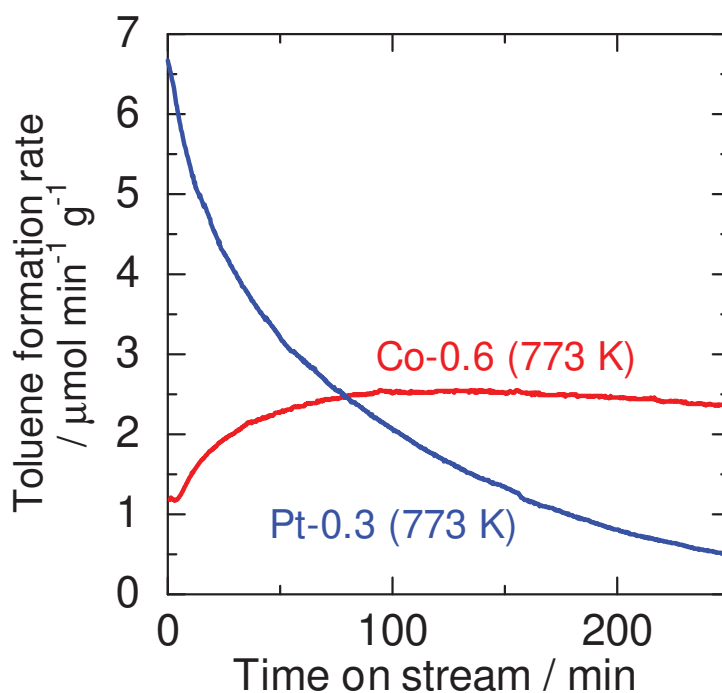
Figure 4-5   Toluene formation rate in methane (94.3kPa) + benzene (0.37 kPa) continuous flow reaction over Co-0.6 and Pt-0.3 at 773 K with time on stream.

4-3-4 *XANES*

Figure 4-6 shows X-ray absorption near edge structure (XANES) of Co, Pd and Pt k-edge on Co, Pd and Pt/MFI, measured before and after the TPR up to 843 K.

In Figure 4-6 (a), the position of Co k-edge on Co/MFI sample was same to that on CoO, regardless to before or after the reaction. It demonstrates that oxidation state of Co on MFI before the reaction was +II, and it was principally maintained during the reaction; we speculate tentative valence change of active Co species in the catalytic cycle for this dehydrogenation type reaction, but apart from it, most of the Co species had oxidation state +II stably in the reaction conditions. On the other hand, the CO_2 formation on Co0.6 in the TPR experiment was observed, but the intensity was small as stated above. The quantity of reduced Co is believed to be small, based on the XANES.

As shown in Figure 4-6 (b), the position of Pd k-edge of the Pd/MFI before the reaction was same to that of PdO. After the reaction, the position and shape of the catalyst changed to those of Pd-foil. This indicates that the Pd species on MFI was reduced from +II to 0 during the reaction. It is also consistent with the observation from TPR shown in Figure 4-1 (c). XANES of Pt/MFI shows that Pt species was completely reduced into metal species after the TPR [Figure 4-6 (c)].

Thus, XANES showed the stable oxidation state of Co held by MFI zeolite and

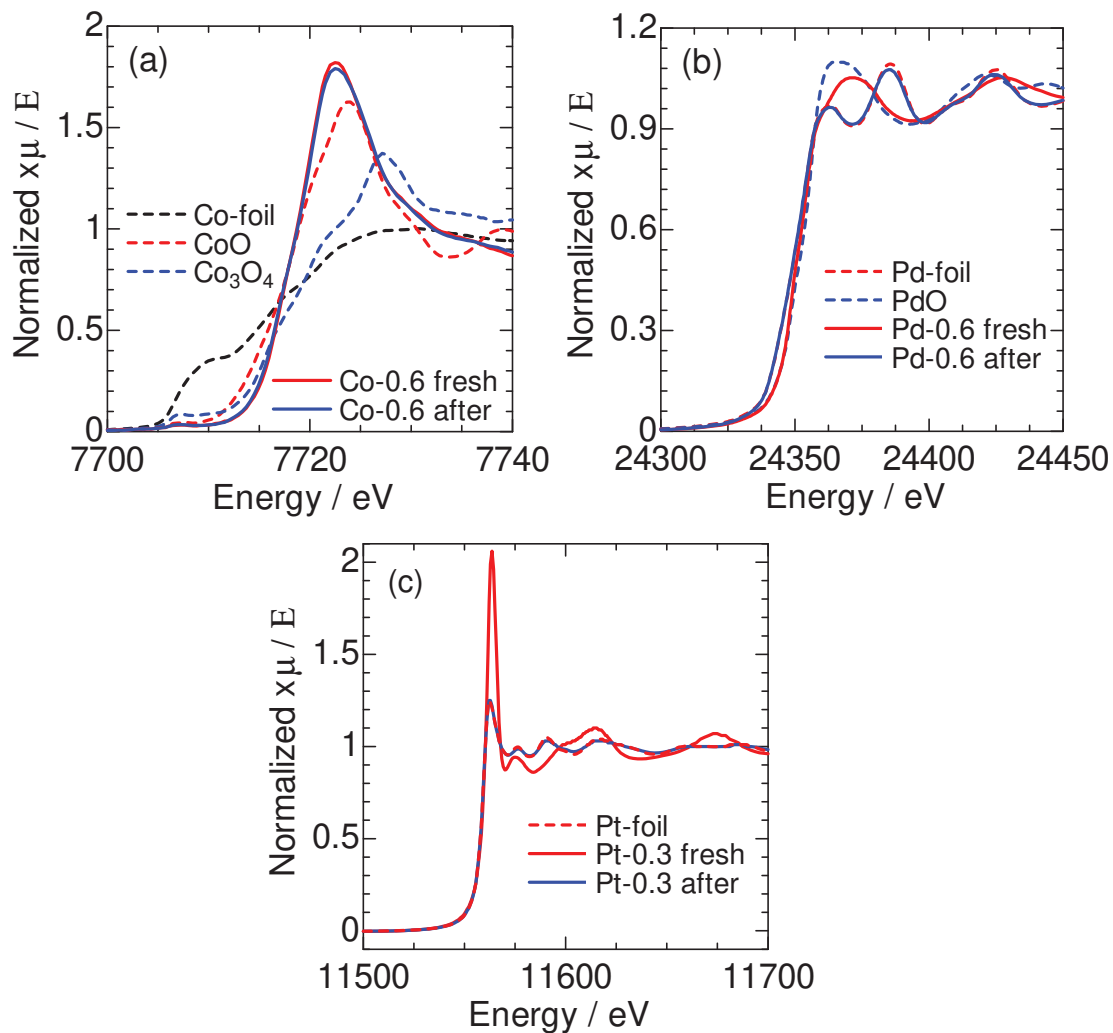the reduction of Pd and Pt in the reaction conditions, supported by the TPR behavior.

Figure 4-6   X-ray absorbed near edge structure (XANES) of (a) Co-0.6, (b) Pd-0.6, and (c) Pt-0.3 with Co-foil, CoO, Co₃O₄, Pd-foil, PdO, and Pt-foil as references.

4-4 Discussion

Reduction behavior

The large peak of CO_2 found on Pd/MFI during the TPR with benzene and methane indicates the easiness of reduction of Pd species, as supported by XANES. In contrast, Co/MFI showed the stable oxidation state (+II) during the reaction conditions as evidenced by XANES. However, the TPR of Co/MFI showed the small peak of CO_2 formation. We have clarified that most of Co(+II) species were located on the ion exchange sites of MFI on this sample (Co-0.6) [16], but from the Co/Al molar ratio 0.6, it is speculated that a fraction of Co was not on the ion exchange site. It has been known that quite high temperature over 1173 K was required for reducing Co cation on the ion exchange site of zeolite by H_2 [36]. It is therefore speculated that the Co species on the ion exchange site was not reduced during the TPR experiments, whereas small amount of Co not held by the ion exchange site was reduced in the experiment. We have reported that the activity for methylation of benzene with methane (1) was mainly generated on the Co species held by the ion exchange site [16]. Therefore, it is considered that the oxidized Co species mainly played a role of active species for the reaction (1).

From the catalytic and reduction behaviors, the employed metal/MFI catalysts were classified into some groups; (i) inactive for methylation of benzene with methane

(NH₄-MFI, Mg, Ca, Cu, Zn, Ga, Ag, and Ru); (ii) active and reduced (Cr, Mn, Fe, and In); (iii) active and kept oxidized (Pb and Mo); (iv) highly active and reduced (Ru, Rh, and Pt); (v) highly active and kept oxidized (Co and Ni).

As shown by non-monotonous dependence of toluene formation rate on the temperature, typically found on In/MFI, the oxidized state and the reduced state of an element showed different catalytic behaviors for the reaction of methane and benzene.

Formation of toluene nor dihydrogen was never found on typical element-promoted MFI (NH₄-MFI, Mg, Ca, Zn, and Ga). The transition metals classified into base metals, Fe, Mo, Cr, Mn, In and Pb, showed relatively low activities for toluene formation, whereas noble metals, i.e., Pt, Rh and Pd showed obviously high activity. Some transition base metals, i.e., Co and Ni, exceptionally showed high activity. The noble metals have been known to possess hydrogenation / dehydrogenation activity, as well as Co and Ni among base metals [37,38]. Dehydrogenation from methane involving the C-H bond cleavage, and the hydrogenation / dehydrogenation ability presumably contributed to generate the ability of formation of intermediate necessary for the methylation of benzene through the cleavage of stable C-H bond in methane.

On all the employed catalysts, the methylation selectivity was low at the start of TPR, i.e., low reaction temperature. The elevation of temperature increased the toluene

105

formation rate and selectivity in the low temperature range (< 650 K) on all the catalysts

which were found to have the activities for the methylation of benzene. On Co, Ni, Cr,

and Fe/MFI, the toluene formation rate continued to monotonously increase up to the

highest temperature in the experimental range, and therefore, the selectivity also showed

approximately monotonous increase against the temperature.

The selectivity was obviously dropped at high temperature on Pt, Rh, Pd, In, and

Mn/MFI, because the toluene formation rate decreased through the maximum, but the

dihydrogen formation rate continued to increase with elevating the temperature. As shown

in the previous section, most of the members of (ii) active and reduced, and all of (iv)

highly active and reduced groups showed this behavior, indicating that the reduction of

element suppressed the selectivity; only Cr and Fe in (ii) showed approximately

monotonous increase of selectivity. All of (iii) active and kept oxidized (Pb and Mo) and

(v) highly active and kept oxidized (Co and Ni) showed monotonous increase of

selectivity against the temperature. The tendency of each group was reasonably explained

according to the standard reduction potential ($E°$, Table 4-2). The species belonging to

the group (iv), Rh, Pd, and Pt, have positive standard reduction potentials, meaning highly

reducible property. The metals in group (ii) were also reducible, although the potentials

were negative. Most members in this group are trivalent, and the loading of metal cation

106

on an ion exchange site of zeolite proceeds preferentially with mono- or divalent cations. The present observation suggests that the cations belonging to the group (ii) were not stabilized by the ion exchange sites. On the other hand, all the metals belonging to (iii) and (v), active and oxidized, have negative $E°$, corresponding to the stability on oxidized states even in a methane flow at high temperature.

It is believed that noble metals, Pt, Pd and Rh, were substantially active for this reaction, and showed high reaction rates at relatively low temperatures. The high activity is consistent with their high activities for dehydrogenation of hydrocarbons [39,]. However, due to the low selectivity of reduced metals as above, the selectivity decreased at too high temperature, and the highest reaction rate was limited.

Thus, a general trend was observed. The elements with high hydrogenation/ dehydrogenation reactivity had activity for the methylation of benzene with methane. The elements with stable oxidized states showed the monotonous increase of the rates of reaction (1) against the reaction temperature, whereas the elements which were reduced in the reaction conditions showed the significant decrease of selectivity at high temperature and the non-monotonous change (in many cases, volcano-shape) of rate against the temperature.

As a result, among the highly active catalysts, high selectivity at high

107

temperature was found on only the element never reduced up to the high temperature, i.e., Co.

Noble metals such as Pt, Rd and Pd showed lower selectivity than others at around 800 K. However, this does not tell us simply that the catalytic performance of noble metals was low. From a practical view, high selectivity at a fixed reaction rate regardless of the reaction temperature should be compared, in order to evaluate potential of the catalysts. For this purpose, plots of selectivity against the rate of desired reaction (1) are shown in Figure 4-4 (b). Compatibility of high reaction rate and high selectivity shows the high catalytic performance regardless of the reaction temperature, and therefore a plot close to the right hand- and upper-corner in Figure 4-4 (b) shows the high performance. High reaction rate was obtained only on Pt, Co, Rh, Pd, and Ni/MFI. Among them, high selectivity was observed only on Pt and Co/MFI. The high selectivities on Pt and Co were observed at ca. 600 and 750 K, respectively. Use of Pt at low reaction temperature and use of Co at high temperature are promising to achieve the high reaction rate and selectivity.

In the continuous flow reaction at a stable temperature, the toluene formation rate on Pt/MFI was high at the initial stage of time on stream, but soon decreased down, while Co/MFI showed stable activity at 773 K. XANES and TPR showed that Pt species

was reduced in the reaction conditions. The nature of Pt contributed to the high reaction rate at the initial stage of time on stream, but the side reaction (2), which should be unavoidable in the reduced state, formed carbonaceous to gradually block the active sites. The noble metals thus showed relatively high reaction rate at low temperature due to their high dehydrogenation activity, but easiness of reduction caused low selectivity and/or catalyst degradation at high temperature. On the contrary, it is shown that Co/MFI had suitable balance between stability of oxidized state and activity for dehydrogenation to show the high activity, selectivity and long catalyst life.

As stated above, the selectivity monotonously increased with elevating the temperature in the low temperature range (< 650 K) on all the catalysts with the activities for the methylation of benzene. It tells us that the methylation of benzene has higher activation energy than that of the side reaction, the simple dehydrogenation of methane, on all the employed metal/MFI. The drop of selectivity at high temperature on the reduced metals (typically found on Pt) may have a different origin. From the deactivation behavior observed in the fixed-temperature experiment, the high reaction rate for the simple dehydrogenation of methane on the reduced metal at the high temperature caused the serious deactivation due to the formed carbonaceous.

4-5 Conclusions

Behaviors of reaction of methane and benzene over metal/MFI catalysts were investigated by temperature programmed reaction technique in 373-843 K. Oxidation state, easiness of reduction and their effects on catalytic nature of metal species were also analyzed, with an aid of XANES. Oxidized Co (+II) species located on ion exchange site of MFI was kept even in reductive conditions of methane flow at 843 K, and it was key point for catalyzing benzene methylation with methane. Ni and noble metals such as Pd, Rh and Pt supported on MFI showed high activity for the methane dehydrogenation as a side reactions, as well as the methylation, resulting in low reaction selectivity at high temperature.

Acknowledgements

References

[1] R. H. Crabtree, *Stud. Surf. Sci. Catal.*, **81**, 85-92 (1994)

[2] B. A. Arndtsen, R.G. Bergman, T.A. Mobley, T.H. Peterson, *Acc. Chem. Res.*, **28**, 154-162 (1995)

[3] R. G. Bergman, *Nature*, **446**, 391-393 (2007)

[4] A. I. Olivos-Suaraz, À. Szécsényi, E. J. M. Hensen, J. Ruiz-Martinez, E. A. Pidko, J. Gascon, *ACS Catal.*, **6**, 2965-2981 (2016)

[5] K. Aasberg-Petersen, I. Dybkjaer, C. V. Ovesen, N. C. Schjodt, J. Sehested, S. G. Thomsen, *J. Nat. Gas Sci. Eng.*, **3**, 423-459 (2011)

[6] C. K. Rofer-DePoorter, *Chem. Rev.*, **81**, 447-474 (1981)

[7] N. V. Beznis, B. M. Weckhuysen, J. H. Bitter, *Catal. Lett.*, **136**, 52-56 (2010)

[8] C. Hammond, M. M. Forde, M. H. Ab Rahim, A. Thetford, Q. He, R. L. Jenkins, N. Dimitratos, J. A. Lopez-Sanchez, N. F. Dummer, D. M. Murphy, A. F. Carley, S. H. Taylor, D. J. Willock, E. E. Stangland, J. Kang, H. Hagen, C. J. Kiely, G. J. Hutchings, *Angew. Chem. Int. Ed.*, **51**, 5129-5133 (2012)

[9] S. I. Chan, Y.-J. Lu, P. Nagababu, S. Maji, M.-C. Hung, M. M. Lee, I.-J. Hsu, P. D. Minh, J. C.-H. Lai, K. Y. Ng, S. Ramalingam, S. S.-F. Yu, M. K. Chan, *Angew. Chem. Int. Ed.*, **52**, 3731-3735 (2013)

[10] E. M. C. Alayon, M. Nachtegaal, A. Bodi, J. A. V. Bokhoven, *ACS Catal.*, **4**, 16-22 (2014)

[11] L. S. Wang, L. X. Tao, M. S. Xie, G. F. Xu, J. S. Huang, Y. D. Xu, *Catal. Lett.*, **21**, 35-41 (1993)

[12] S. Ma, X. Guo, L. Zhao, S. Scott, X. Bao, *J. Energy Chem.*, **22**, 1-20 (2013)

[13] B. Liu, Y. Yang, A. Sayari, *Appl. Catal. A*, **214**, 95-102 (2001)

[14] T. Baba, Y. Abe, K. Nomoto, K. Inazu, T. Echizen, A. Ishikawa, K. Murai, *J. Phys. Chem. B*, **109**, 4263-4268 (2005)

[15] A. A. Gabrienko, S. S. Arzumanov, I. B. Moroz, I. P. Prosvirin, A. V. Toktarev, W. Wang, A. G. Stepanov, *J. Phys. Chem. C*, **118**, 8034-8043 (2014)

[16] K. Nakamura, A. Okuda, K. Ohta, H. Matsubara, K. Okumura, K. Yamamoto, R. Itagaki, S. Suganuma, E. Tsuji, N. Katada, *ChemCatChem*, **10**, 3806-3812 (2018)

[17] M. H. Groothaert, P. J. Smeets, B. F. Sels, P. A. Jacobs, R. A. Schoonheydt, *J. Am. Chem. Soc.*, **127**, 1394-1395 (2005)

[18] P. J. Smeets, R. G. Hadt, J. S. Woertink, P. Vanelderen, R. A. Schoonheydt, B. F. Sels, E. I. Solomon, *J. Am.Chem. Soc.*, **132**, 14736-14738 (2010)

[19] Y. Tang, Y. Li, V. Fung, D. Jiang, W. Huang, S. Zhang, Y. Iwasawa, T. Sakata, L. Nguyen, X. Zhang, A. I. Frenkel, F. Tao, *Nature Commun.*, **9**, 1231-1241 (2018)

[20] L. S. Wang, L. X. Tao, M. S. Xie, G. F. Xu, J. S. Huang, Y. D. Xu, *Catal. Lett.*, **21**, 35-41 (1993)

[21] K. Okumura, S. Matsumoto, N. Nishiaki, M. Niwa, *Appl. Catal. B*, **40**, 151-159 (2003)

[22] F. Ljnyi, H. E. Solt, J. Valyon, A. Boix, L. B. Gutierrez, *Appl. Catal. B*, **117**, 212-223 (2012)

[23] A. Oda, H. Torigoe, A. Itadani, T. Ohkubo, T. Yumura, H. Kobayashi, Y. Kuroda, *J. Phys. Chem. C*, **117**, 19525-19534 (2013)

[24 E. M. Stuve, R. J. Madix, *J. Phys. Chem.*, **89**, 105-112 (1985)

[25] M. W. Balakos, S. S. C. Chuang, *J. Catal.*, **138**, 733-745 (1992)

[26] H. E. Curry-hyde, H. Musch, A. Baiker, M. Schraml-Marth, A. Wokaun, *J. Catal.*, **133**, 397-414 (1992)

[27] T. Sano, K. Okabe, H. Hagiwara, H. Takaya, *J. Mol. Catal.*, **40**, 113-117 (1987)

[28] E. M. Kennedy, F. Lonyi, T. H. Ballinger, M. P. Rosynek, J. H. Lunsford, *Energy & Fuels,* **8**, 846-850 (1994)

[29] L. Zardin, O. W. Perez-Lopez, *Int. J. Hydrogen Energy,* **42**, 7895-7907 (2017)

[30] J. Jansson, A. E. C. Palmqvist, E. Fridell, M. Skoglundh, L. Österlund, P. Thormählen, V. Langer, *J Catal.*, **211**, 387-397 (2002)

[31] J. Majewska, B. Michalkiewicz, *New Carbon Mater.*, **29**(2), 102-108 (2014)

[32] C. Anjaneyulu, G. Naresh, V. V. Kumar, A. H. Padmasri, J. Tardio, S. K. Bhargava, A. Venugopal, *RSC Adv.*, **6**, 34600-34607 (2016)

[33] L. Guczi, K.V. Sarma, L. Borkó, *Catal. Lett.*, **39**, 43-47 (1996)

[34] D. B. Lukyanov, T. Vazhnova, *J. Mol. Catal. A: Chem.*, **305**, 95-99 (2009)

[35] W. M. Haynes in *Handbook of Chemistry and Physics ninety-fourth ed.* (Eds.: D. R. Lide, T. J. Bruno), CRC Press, Florida, pp. section5 80-84 (2013)

[36] A. Bellmann, H. Atia, U. Bentrup, A. Brückner, *Appl. Catal. B: Environ.*, **230**, 184-193 (2018)

[37] Y. Zhang, G. Bai, X. Yan, Y. Li, T. Zeng, J. Wang, H. Wang, J. Xing, D. Luan, X. Tang, L. Chen, *Catal. Commun.*, **8**, 1102-1106 (2007)

[38] G. Liang, L. He, H. Cheng, W. Li, X. Li, C. Zhang, Y. Yu, F. Zhao, *J. Catal.*, **309**, 468-476 (2014)

[39] B. W., Wolfgang, M. H. Sachtler, *Appl. Catal. A: Gen.*, **229**, 11-22 (2002)

[40] U. Obenaus, F. Neher, M. Scheibe, M. Dyballa, S. Lang, M. Hunger, *J. Phys. Chem. C*, **120**, 2284-2291 (2016)

Chapter 5 Enhancement of Methylation Selectivity of Benzene Methylation with Methane over Designed Co/MFI catalyst

5-1 Introduction

Development of processes which can convert methane into chemical products has been strongly demanded for utilizing methane as substitute of petroleum in chemical resources [1,2]. Direct partial oxidation of methane into methanol [3,4] and aromatization of methane into aromatics such as BTX [5,6] have been studied. However, big problems such as low selectivity of the target reaction and/or energy loss have made the challenges difficult.

We have recently suggested direct methylation of benzene with methane as a desirable reaction. In our previous study, cobalt supported on MFI-type zeolite (Co/MFI) was distinctly active for benzene methylation with methane [reaction (1)] in various metal/MFI catalysts [7,8].

$$CH_4 + C_6H_6 \ \rightarrow \ C_6H_5\text{-}CH_3 + H_2 \qquad\qquad (1)$$
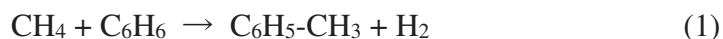
However, on Co/MFI, methane dehydrogenation [reaction (2)] accompanied as a side

reaction, as well as the methylation.

$$CH_4 \rightarrow C + 2H_2 \qquad\qquad (2)$$

In addition to that, toluene formation rate has been still low with c.a. 2.0 µmol g^{-1} min^{-1} at 773 K. To accelerate toluene formation rate, elevation of reaction temperature was tried. Unfortunately, reaction rate of hydrogenation (2) became much higher than methylation (1) in high temperature over 800 K. Therefore, it is needed that accurate active species of Co/MFI for the target and side reactions were clarified.

From characterization of Co/MFI with X-ray absorbed spectroscopy (XAS) and ammonia infrared mass spectrometer / temperature programmed desorption (NH$_3$-IRMS-TPD), it was cleared that the active species of Co/MFI was Co(+II) species on mono-atomically dispersed on ion exchange site of MFI (Chapter 3,[7]). In addition to that, results of methane + benzene TPR experiments over metal/MFI showed that balance between Lewis acidity and ability of dehydrogenation was important for the target reaction (Chapter 4). However, the active species for dehydrogenation of methane was not clarified.

Based on these backgrounds, methane + benzene TPR experiments over various

Co/MFI with different [Co] and [Al] were performed to identify active species of methane

dehydrogenation and get a hint for improving the Co/MFI catalyst. In this study, we

reported that Co/MFI with low [Al] prepared by impregnation method showed high

selectivity and long catalytic life in high temperature where the toluene formation rate

was over 2.0 μmol g^{-1} min^{-1}.

5-2 Experimental

5-2-1 *Catalyst preparation*

Samples of Na-MFI zeolite with $SiO_2/Al_2O_3 = 22.1$ (supplied by Tosoh), 30, 48

(Mizusawa), 61 (Zeolyst), and 90 (Craliant) were ion-exchanged into NH$_4$-form. Co

species was impregnated from aqueous solutions of Co nitrate [Co(NH$_3$)$_2$] on NH$_4$-MFI.

Most of the solvent was removed by drying at 343 K with stirring at 400 rpm. The yielded

solid was dried again at 383 K overnight in an oven and then stored without further

calcination at higher temperatures. Ion exchange method was also performed for the

catalyst preparation as follows: NH$_4$-MFI with $SiO_2/Al_2O_3 = 22.1$ was put into an aqueous

Co(NO$_3$)$_2$ solution with desired Co content, and the solution was stirred and heated at 343

K for 4 h. The solid was then filtrated, washed 3 times and dried at 383 K. The Co and Al

contents on the ion-exchanged samples were measured by means of inductively coupled

plasma emission spectroscopy (ICP-AES, Rigaku ICP CIROS). The prepared samples are

listed in Table 5-1 with their abbreviations.

Table 5-1   Prepared samples.

Abbreviation	Preparation method	[Al] / mol kg^{-1}	[Co] / mol kg^{-1}	SiO$_2$/Al$_2$O$_3$ in support	Co/Al in solution	Co/Al in solid
22-IE-Co-0.39	Ion exchange	1.35	0.53	22.1	2.0	0.39*
22-IE-Co-0.41	Ion exchange	1.35	0.55	22.1	10.0	0.41*
22-IMP-Co-0.6	Impregnation	1.35	0.81	22.1	0.6	0.6**
22-IMP-Co-1.8	Impregnation	1.35	2.43	22.1	1.8	1.8**
30-IMP-Co-0.6	Impregnation	1.02	0.61	30	0.6	0.6**
48-IE-Co-0.15	Ion exchange	0.66	0.10	48	10.0	0.15*
48-IMP-Co-0.6	Impregnation	0.66	0.39	48	0.6	0.6**
52-IMP-Co-0.6	Impregnation	0.61	0.37	52	0.6	0.6**
61-IMP-Co-0.6	Impregnation	0.52	0.31	61	0.6	0.6**
90-IMP-Co-0.6	Impregnation	0.36	0.22	90	0.6	0.6**

*: Measured by inductively coupled plasma emission spectroscopy (ICP-AES).

**: Based on the amounts of Co in the impregnated solution and Al in the used zeolite.

5-2-2 *Temperature-programmed reaction (TPR)*

Catalytic activity and selectivity of metal/MFI over a wide range of temperature were studied with temperature-programmed reaction (TPR) in a fixed-bed flow reactor (i.d. = 10 mm). Metal/MFI (0.300 g) was pretreated in oxygen (99.9% from Hinomaru Industry) flow with 1.23 mmol min^{-1} of the flow rate in atmospheric pressure at 823 K for 1 hour, then catalyst bed was cooled to 373 K. A mixture of methane (99.9% from Iwatani), benzene (special grade from Wako), and helium (as internal standard, 99.9% from Taiyo Nippon Sanyo) with 1.14×10^3, 4.46 and 81.7 µmol min^{-1}, respectively, was fed with recording the mass spectra continuously by using a mass spectrometer (Pfeiffer Vacuum, QMG220) connected to the outlet of reactor. After the ion currents were stabilized, the catalyst bed was heated again to 843 K at a ramp rate of 10 K min^{-1}. Benzene, toluene, and dihydrogen were quantitated from their ion currents, as well as other mass spectral signals within *m/e* (mass / charge ratio) = 1 to 200.

5-2-3 *Steady state reaction*

Steady state reactions were performed with same procedure to the TPR until the MS stabilization step. Then, temperature of the catalyst bed was elevated to 773 K at a

ramp rate of 10 K min^{-1}. It was defined as a reaction started point when the temperature

became 773 K. Benzene, toluene, and dihydrogen were quantitated from their ion currents.

5-3 Results and Discussion

Figure 5-1 shows TPR profiles which are plots of ion currents against temperature during heating the catalyst bed from 373-843 K using Co/MFI with different [Co] loaded by ion exchange and impregnation method. The result of 22-IMP-Co-0.6 is totally same to one reported in Chapter 4. In all of the profiles, ion currents at $m/z = 4$
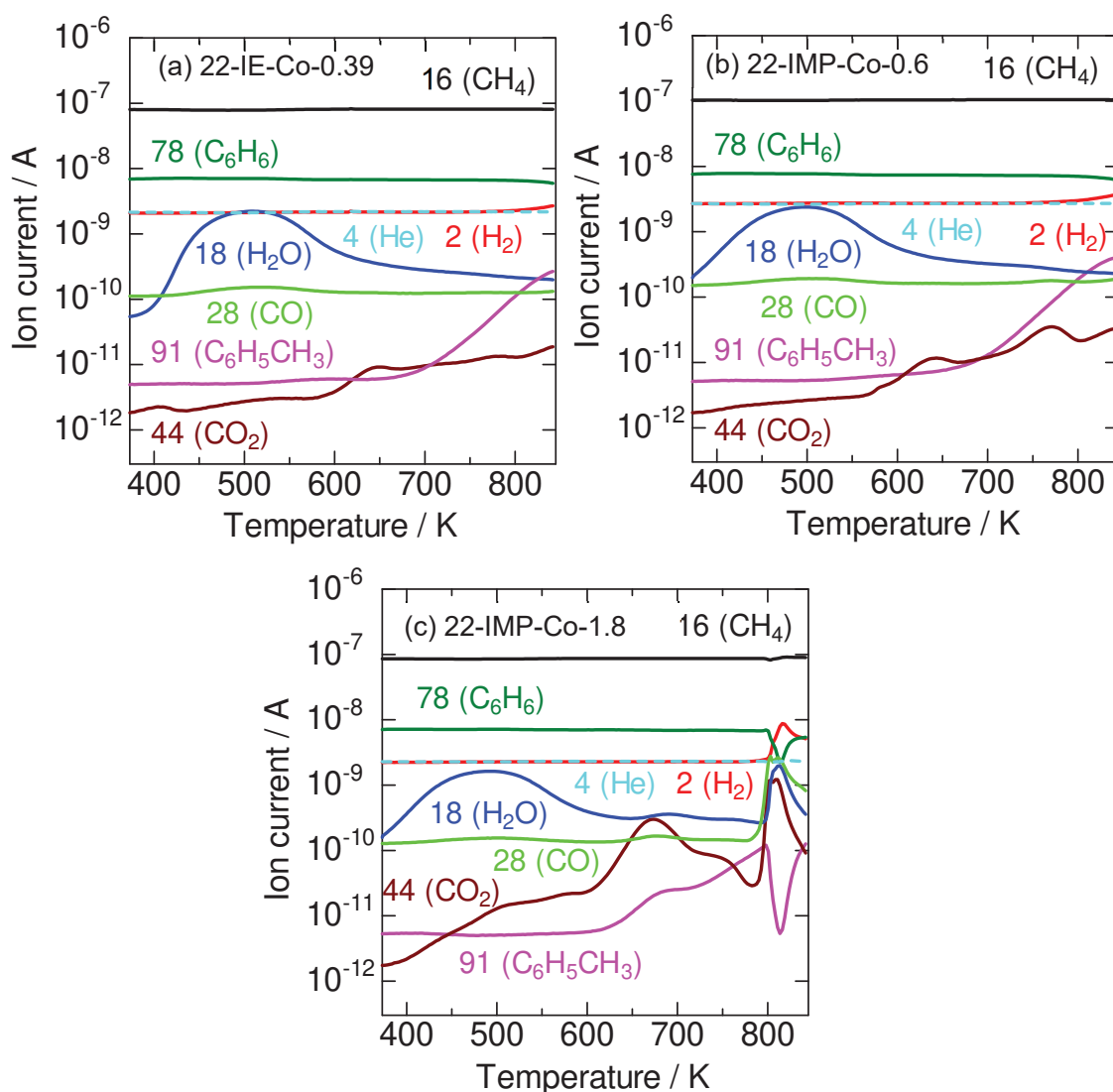
Figure 5-1　TPR profiles under methane (94 kPa) + benzene (0.37 kPa) in 373-843 K over (a) 22-IE-Co-0.39, (b) 22-IMP-Co-0.6, and (c) 22-IMP-Co-1.8.

attributed to helium as inner standard were stable, meaning that these reactions were performed stably. Ion currents of $m/z = 16$ attributed to methane were also stable in the temperature range because they were flowed in surplus, so we could not observed decrease of current in the temperature range. Broad peaks of ion current at $m/z = 18$ attributed to water observed in 400-600 K in all the experiments were caused by H_2O desorbed from catalysts, implying that small amount of water existed in benzene as an impurity and it was adsorbed on the catalyst during MS stabilization step. On 22-IMP-Co-0.6 and 22-IMP-Co-1.8, some peaks of ion currents at $m/z = 44$ attributed to carbon dioxide were observed. It indicates that some Co species were reduced by methane into reduced Co species such as Co^0. On 22-IE-Co-0.39 and 22-IMP-Co-0.6, ion currents at $m/z = 91$ attributed to toluene was elevated from c.a. 700K monotonously against temperature. This means that toluene was produced in the temperature range. On 22-IMP-Co-1.8, the toluene production was observed with two steps, 650-700 K and > 700 K. The former step was observed at the same time to the large reduction peak. It implies that toluene was produced by methylation of benzene with other than methane reagent such as methanol produced by Co reduction [9,10]. Ion current at $m/z = 2$ attributed to dihydrogen was remarkable on 22-IMP-Co-1.8 over 800 K after the large reduction peak of $m/z = 44$ (CO_2). This indicates that reduced Co^0 species promoted methane

122

dehydrogenation as a side reaction (2).

Based on the ion currents, toluene and dihydrogen formation rates were calculated as shown in Figure 5-2. The order of toluene formation rate was cleared as 22-IMP-Co-0.6 > 22-IE-Co-0.39 > 22-IMP-Co-1.8 apparently from Figure 5-2 (a), consisted to the results of continuous flow reactions shown in Chapter 3. Temporary decrease of the rate was observed in 800-820 K on 22-IMP-Co-1.8. This was because methane was consumed for reduction of Co species on MFI. The order of dihydrogen rate was also same to the results of continuous flow reactions.

Then, based on these rates, we could calculate methylation selectivity which is ratio of methane consumed for the target reaction (1).
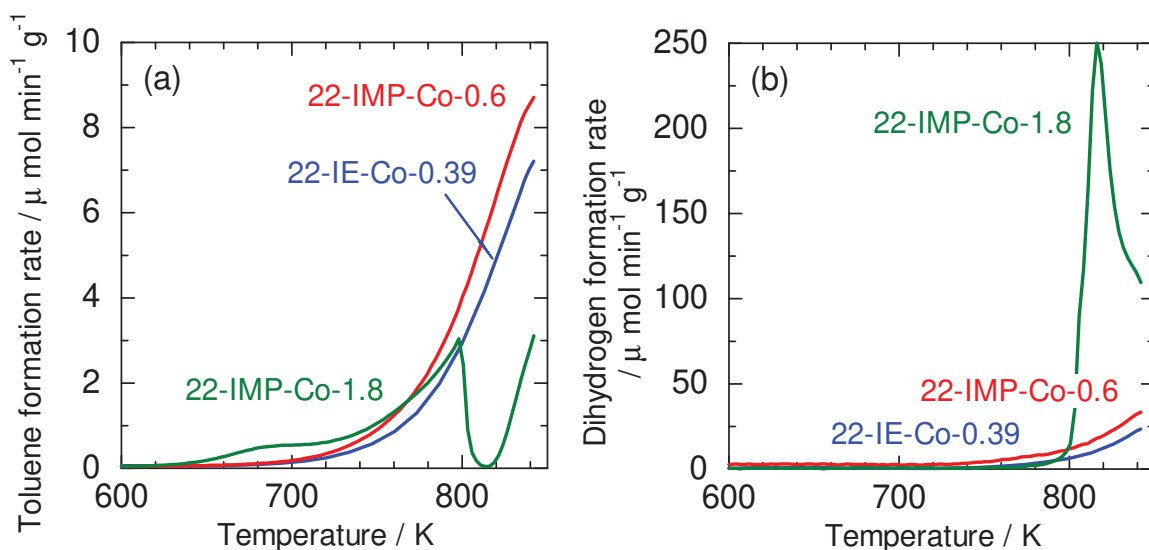
Figure 5-2   (a) toluene and (b) dihydrogen formation rates calculated from ion currents shown in Figure 5-1.

$$S_{\text{Methyl}} (\%) = \frac{r_{\text{Toluene}}}{r_{\text{Toluene}} + \frac{r_{\text{Dihydrogen}} - r_{\text{Toluene}}}{2}} \times 100 \qquad (3)$$

where, S_{Methyl}, r_{Toluene}, $r_{\text{Dihydrogen}}$ are methylation selectivity, toluene formation rate, and

dihydrogen formation rate, respectively. The methylation selectivity was shown in Figure

5-3. On all the samples, methylation selectivity was started at left-hand and bottom region

at low temperature and went to right-upper side with increasing toluene formation rate

[Figure 5-3 (a)]. The selectivity decreased in high temperature over 800 K. It indicates

that dehydrogenation of methane was much promoted compared to the methylation in this

region. Relationship between activity and selectivity was summarized as shown Figure

5-3 (b). In this figure, a catalyst plotted at right-upper side is desirable. Although 22-IMP-

Co-0.6 showed highest activity in the three catalyst, the methylation selectivity was under
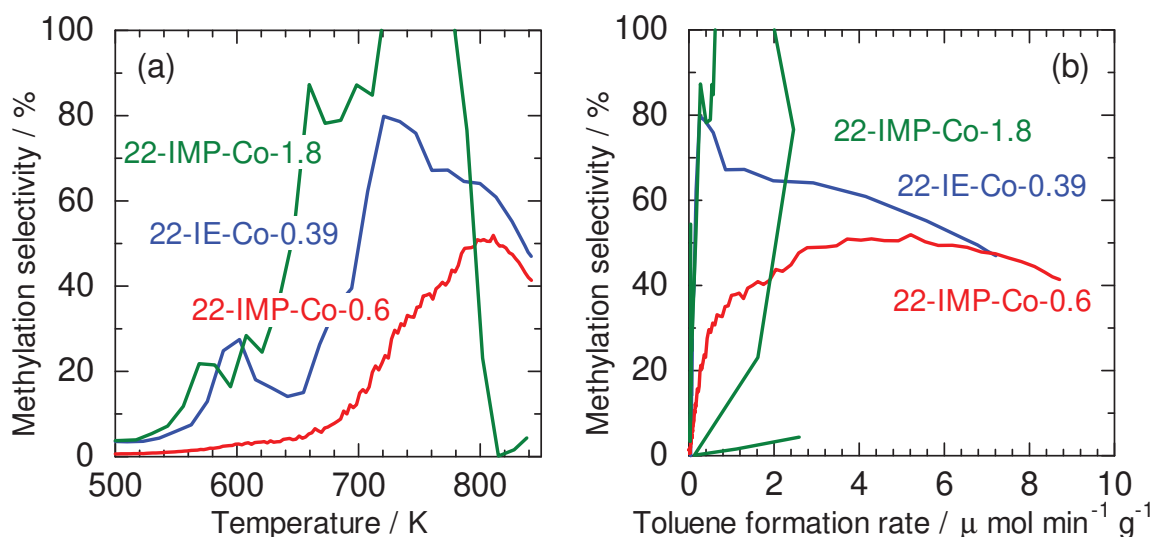
Figure 5-3   Relationship between methylation selectivity and (a) temperature and (b) toluene formation rate.
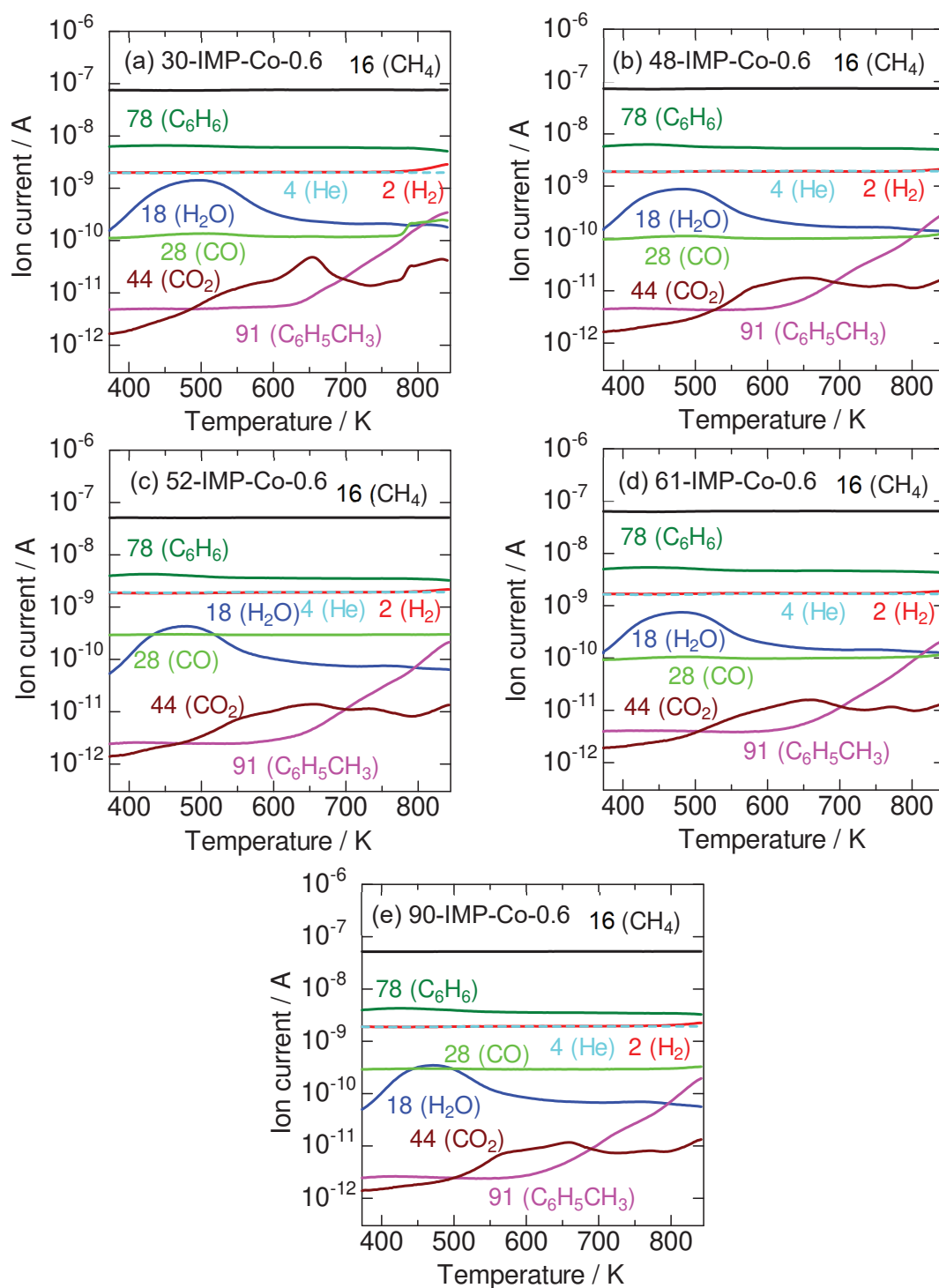
Figure 5-4   TPR profiles under methane (94 kPa) + benzene (0.37 kPa) in 373-843 K over (a) 30-, (b) 48-, (c) 52-, (d) 61-, and (e) 90-IMP-Co-0.6.

50%. It is needed that more selective catalyst is designed and developed.

Figure 5-4 shows TPR profiles which are plots of ion currents against temperature during heating the catalyst bed from 373-843 K using Co/MFI with different [Al]. On all the catalysts except for 30-IMP-Co-0.6, changes of the ion currents such as position of H_2O desorption and CO_2 formation peak were similar. On 30-IMP-Co-0.6, comparably large reduction peaks were observed at 650 and 800 K. This indicates that some Co species was existed on other than ion exchange site of MFI. It was reported that crystallite size was large, and that the surface area was quite low [11]. Therefore, Co^{2+} species were not loaded to ion exchange site of MFI by impregnation method effectively.

Then, toluene and dihydrogen formation rates were calculated, followed by methylation selectivity, and relationship between activity and selectivity for the target reaction was summarized in Figure 5-5 like Figure 5-3 (b). Although 22-IMP-Co-0.6 and 30-IMP-Co-0.6 which had high [Al] comparably showed high activity for the target reaction, the selectivities were under 50%. On the other hand, 48-IMP-Co-0.6 and 61-IMP-Co-0.6 showed high selectivity in the range where toluene formation rate was over 6 μmol g^{-1} min^{-1}. These results may be related to the fact that the active species of Co/MFI was dispersed Co^{2+} species on ion exchange site of MFI, cleared in Chapter 3.
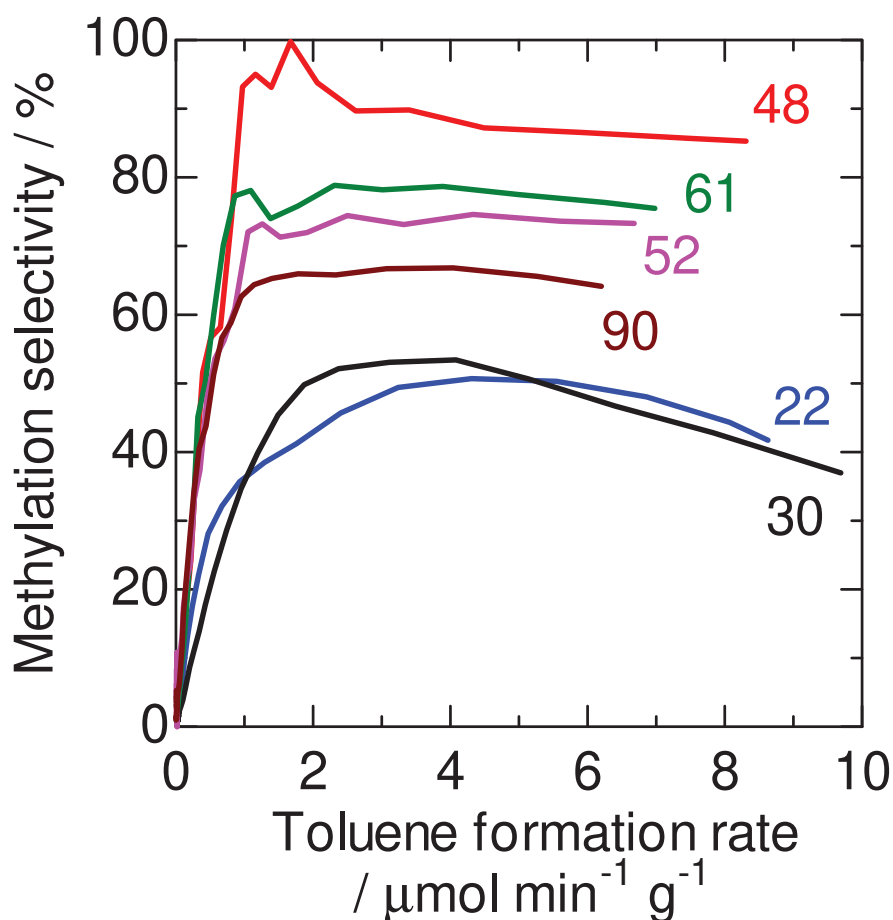
Figure 5-5   Relationship between activity and selectivity for benzene methylation with methane calculated from the results methane (94kPa) + benzene (0.37 kPa) TPR in 373-843K over Co/MFI with different [Al] and fixed Co/Al =0.6 prepared by impregnation method (numeral means SiO_2/Al_2O_3 of MFI).

In the TPR experiments, it was demonstrated that 48-IMP-Co-0.6 had high

methylation selectivity in high temperature realizing high toluene formation rate.

Therefore, the catalytic stabilities of 48-IMP-Co-0.6 and 22-IMP-Co-0.6 were compared

in continuous flow reaction at 813 K which was severe conditions, and the results were

shown in Figure 5-6. Although 22-IMP-Co-0.6 showed high toluene formation rate at

initial stage of the reaction (< 5 h) compared to 48-IMP-Co-0.6, the rate decreased rapidly

and became below that of 48-IMP-Co-0.6 over 5 h with time on stream. Finally at 30 h, the rate dropped to only 3% of the maximum rate, and turn over number (TON) became 3.1 $mol_{toluene}/mol_{Co}$. On the other hand, 48-IMP-Co-0.6 showed high catalytic stability. The toluene formation rate was kept to 60% of the maximum rate at 30 h with time on stream, and TON reached 15.0 $mol_{toluene}/mol_{Co}$. These results demonstrated that Co/MFI with high methylation selectivity showed high catalytic stability.
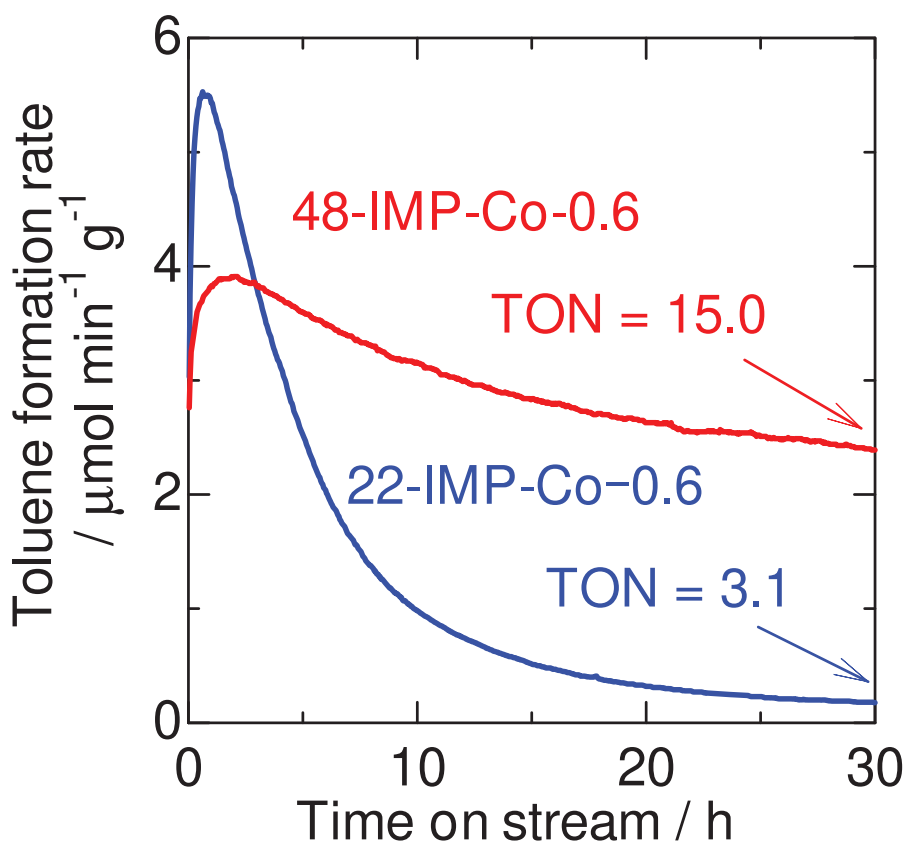
Figure 5-6   Change of the toluene formation rates in continuous flow reaction of methane (94 kPa) + benzene (0.37 kPa) at 813 K over 22-IMP-Co-0.6 and 48-IMP-Co-0.6.

Why the catalytic performance was so different? The clue to solve the question was speculated to be hidden in the MFI zeolite as support, especially for the crystal locations of Al atoms in MFI. It has been known that Al atoms providing ion exchange sites in zeolites were distinguished into 2 types; pair sites and single sites. The former sites are originated by Al atoms which exists closely each other. The latter sites are done with distant Al atoms. The amount of each site was speculated from the amount of Co (+II) species exchanged into MFI by ion exchange method. In Table 5-1, MFI zeolites with SiO_2/Al_2O_3 = 22 was ion exchanged to Co/Al = 0.41 in solution with Co/Al = 10. On the other hand, MFI sample with SiO_2/Al_2O_3 = 48 was ion exchanged to only Co/Al = 0.15 in Co/Al = 10. It was speculated that Co (+II) species was introduced on Al pair sites shown in Figure 5-7. These means that MFI with SiO_2/Al_2O_3 = 22 had much more
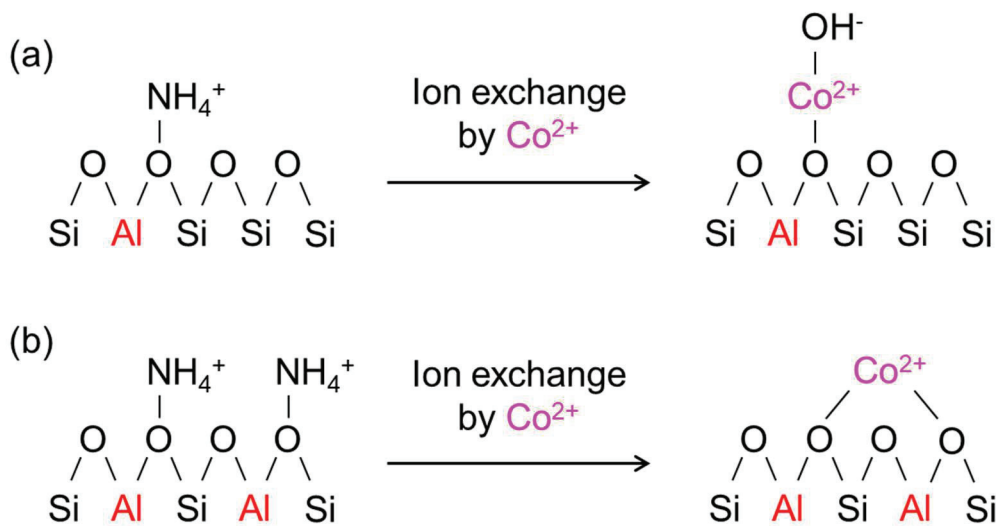
Figure 5-7   Speculated models of Co^{2+} species ion exchange into (a) Al single sites and (b) Al pair sites.
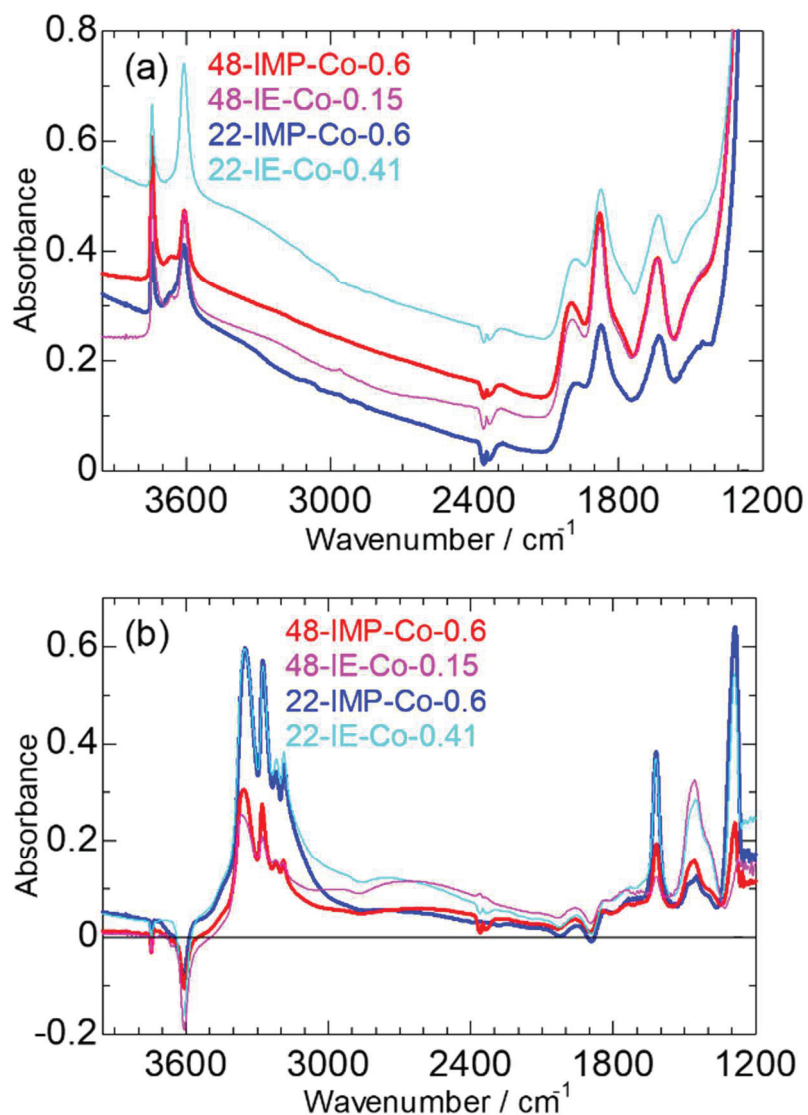
129

Figure 5-8   IR spectra in the (a) reference and (b) difference steps at 373 K
in ammonia IRMS-TPD measurement of Co/MFI.

Al pair sites than that with $SiO_2/Al_2O_3 = 48$, because Co species on the MFI was stable

+II regardless of preparation methods [7].

Figure 5-8 shows IR spectra in the ammonia IRMS-TPD measurements of

Co/MFI. In the Figure 5-8 (a), absorption spectra were observed due to SiOH(3745 cm^{-1}) , acidic OH (3608 cm^{-1}), and SiO framework (2000, 1800, 1600, 1100 cm^{-1}). They are

observed in typical zeolite samples [12]. In addition, on 48-IMP-Co-0.6 and 48-IE-Co-0.15, another band was observed at 3660 cm^{-1} due to AlOH associated with extra-framework [13]. This means that MFI samples with $SiO_2/Al_2O_3 = 48$ had extra-framework aluminum species. Figure 5-8 (b) shows difference (before adsorption of NH_3 – after adsorption of NH_3) spectra. Some NH stretching vibration bands were observed around 3000-3500 cm^{-1} [14]. Positive bands observed at ca. 1440, 1320, and 1620 cm^{-1} were attributed to stretching of NH_4 (ν_4) on Brønsted acid site, symmetric vibration of NH_3 (δ_s) on Lewis acidic metal, and asymmetric vibration of NH_3 (δ_d) on Lewis acidic metal, respectively [15]. Negative bands at 3750 and 3600 cm^{-1} mean disappearances of OH stretching bands caused by adsorption of NH_3 on them. Based on these spectra, we could get the amount of Brønsted and Lewis acid sites of the samples. Amount of Lewis acid
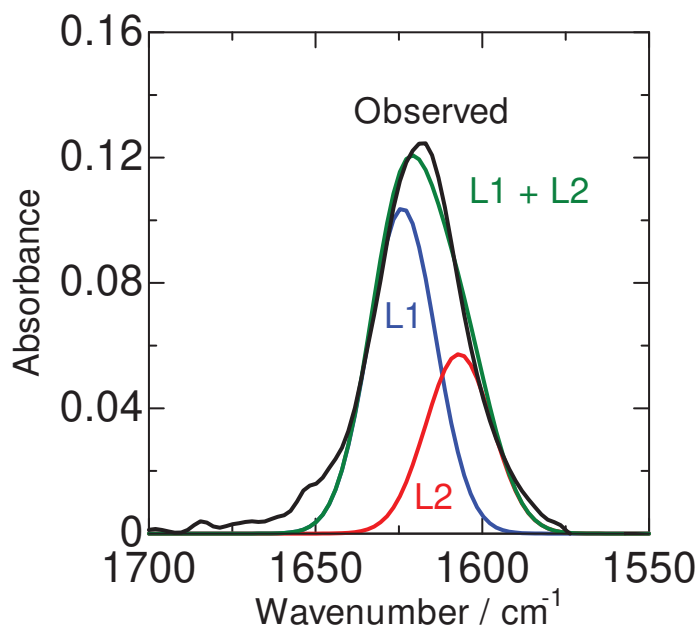

Figure 5-9   Example of deconvolution of δ_d band (48-IMP-Co- 0.6 at 373 K).

131

Table 5-2   Acidic properties of Co/MFI.

Sample	[Al]	Total desorbed NH$_3$	B sum	L sum	L1	L2
	mol kg^{-1}	mol kg^{-1}	mol kg^{-1}	mol kg^{-1}	mol kg^{-1}	mol kg^{-1}
22-IMP-Co-0.6	1.35	1.40	0.09	1.08	0.19	0.89
22-IE-Co-0.41	1.35	1.05	0.14	0.78	0.16	0.62
48-IMP-Co-0.6	0.66	0.53	0.07	0.37	0.05	0.32
48-IE-Co-0.15	0.66	0.60	0.29	0.19	0.05	0.14

sites were calculated from the band of δ_d in contrast of the case in Chapter 3, because the band of δ_s was overlapped by SiO vibration on low [Co] samples such as 48-IE-Co-0.15. In addition, the band of δ_d was deconvoluted into 2 bands; 1624 (L1) and 1607 (L2) cm^{-1} shown in Figure 5-9. Acidic properties of the Co/MFI samples were summarized in Table 5-2. Amount of Brønsted acid (B sum) was low even on Co/MFI samples prepared by impregnation method. This means that Co^{2+} species were effectively ion exchanged on ion exchange sites of MFI. On Co/MFI samples with SiO$_2$/Al$_2$O$_3$ = 22, no apparent changes in acidity were observed in preparation methods. On the other hand, on those with with SiO$_2$/Al$_2$O$_3$ = 48, 48-IMP-Co-0.6 had more L2 than 48-IE-Co-0.15, althogh amounts of L1 were not changed. This implies that amount of L2 is related to that of Co species on Al single sites. However, discussion of amount of Co species on Al sigle sites

should be done carefully, because 22-IE-Co-0.41 also had much L2. Therefore, further characterization of these samples is needed by spectroscopic techniques such as *in-situ* Ultraviolet-visible (*in-situ* UV-vis) in the future works, in order to clarify precise active species promoting the methylation of benzene with methane.

5-4 Conclusions

Methane and benzene TPR experiments were performed over Co/MFI with various [Co] and [Al] prepared by ion exchange and impregnation method. Co/MFI loaded excess Co showed quite low methylation selectivity because Co species on external surface of MFI was reduced into metal Co^0 promoting methane dehydrogenation. On the other hand, Co/MFI with high [Al] which was expected to be dispersed Al in MFI was high methylation selectivity at high temperature realizing high toluene formation rate. From the results of continuous flow reaction of methane + benzene in severe conditions, it was demonstrated that high selective Co/MFI showed high catalytic stability.

Acknowledgement

References

[1] D. A. Wood, C. Nwaoha, B. F. Towler, *J. Nat. Gas Sci. Eng*., **9**, 196-208 (2012)

[2] R. Z. Ríos-Mercado, C. Borraz-Sánchez, *Appl. Energ*., **147**, 536-555 (2015)

[3] N. V. Beznis, B. M. Weckhuysen, J. H. Bitter, *Catal. Lett*., **136**, 52-56 (2010)

[4] E. M. C. Alayon, M. Nachtegaal, A. Bodi, J. A. V. Bokhoven, *ACS Catal*., **4**, 16-22 (2014)

[5] L. S. Wang, L. X. Tao, M. S. Xie, G. F. Xu, J. S. Huang, Y. D. Xu, *Catal. Lett*., **21**, 35-41 (1993)

[6] S. Ma, X. Guo, L. Zhao, S. Scott, X. Bao, *J. Energy Chem*., **22**, 1-20 (2013)

[7] K. Nakamura, A. Okuda, K. Ohta, H. Matsubara, K. Okumura, K. Yamamoto, R. Itagaki, S. Suganuma, E. Tsuji, N. Katada, *ChemCatChem*, **10**, 3806-3812 (2018)

[8] H. Matsubara, E. Tsuji, Y. Moriwaki, K. Okumura. K. Yamamoto, K. Nakamura, S. Suganuma, N. Katada, *Catal. Lett.,* **149**, 2627-2635 (2019)

[9] L. Zardin, O. W. Perez-Lopez, Int. J. Hydrogen Energy, **42**, 7895-7907 (2017)

[10] J. Jansson, A. E. C. Palmqvist, E. Fridell, M. Skoglundh, L. Österlund, P. Thormählen, V. Langer, J Catal., **211**, 387-397 (2002)

[11] D. Mitsuyoshi, K. Kuroiwa, Y. Kataoka, T. Nakagawa, M. Kosaka, K. Nakamura, S.

Suganuma, Y. Araki, N. Katada, *Micropor. Mesopor. Mater.*, **242**, 118-126 (2017)

[12] F. Geobaldo ,B.Onida, P. Rivolo, F. DiRenzo, F. Fajula, E. Garrone, *Catal.Today*, **70**, 107-119 (2001)

[13] L. Kubelkova, J. Novakova, K. Nedomova, *J. Catal*., **124**, 441-450 (1990)

[14] N. Katada, T. Tsubaki, M. Niwa, *Appl. Catal. A: Gen.*, **340**, 76-86 (2008)

[15] S. Suganuma, Y. Murakami, J. Ohyama, T. Torikai, K. Okumura, N. Katada, *Catal. Lett.*, **145**, 1904-1912 (2015)

Chapter 6   Synthesis of Benzene Derivatives from Reaction of Ethane and Benzene over Pb/MFI Catalyst

6-1 Introduction

Natural gas has attracted world's interest as a substitute of petroleum, and amount of mined natural gas has increased since the shale gas revolution occurred [1-4]. Ethane is a component of natural gas. Some processes which gain value-added chemical compounds from ethane have been performed industrially all over the world [5]. In those processes, first of all, ethane is dehydrogenated into ethylene (1),

$$C_2H_6 \rightarrow C_2H_4 + H_2 \qquad\qquad (1)$$

and then the ethylene is converted to the chemicals via condensation and additive reactions [6-9]. However, these processes consumed much energy due to multistep and endothermal reactions [10].

Therefore, developing processes which convert the ethane into chemicals directly has been demanded. It is a choice that ethane is utilized as a direct ethylation reagent. Especially, ethylation of aromatics is promising, because ethylated aromatics and

its derivatives such as ethylbenzene, styrene and diethylbenzene can be a feedstock of various polymer [11,12]. So, reaction of ethane + benzene to synthesize ethylbenzene (2),

$$C_2H_6 + C_6H_6 \rightarrow C_6H_5\text{-}C_2H_5 + H_2 \qquad (2)$$
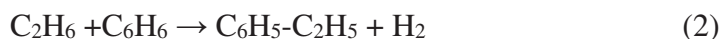
is considered to be the best as a target reaction.

The reaction (2) has been studied by some researchers. Suzuki et al. found that ethylbenzene was produced from a mixed gas of ethane + benzene over Pt supported on MFI-type zeolite [13,14]. Lukyanov et al. demonstrated the reaction pathways as follows. First, Pt particles on MFI promoted the reaction (1) to produce ethylene. Then, Brønsted acid sites of MFI zeolite catalyzed additive reaction of benzene with the ethylene (3).

$$C_2H_4 + C_6H_6 \rightarrow C_6H_5\text{-}C_2H_5 \qquad (3)$$

Namely, the reaction (2) was promoted in the system seemingly, but actually, multistep reactions of (1) + (3) proceeded on the Pt/MFI [15,16]. Although it is very attractive to produce ethylbenzene from ethane + benzene in one system, olefins such as ethylene which is synthesized by the reaction (1) tend to be polymerized into carbon species, cause

catalyst deactivation [17]. Therefore, it is considered to be desirable that reaction (2) proceeds by one step or without via olefins.

To realize those, two choices can be possible. The first is pathways via oxidative reaction. Ethane is oxidized into ethanol, then the ethanol is added into benzene to produce ethylbenzene. It was reported that H-MFI zeolite catalyzed the process [18]. In this process however, it is difficult to regulate progress of complete oxidation of ethane into carbon dioxide as a side reaction. The second one is direct ethylation of benzene with ethane in non-oxidative conditions, (2) exactly. Gerzeliev et al. reported a possibility that H-MFI catalyzed the process by utilizing quantum-chemical simulation [19]. Furthermore, it was reported that Co/MFI catalyze direct methylation of benzene with methane in our previous study [20,21]. Anyway, metal supported MFI-type zeolite is promising as the catalyst.

Based on the background mentioned above, a metal/MFI which can catalyze the reaction of ethane + benzene in non-oxidative conditions with a fixed-bed flow reactor was researched for. We evaluated the catalytic stability and speculated the reaction pathways on some active catalysts by comparing changes of formation rates and distribution of the products. Then suitable chemical composition such as metal/Al molar ratio and Al content in MFI, and an effect of reaction temperature on the activity were

139

clarified. This paper shows high and stable catalytic activity of Pb/MFI for the reaction of ethane + benzene, and speculated reaction pathways on the Pb/MFI.

6-2 Experimental

6-2-1 *Catalyst preparation*

Various metal/zeolites were prepared by impregnation method as reported our previous paper [20]. A NH$_4$-MFI zeolite (Tosoh, [Al] = 1.3 mol kg^{-1}, SiO$_2$/Al$_2$O$_3$ molar ratio = 22.1) was put into aqueous solution from nitrates (Cr, Mn, Fe, Co, Ni, Cu, Zn, Ga, Ag, In, Pb, and Bi), and chlorides (Rh and Ru), chlorides of ammine complexes (Pd, and Pt), or (NH$_4$)$_6$Mo$_7$O$_{24}$ as a precursor. The mixture was heated at 343 K with stirring at 400 rpm until most of the water was dried. The yielded slightly wet solid was dried again at 383 K for 3 h. In addition to these, some Pb/MFI samples, Pb/zeolites and Pb/SiO$_2$ were also prepared with NH$_4$-MFI (ion exchanged from Na-MFI, Mizusawa, Mizusawa, Zeolyst, and Clariant), NH$_4$-*BEA (ion exchanged from Na-*BEA, Clariant), NH$_4$-MOR (as supplied from Tosoh), NH$_4$-FER (as supplied from Tosoh), and NH$_4$-FAU (ion exchanged from Na-FAU, JGC Catalysts and Chemicals) with SiO$_2$/Al$_2$O$_3$ = 30, 48, 61, 90, 25, 15, 18.5 and 4.8, respectively, and SiO$_2$ (JGC Catalysts and Chemicals) as a

support of Pb species. Some Pb/MFI samples were prepared by means of ion exchange method. A NH_4-MFI with SiO_2/Al_2O_3 = 22.1, 52, and 63 supplied from Tosoh, Mizusawa, Mizusawa, respectively, were put into the $Pb(NO_3)_2$ aqueous solution. After the solution was stirred and heated at 343 K for 4 h, the solid was filtrated and washed 3 times, and dried at 383 K for 3 h. The Pb and Al contents on the ion-exchanged samples were measured by means of inductively coupled plasma emission spectroscopy (ICP-AES, Agilent, 5110 ICP-OES). The prepared samples are summarized in Table 6-1.

Table 6-1   Prepared catalysts.

Abbreviation	Transition metal source	Preparation method	Structure of support	[Al] / mol kg^{-1}	[Metal] / mol kg^{-1}	SiO$_2$/Al$_2$O$_3$ in support	Metal / Al molar ratio
NH$_4$/-MFI	-	-	MFI	1.3	0	22.1	0
22-IMP-Pb-Y	Pb(NO$_3$)$_2$	Impregnation	MFI	1.3	$1.3 \times Y*$	22.1	$Y*$
30-IMP-Pb-0.6	Pb(NO$_3$)$_2$	Impregnation	MFI	1.0	0.60	30	0.6
48-IMP-Pb-0.6	Pb(NO$_3$)$_2$	Impregnation	MFI	0.66	0.40	48	0.6
61-IMP-Pb-0.6	Pb(NO$_3$)$_2$	Impregnation	MFI	0.52	0.31	61	0.6
90-IMP-Pb-0.6	Pb(NO$_3$)$_2$	Impregnation	MFI	0.36	0.22	90	0.6
22-IE-Pb-Y	Pb(NO$_3$)$_2$	Ion exchange	MFI	1.3	$1.3 \times Y**$	22.1	$Y**$
52-IE-Pb-0.41	Pb(NO$_3$)$_2$	Ion exchange	MFI	0.61	0.25	52	0.41
63-IE-Pb-0.38	Pb(NO$_3$)$_2$	Ion exchange	MFI	0.51	0.19	63	0.38
Pb/FER	Pb(NO$_3$)$_2$	Impregnation	FER	1.6	0.95*	18.5	0.60*
Pb/*BEA	Pb(NO$_3$)$_2$	Impregnation	BEA	1.2	0.72*	25	0.60*
Pb/MOR	Pb(NO$_3$)$_2$	Impregnation	MOR	1.9	1.14*	15	0.60*
Pb/FAU	Pb(NO$_3$)$_2$	Impregnation	FAU	4.5	2.71*	4.8	0.60*
Pb/SiO$_2$	Pb(NO$_3$)$_2$	Impregnation	Amorphous (silica gel)	0	0.59*	∞	∞
22-IMP-Mg-0.6	Mg(NO$_3$)$_2$	Impregnation	MFI	1.3	0.81*	22.1	0.60*
22-IMP-Cr-0.4	Cr(NO$_3$)$_3$	Impregnation	MFI	1.3	0.54*	22.1	0.40*
22-IMP-Mn-0.6	Mn(NO$_3$)$_2$	Impregnation	MFI	1.3	0.81*	22.1	0.60*
22-IMP-Fe-0.4	Fe(NO$_3$)$_3$	Impregnation	MFI	1.3	0.54*	22.1	0.40*
22-IMP-Ni-0.6	Ni(NO$_3$)$_2$	Impregnation	MFI	1.3	0.81*	22.1	0.60*
22-IMP-Cu-0.6	Cu(NO$_3$)$_2$	Impregnation	MFI	1.3	0.81*	22.1	0.60*
22-IMP-Zn-0.6	Zn(NO$_3$)$_2$	Impregnation	MFI	1.3	0.81*	22.1	0.60*
22-IMP-Ga-0.4	Ga(NO$_3$)$_3$	Impregnation	MFI	1.3	0.54*	22.1	0.40*
22-IMP-Mo-0.6	(NH$_4$)$_6$Mo$_7$O$_{24}$	Impregnation	MFI	1.3	0.81*	22.1	0.60*
22-IMP-Ru-0.4	RuCl$_3$	Impregnation	MFI	1.3	0.54*	22.1	0.40*
22-IMP-Rh-0.4	RhCl$_3$	Impregnation	MFI	1.3	0.54*	22.1	0.40*
22-IMP-Pd-0.6	[Pd(NH$_3$)$_4$]Cl$_2$	Impregnation	MFI	1.3	0.81*	22.1	0.60*
22-IMP-Ag-1.2	AgNO$_3$	Impregnation	MFI	1.3	1.62*	22.1	1.20*
22-IMP-In-0.4	In(NO$_3$)$_3$	Impregnation	MFI	1.3	0.54*	22.1	0.40*
22-IMP-Pt-0.3	H$_2$[PtCl$_6$]	Impregnation	MFI	1.3	0.41*	22.1	0.30*
22-IMP-Bi-0.4	Bi(NO$_3$)$_3$	Impregnation	MFI	1.3	0.54*	22.1	0.40*

*: Based on the amounts of Pb in the impregnated solution and Al in the used zeolite.

**: Measured by inductively coupled plasma emission spectroscopy (ICP-AES).

6-2-2 *Catalytic test*

Catalytic tests were performed in a fixed-bed flow reactor. Ethane (99.7 % from Taiyo Nippon Sanyo) and benzene (special grade, Wako) were used. In standard conditions, powder sample (0.300 g) was placed in a Pyrex tube (i.d.: 10 mm) and pretreated in a flow of nitrogen (73.6 mmol h^{-1}, 99.9% from Iwatani) in the atmospheric pressure at 823 K for 1 h. Then, a mixture of ethane and benzene (99.0 and 2.3 kPa, 73.6 and 1.72 mmol h^{-1}, respectively, corresponding to W_{cat} / $F_{totalgas}$ = 3.98 g$_{cat}$ h mol$_{totalgs}$$^{-1}$) was fed to the catalyst bed at 773 K. The outlet materials were loaded by 6-ways valve into and analyzed with flame ionization detector-gas chromatograph (FID-GC, Shimadzu GC-2014) equipped with capillary column (Agilent, CP-PoraBOND Q) directly connected to the outlet of a reactor.

6-3 Results

Figure 6-1 compares the catalytic activities of metal/zeolites for the reaction of ethane + benzene. Ethylene, C_{3-5} hydrocarbon, toluene, ethylbenzene, styrene, diethylbenzene, naphthalene, and methylnaphthalene were observed as the main products in the reaction. In this study, ethylbenzene, styrene and diethylbenzene were regarded as target products. C_{3_5} hydrocarbon and toluene, and naphthalene and methylnaphthalene were regarded as byproducts via hydrogenolysis of benzene [22] and dehydrocyclization of diethylbenzene [23], respectively. Parent NH_4-MFI was inactive for the target reactions. On Zn, Mo, Pt, and Pb/MFI, formation rates of the target products were higher than other metal/MFI catalysts and parent NH_4-MFI (*in-situ* H-type MFI). On Zn and Pt/MFI, formation rates of byproducts were also high. Pt/MFI showed the highest activity for the
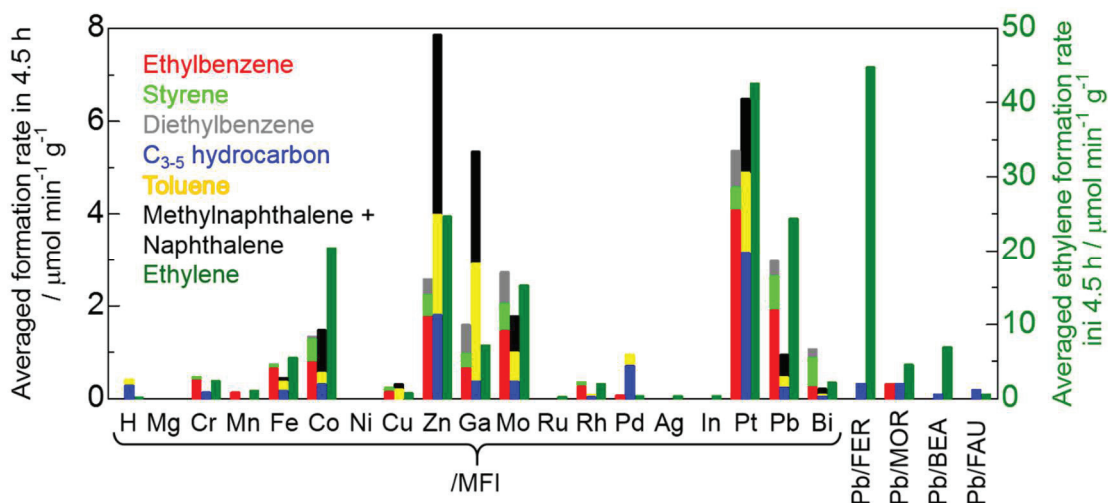
Figure 6-1   Averaged formation rates of ethylbenzene + styrene + diethylbenzene, C_{3-5} hydrocarbon + toluene + naphthalene + methylnaphthalene, and ethylene in the reaction of ethane + benzene over metal/zeolites in 4.5 h (773 K, P_{C2C6} = 99.0 kPa, P_{C6H6} = 2.3 kPa).

target reaction in 4.5 h in this reaction conditions as reported previously [13,15]. On the

other hand, Pb/MFI was less active for the side reactions. Ethylene formation rates on Zn,

Mo, Pt, and Pb/MFI were comparably high among the metal/MFI catalysts.

Figure 6-2 shows time courses of the formation rates in the reaction of ethane +

benzene over Zn, Mo, Pt, and Pb/MFI which showed high activity for the target reactions.

On Zn, Pt, and Mo/MFI, the formation rates of the target products gradually fell with time
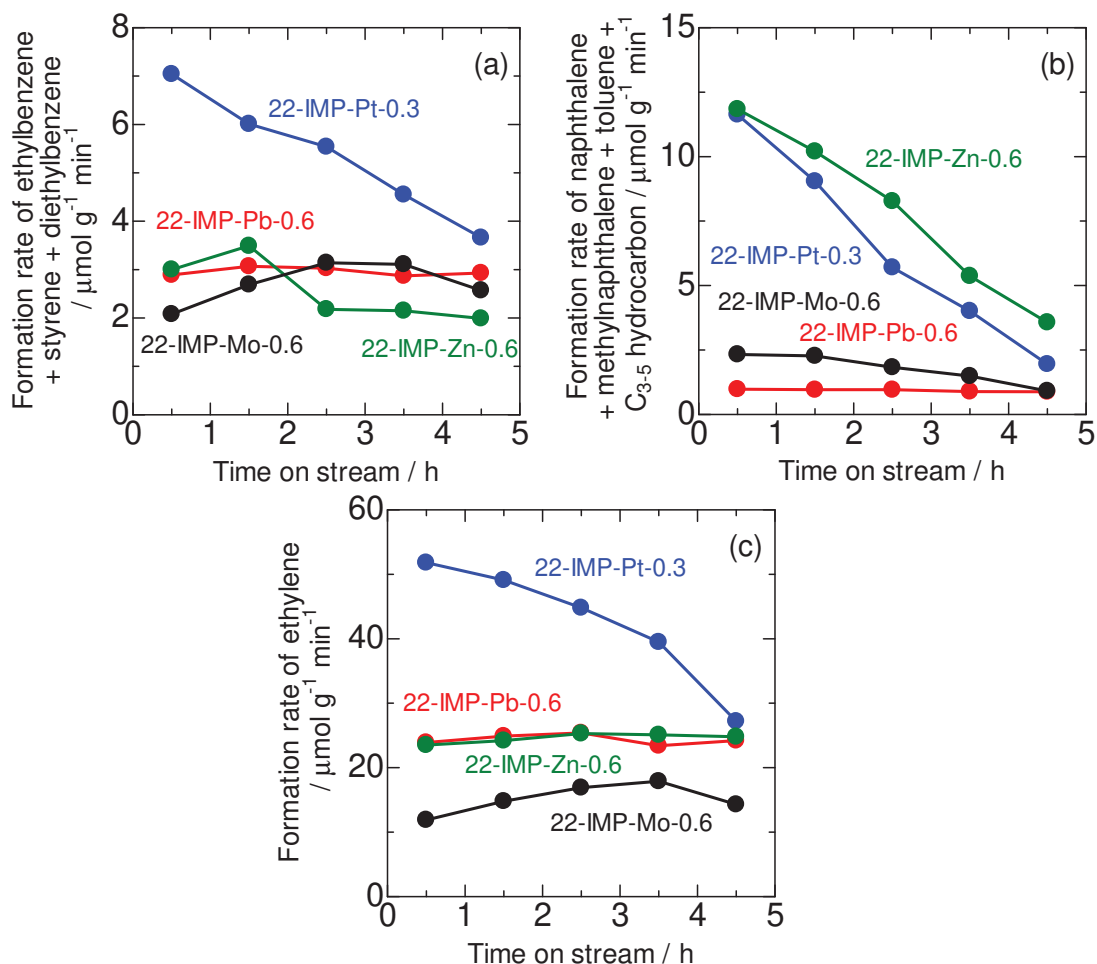
Figure 6-2   Changes in formation rates of (a) ethylbenzene + styrene + diethylbenzene, (b) C_{3-5} hydrocarbon + toluene + naphthalene + methylnaphthalene, and (c) ethylene with time on stream in the reaction of ethane + benzene over Zn, Mo, Pt, and Pb/MFI (773 K, P_{C2C6} = 99.0 kPa, P_{C6H6} = 2.3 kPa).

on stream in 4.5 h, whereas Pb/MFI showed stable activity [Figure 6-2 (a)]. This tendency

was also observed in Figure 6-2 (b). Ethylene formation rates fell on Pt and Mo/MFI,

whereas were stable on Zn and Pb/MFI [Figure 6-2 (c)]. The ethylene formation rates

were in the order with Pt/MFI > Zn/MFI = Pb/MFI > Mo/MFI.

Based on the screening of catalysts for ethane + benzene reaction, it was

demonstrated that Pb/MFI had stable activity for the target reaction and did not promoted

side reactions so much. Furthermore other Pb/zeolites such as Pb/MOR were inactive for

the target reaction shown in Figure 6-1. Therefore, we researched about Pb/MFI for

suitable composition of the catalyst and speculation of the reaction pathway.

Figure 6-3 showed the relationship between catalytic activities for the target

reactions and catalyst compositions of X-IMP-Pb-0.6. It was observed that the catalytic

activity was almost saturated at even low Al content in MFI ([Al]) = 0.36 (SiO$_2$/Al$_2$O$_3$ =

91) and not changed so much with concentrating the [Al].

Figure 6-4 compares the catalytic activity for the target reactions of 22-IMP-Pb-

Y and 22-IE-Pb-Y in the Pb/Al molar ratio and the preparation method. On 22-IMP-Pb-Y,

the activity increased in range of Pb/Al = 0-0.5 and fell > 0.5. On 22-IE-Pb-Y, the activity

was low in range of Pb/Al = 0-0.2, whereas drastically increased in range of Pb/Al = 0.2-
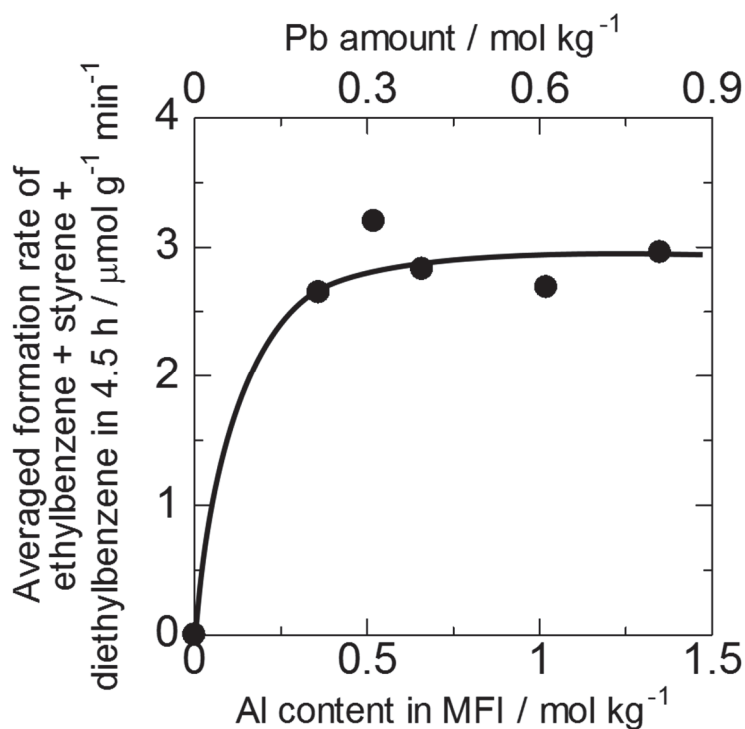
Figure 6-3   Averaged formation rates of ethylbenzene + styrene + diethylbenzene in the
reaction of ethane + benzene over X-IMP-Pb-0.6 in 4.5 h (X = 22, 30, 48, 61, and 90, 773
K, P_{C2C6} = 99.0 kPa, P_{C6H6} = 2.3 kPa).

0.5. The Pb/Al molar ratio of Pb/MFI was saturated in ca. 0.5 even by preparation with excessive Pb solution. 22-IE-Pb-Y showed higher catalytic performance than 22-IMP-Pb-Y in around Pb/Al = 0.5.

22-IE-Pb-Y with high Y showed high catalytic activity. Then, effects of X (= [Al]) of X-IE-Pb-Y with high Y and reaction temperature on catalytic performances was investigated.
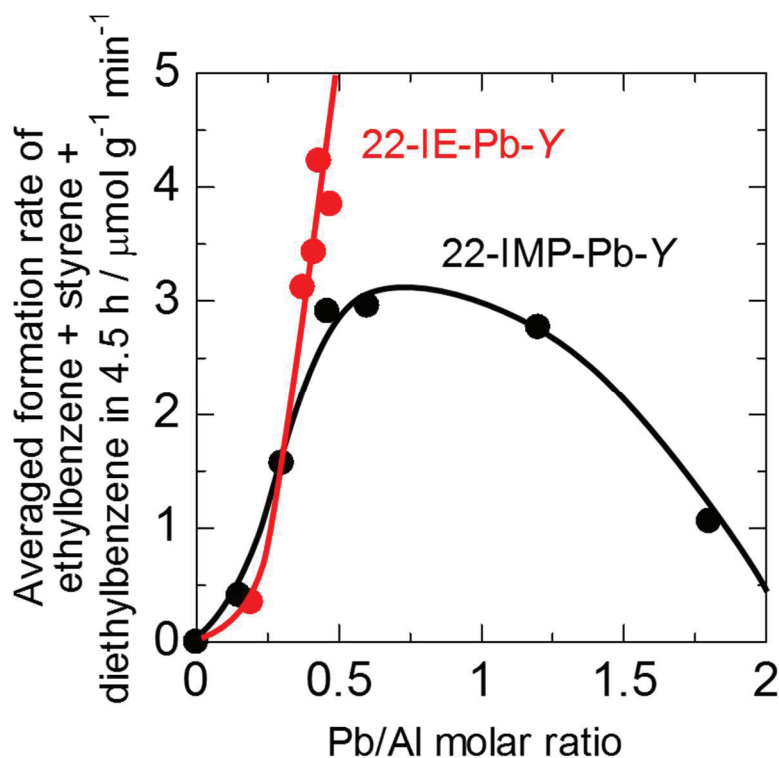
Figure 6-4   Averaged formation rates of ethylbenzene + styrene + diethylbenzene in the reaction of ethane + benzene over 22-IMP-Pb-Y, and 22-IE-Pb-Y in 4.5 h (773 K, P_{C2C6} = 99.0 kPa, P_{C6H6} = 2.3 kPa).

Figure 6-5 shows formation rates of target products, byproducts, and ethylene in the reaction of ethane + benzene over 22-IE-Pb-0.47, and 52-IE-Pb-0.41 and 63-IE-Pb-0.38. The catalytic performances were different among the catalysts. On 22-IE-Pb-0.47, changes of the formation rates of target and side reactions were not monotonous against reaction temperature. 22-IE-Pb-0.47 showed the highest formation rates of the target products in the reaction temperature <= 798 K among the three catalysts. But, the rate
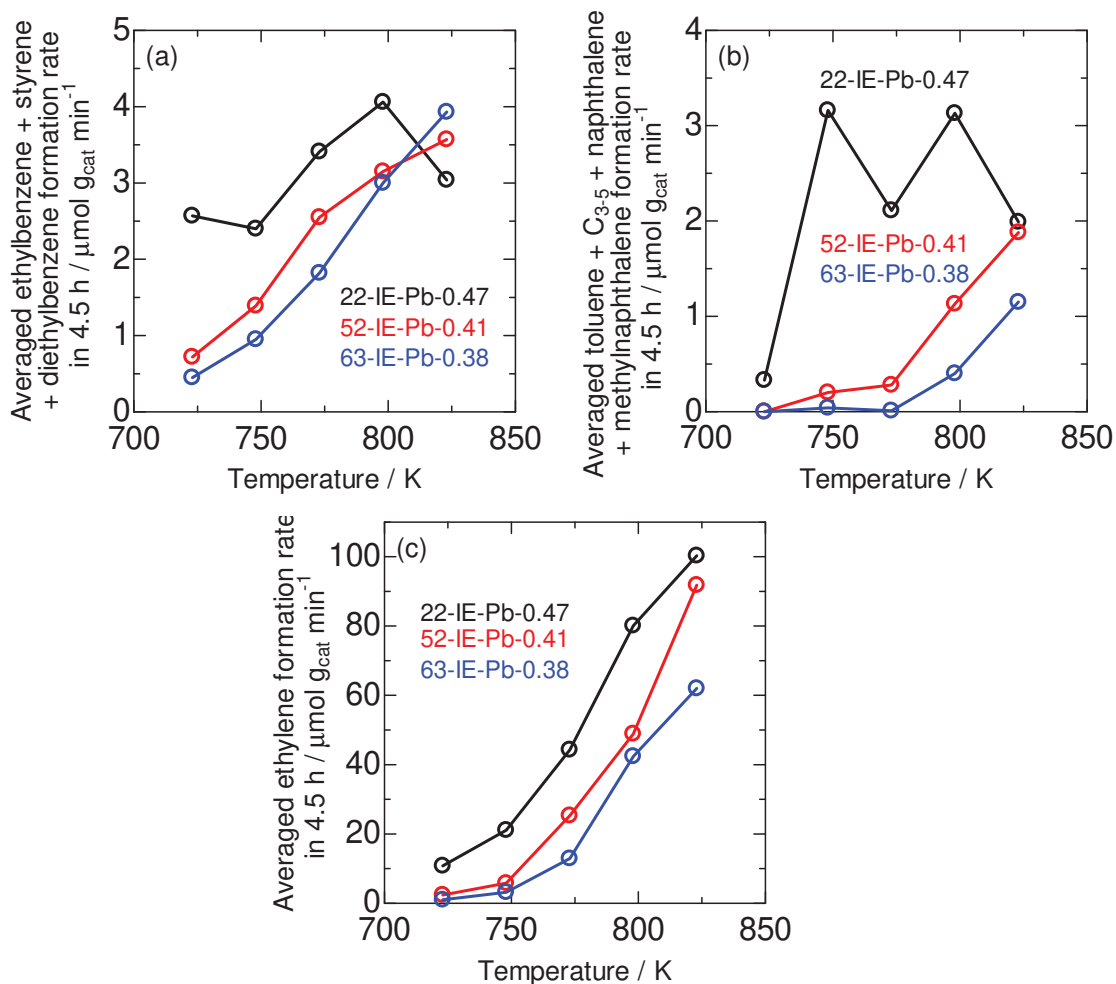
Figure 6-5   Averaged formation rates of (a) ethylbenzene + styrene + diethylbenzene, (b) C_{3-5} hydrocarbon + toluene + naphthalene + methylnaphthalene, and (c) ethylene in the reaction of ethane + benzene over 22-IE-Pb-0.47, 52-IE-Pb-0.41, and 63-IE-Pb-0.38 in 4.5 h against reaction temperature   (P_{C2C6} = 99.0 kPa, P_{C6H6} = 2.3 kPa).

was the lowest at 823 K. 22-IE-Pb-0.47 showed the highest activity for the side reactions in temperature range of 723-823 K. On the other hand, on 52-IE-Pb-0.41 and 63-IE-Pb-0.38, changes of the formation rates of target and side reactions monotonously increased against reaction temperature. The ethylene formation rates were elevated with increasing temperature in all the three catalysts, and the order was 22-IE-Pb-0.47 > 52-IE-Pb-0.41 > 63-IE-Pb-0.38 in the range of the reaction temperature, consisted with the order of [Al] of the catalysts.

The reaction of ethane + benzene over 52-IE-Pb-0.41 were performed with some conditions of $W_{cat}/F_{totalgas}$ at 773 K to speculate the reaction pathway. Figure 6-6 shows
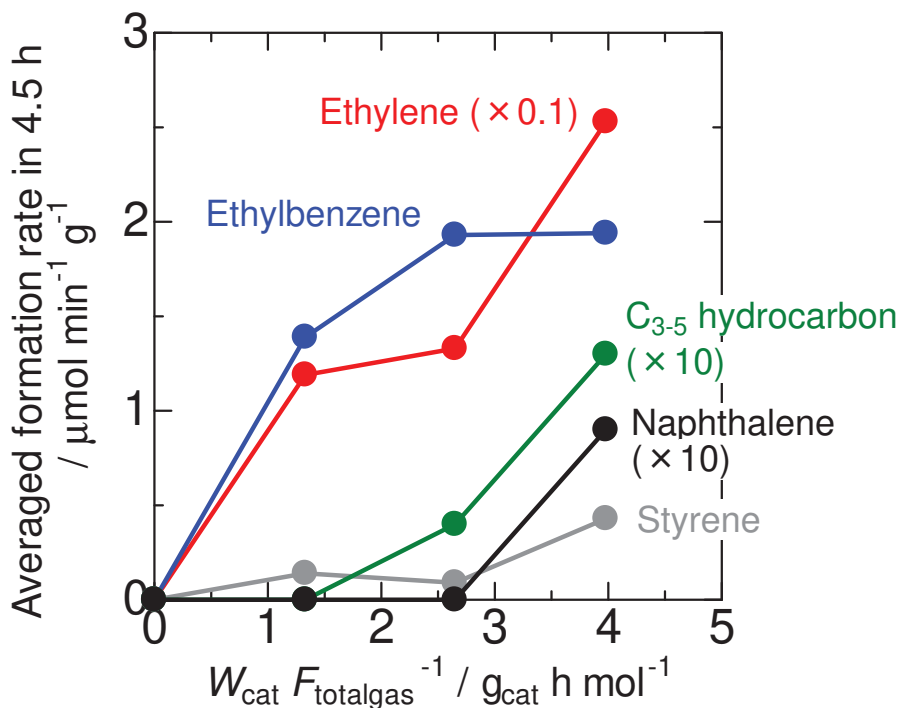
Figure 6-6   Averaged formation rates of the products in the reaction of ethane + benzene over 52-IE-Pb-0.41 in 4.5 h against $W_{cat}/F_{totalgas}$ (773 K, P_{C2C6} = 99.0 kPa, P_{C6H6} = 2.3 kPa).

relationship between the formation rates of the reaction products and $W_{cat}/F_{totalgas}$. The reaction did not proceed with no catalyst. Ethylene and ethylbenzene were produced with even low $W_{cat}/F_{totalgas}$ = 1.33 g_{cat} h mol^{-1}, their formation rates increased with elevating $W_{cat}/F_{totalgas}$ to 2.65 g_{cat} h mol^{-1}. Ethylene formation rates increased with elevating the $W_{cat}/F_{totalgas}$. to 3.98 g_{cat} h mol^{-1}, whereas ethylbenzene formation rate was saturated then. On the contrary, C3-5 hydrocarbon, naphthalene, and styrene were almost not observed at low $W_{cat}/F_{totalgas}$ = 1.33 g_{cat} h mol^{-1}, but they were observed $W_{cat}/F_{totalgas}$ < 2.65 g_{cat} h mol^{-1}.

6-4 Discussion

6-4-1 *Requirements for stable catalytic activity*

Among various metal/MFI catalysts, Zn, Mo, Pt, and Pb/MFI showed high catalytic activities for the target reaction, however the products distribution was different. For example Zn and Pt/MFI showed high activities for the side reactions producing C_{3-5} hydrocarbon, toluene, and naphthalene. C_{3-5} hydrocarbons and toluene were produced by hydrogenolysis of benzene on Brønsted acid sites of MFI [22]. In this case, the hydrogen source was considered to be from ethane dehydrogenation into ethylene. Indeed, production of ethylene was observed on the catalysts. Although ethylene was also produced on Mo and Pb/MFI, amounts of the C_{3-5} hydrocarbons and toluene were few, compared to those using Zn and Pt/MFI. This might be because of difference of Brønsted acidity. On the other hand, naphthalene was produced by dehydrocyclization of diethylbenzene [23]. Therefore, Zn and Pt/MFI which promoted side reactions were highly active for dehydrogenation of hydrocarbon as reported [16, 24]. Generally, catalysts which have high activity for dehydrogenation are tend to be deactivated by covering active sties with carbon species produced from the dehydrogenation [17]. Indeed, deactivation was observed on Zn and Pt/MFI. Deactivation was also observed on Mo/MFI slightly in 4.5 h with time on stream, although amount of the byproducts was few

comparably. This means that amount of active sites was few due to difficulty of dispersing Mo species on the support. It has been reported that Mo species were aggregated on external surface of zeolite supports in Mo/zeolites [25]. On Pb/MFI, the formation rates of the byproducts were low. It means that deposition rate of carbon species was slow, resulting in stable activity for the target reaction.

6-4-2 *Speculated reaction pathway for ethylbenzene production*

Two possibilities are expected for pathway of ethylbenzene production from the reaction of ethane + benzene. The first pathway is direct ethylation of benzene with ethane. The second one is dehydrogenation of ethane into ethylene + dihydrogen, followed by alkylation of benzene with ethylene. It has been reported that the latter pathway proceeded on Pt/MFI [15,16]. Changes of product formation rates when using Zn/MFI were similar to Pt/MFI, indicating that the latter pathway proceeded on Zn/MFI [26]. Although the ethylene and target formation rates on Pb/MFI were similar to on Zn/MFI, the formation rates of byproducts were totally different. This means that reaction pathway was different from Zn/MFI, namely the former pathway, or both pathways might proceed on Pb/MFI.

6-4-3 *Suitable chemical composition of Pb/MFI*

No activity for the target reaction was observed on Pb/SiO$_2$ and Pb/zeolites other than Pb/MFI. This means that the active species of Pb/MFI requires ion exchange site of MFI zeolite. The low activity of Pb/MFI loaded excess Pb by impregnation method implies that Pb species other than ion exchange sites promoted side reaction to lead deactivation. Fast deactivation was observed on 22-IMP-Pb-1.2 and 22-IMP-Pb-1.8 (not shown). In addition to that, maximum amount of Pb loaded on MFI with ion exchange method was around Pb/Al = 0.5, and the activity of 22-IE-Pb-*Y* was higher than 22-IMP-Pb-*Y* with around Pb/Al =0.5. Based on these facts, it is speculated that Pb species was ion-exchanged onto MFI with oxidation state = +II, and that the Pb^{2+} species on ion exchange sites were active species for the target reaction. Amount of Pb loaded on ion exchange sites of MFI decreased with decreasing the [Al] in MFI, meaning that amount of Al pair sites in MFI which can supported divalent cations was few in a MFI with low [Al]. Difference in the activity of *X*-IMP-Pb-0.6 (*X* = 22, 30, 48, 61, and 90) was small. This may be because Pb species was not loaded on ion exchange sites of MFI with high [Al] by impregnation method effectively.

Products distributions were different in dependency of reaction temperature among Pb/MFI catalysts with different [Al] prepared by ion exchange method.

High activity for the side reactions in wide range of reaction temperature on 22-IE-Pb-0.47 with high [Al] compared to 52-IE-Pb-0.41 and 63-IE-Pb-0.38, although difference in ethylene formation rates were small. It implies that 22-IE-Pb-0.47 had strong Brønsted acid sites comparably, or that some Pb^{2+} species which promotes the side reactions existed. Niessen et al. mentioned a possibility that Pb-ion exchanged zeolite had some Pb species [27]. Decrease of the catalytic activity for the target reactions at high reaction temperature on 22-IE-Pb-0.47 was due to fast deactivation from the side reactions. On the other hand, on 52-IE-Pb-0.41 and 63-IE-Pb-0.38, the formation rates of all the products increased with elevating the reaction temperature, indicating that these catalysts have simple Pb^{2+} species. Therefore, it is seemed to be suitable for this reaction that a Pb/MFI which has much Pb^{2+} species loaded on ion exchange sites of MFI with low [Al] such as 52-IE-Pb-0.41 and 63-IE-Pb-0.38.

6-4-4 *Speculated reaction pathways on Pb/MFI*

In the reactions of ethane + benzene with different amount of 52-IE-Pb-0.41 as a catalyst, ethylbenzene was produced at low $W_{cat}/F_{totalgas}$ and saturated in range of $W_{cat}/F_{totalgas}$ = 2.65-3.98 g_{cat} h mol^{-1}, whereas byproducts such as C_{3-5} hydrocarbon and naphthalene was produced in range of $W_{cat}/F_{totalgas}$ = 2.65-3.98 g_{cat} h mol^{-1}. This

155

demonstrates that ethylbenzene was first product, and C$_{3-5}$ hydrocarbon and naphthalene were sequential products. In addition to that, ethane dehydrogenation into ethylene + dihydrogen proceeded dependently. Based on these results and discussion, reaction pathways in this reaction system was speculated in Figure 6-7. Ethylbenzene was produced by both direct ethylation of benzene with ethane and ethane dehydrogenation into ethylene, followed by additive reaction of benzene with the ethylene. The ethylbenzene was converted into styrene by dehydrogenation and diethylbenzene by second ethylation. The diethylbenzene was dehydrocyclizated into naphthalene, and finally into coke species. In addition to these reaction, C$_{3-5}$ hydrocarbon and toluene were
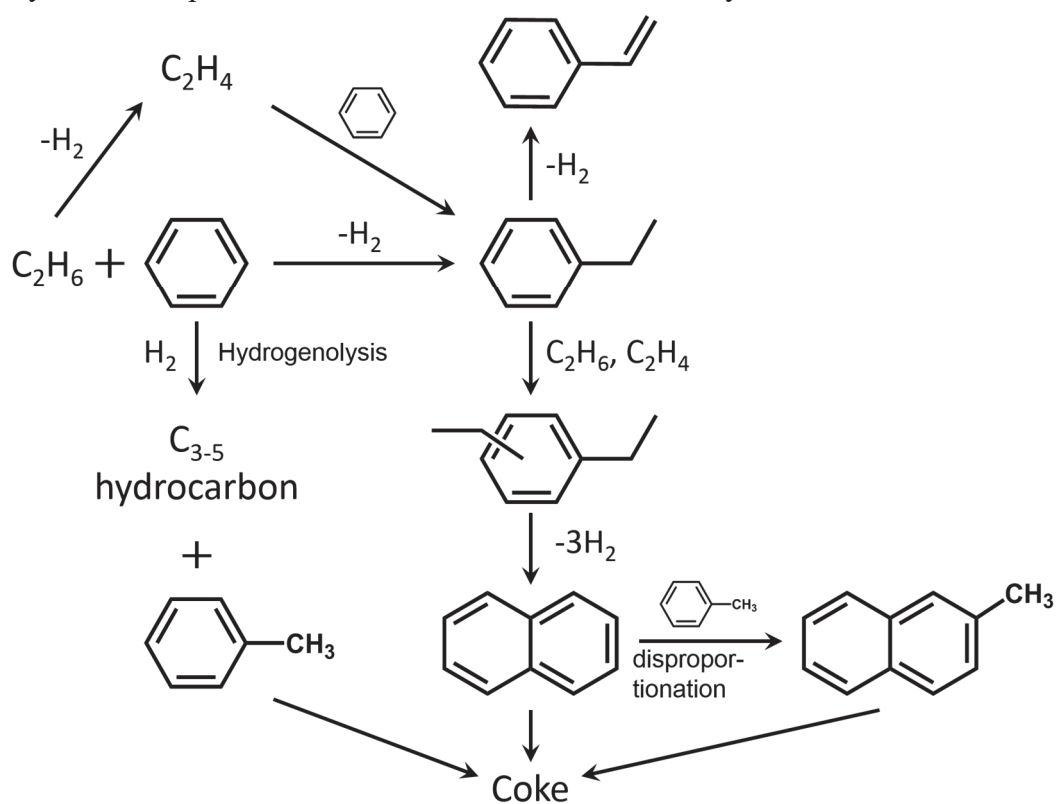
Figure 6-7   Speculated reaction pathways in the reaction of ethane + benzene over Pb/MFI.

156

produced via hydrogenolysis with dihydrogen produced from other reactions. The toluene

was also converted coke species finally.

Detail characterization of the Pb/MFI including acidity, oxidation state, and fine

structure around active Pb species are needed in the future works to enhance the activity,

because an example that Pb/MFI showed high catalytic activity was quite few [28].

6-5 Conclusions

Reactions of ethane + benzene were performed on various metal/zeolites as catalysts at 773 K to find a catalyst producing ethylbenzene, styrene, and diethylbenzene. Zn, Mo, Pt, Pb/MFI showed high catalytic activity for the target reactions. Deactivation of the activities was observed on Zn, Mo and Pt/MFI, whereas stable activity was observed on Pb/MFI. Pb/MFI prepared by ion exchange method showed higher activity for the target reactions than that of by impregnation method, due to effective loading Pb^{2+} species on ion exchange sites of MFI. Formation rates of byproducts such as C_{3-5} hydrocarbon, toluene, and naphthalene were slow on Pb/MFI with low Al content prepared by ion exchange method. Byproducts from side reactions were converted into coke species finally, resulting in deactivation of the catalyst.

References

[1] D. A. Wood, C. Nwaoha, B. F. Towler, *J.Nat. Gas Sci. Eng.*, **9** 196-208 (2012)

[2] J. N. Armor, *J. Energy Chem.*, **22**, 21-26 (2013)

[3] R. Z. Ríos-Mercado, C. Borraz-Sánchez, *Appl. Energ.*, **147**, 536-555 (2015)

[4] Y. Alcheikhhamdon, M. Hoorfar, *J.Nat. Gas Sci. Eng.*, **34** 689-701 (2016)

[5] C. He, F. You, *Ind. Eng. Chem. Res.*, **53**, 11442-11459 (2014)

[6] J. Heveling, C. P. Nicolaides, M. S. Scurrell, *Appl. Catal. A: Gen.*, **173**, 1-9 (1998)

[7] D. M. Ginosar, K. Coates, D. N. Thompson, *Ind. Eng. Chem. Res.*, **41**, 6537-6545 (2002)

[8] M. Lallemand, A. Finiels, F. Fajula, V. Hulea, *Appl. Catal. A: Gen.*, **301**, 196-201 (2006)

[9] W. Taifan, J. Baltrusaitis, *Appl. Catal. B: Environ.*, **198**, 525-547 (2016)

[10] T. Ren, M. Patel, K. Blok, *Energy*, **31**, 425-451 (2006)

[11] V. V. Bokade, G. D. Yadav, *J. Mol. Catal. A: Chem*, **285**, 155-161 (2008)

[12] T. F. Degnan Jr., C. M. Smith, C. R. Venkat, *Appl. Catal. A: Gen.*, **221**, 283-294 (2001)

[13] S. Kato, K. Nakagawa, N. Ikenaga, T. Suzuki, *Chem. Lett.*, **28**, 207-208 (1999)

[14] S. Kato, K. Nakagawa, N. Ikenaga, T. Suzuki, *Chem. Lett.*, **73**, 175-180 (2001)

[15] D. B. Lukyanov, T. Vazhnova, *J. Mol. Catal. A: Chem.*, **279**, 128-132 (2008)

[16] D. B. Lukyanov, T. Vazhnova, *J. Catal.*, **257**, 382-389 (2008)

[17] L. Chen, L. Lin, Z. Xu, X. Li, T. Zhang, *J. Catal.*, **157**, 190-200 (1995)

[18] T. Odedairo, S. Al-Khattaf, *Appl. Catal. A: Gen.*, **385**, 31-45 (2010)

[19] I. M. Gerzeliev, D. A. Shavaleev, A. M. Gyul'maliev, *Petrol. Chem.*, **57**, 424-429

(2017)

[20] K. Nakamura, A. Okuda, K. Ohta, H. Matsubara, K. Okumura, K. Yamamoto, R. Itagaki, S. Suganuma, E. Tsuji, N. Katada, *ChemCatChem*, **10**, 3806-3812 (2018)

[21] H. Matsubara, E. Tsuji, Y. Moriwaki, K. Okumura, K. Yamamoto, K. Nakamura, S. Suganuma, N. Katada, *Catal. Lett.*, 149, 2627-2635 (2019)

[22] T. Sano, K. Okabe, H. Hagiwara, H. Takaya, H. Shoji, K. Matsuzaki, *J. Mol. Catal.*, **40**, 113-117 (1987)

[23] L. Forni, G. Cremona, F. Missineo, G. Bellussi, C. Perego, G. Pazzuconi, *Appl. Catal. A: Gen.*, **121**, 261-272 (1995)

[24] I. V. Asaftei, N. Bilba, I. Sandu, *Rev. Chim-Bucharest*, **64**, 838-843 (2013)

[25] E. Mannei, F. Ayari, M. Mhamdi, M. Almohalla, A. G. Ruiz, G. Delahay, A. Ghorbel, *Micropor. Mesopor. Mater.*, **219**, 77-86 (2016)

[26] J. Gao, L. Zhang, J. Hua, W. Li, J. Wang, *Catal. Commun.*, **10**, 1615-1619 (2009).

[27] H. G. Niessen, M. V. Buskirk, C. Dybowski, D. R. Corbin, J. A. Reimer, A. T. Bell, *J. Phys. Chem. B*, **105**, 2945-2950 (2001)

[28] S. J. Kulkarni, R. R. Rao, M. Subrahmanyam, A. V. R. Rao, *Appl. Catal. A: Gen.*, **113**, l-7 (1994)

Chapter 7   Conclusions

The author studied conversion reactions of aromatic hydrocarbons on zeolite-based catalyst to clarify catalysis of them and develop a new catalyst promoting challenging reactions converting natural gas into useful chemicals. The knowledges from this study is desirable to be applied for designing catalysts which supports next generation.

Concluding remarks are shown below.

Chapter 2

Toluene disproportionation and cumene cracking were performed over various solid acid catalysts in 723-823 K and 1 MPa of total pressure. Based on the conversion of reactants, each reactions was analyzed kinetically, and activation enthalpy ($\Delta H^{*\circ}$) and entropy ($\Delta S^{*\circ}$) were calculated. Compensation effect was observed between $\Delta H^{*\circ}$ and $\Delta S^{*\circ}$. The slopes was depended on the bulkiness of reactant molecule as cumene > toluene > small alkane. On the other hand, the intercept of $\Delta H^{*\circ}$ in the effect may be index of difficulty for activating a reactant regardless of the degree of freedom.

Chapter 3

Methane and benzene were flowed on various elements supported on MFI zeolite at 773 K in 101 kPa of total pressure. Co/MFI showed distinctly high catalytic activity for direct methylation of benzene. Co/MFI was characterized with various spectroscopies such as NH$_3$-IRMS-TPD and XAS. It was clarified that Lewis acidic cobalt (+II) on ion exchange site of MFI was the active species for the reaction.

Chapter 4

Reactivity of methane and benzene over various elements supported on MFI zeolite was evaluated with temperature programmed reaction in 373-843 K. Ni, Co, and noble metals such as Rh, Pd, Pt showed high activity for benzene methylation with methane. Ni and noble metals were also highly active for dehydrogenation of methane, resulting in low methylation selectivity. Co species was stable with oxidized state (+II) during the reaction. It leads the stable activity for the reaction.

Chapter 5

Methane + benzene TPR experiments over various Co/MFI with different [Co] and [Al] were performed. Co species on external surface of MFI was reduced into metal Co0 species during the reaction and it promoted methane dehydrogenation. Co/MFI with low [Al] showed high methylation selectivity and long catalytic stability in high temperature where toluene formation rate over 2.0 µmol g^{-1} min^{-1}.

Chapter 6

Reactivity of ethane + benzene were evaluated over metal/MFI catalysts at 773 K. Zn, Mo, Pt and Pb/MFI showed high activity for production of target compounds such as ethylbenzene, styrene, and diethylbenzene. Zn, Mo, and Pt/MFI showed also high activity for production of byproducts such as naphthalene, toluene, and C$_{3-5}$ hydrocarbon, leading catalytic deactivation. Pb/MFI showed had high selectivity for the target products, resulting in high catalytic stability.

List of publications

[1]   Compensation between Activation Entropy and Enthalpy in Reactions of

Aromatic Hydrocarbons Catalyzed by Solid Acids

Koshiro Nakamura, Ryo Mizuta, Satoshi Suganuma, Etsushi Tsuji, Naonobu Katada

Catalysis Communication, **102**, 103-107 (2017)

[2]   Direct Methylation of Benzene with Methane Catalyzed by Co/MFI Zeolite

Koshiro Nakamura, Akihito Okuda, Kiyotaka Ohta, Hitoshi Matsubara, Kazu Okumura,

Kana Yamamoto, Ryosuke Itagaki, Satoshi Suganuma, Etsushi Tsuji, Naonobu Katada

ChemCatChem, **10**, 3806-3812 (2018)

[3]   Reactivity of Methane and Benzene over Metal/MFI Zeolite Analyzed with

Temperature-Programmed Reaction Technique

Koshiro Nakamura, Kazu Okumura, Etsushi Tsuji, Satoshi Suganuma, Naonobu Katada

ChemCatChem, in press (DOI: 10.1002/cctc.202000030)

Supplementary publications

[1]   Dealkylation of Alkyl Polycyclic Aromatic Hydrocarbon over Silica Monolayer Solid Acid Catalyst

Naonobu Katada, Yusuke Kawaguchi, Kazuki Takeda, Taku Matsuoka, Naoki Uozumi, Kazuki Kanai, Shohei Fujiwara, Keisuke Kinugasa, Koshiro Nakamura, Satoshi Suganuma, Masato Nanjo

Applied Catalysis A: General, **530**, 93-101 (2016)

[2]   Shape Selectivity in Toluene Disproportionation into Para-xylene Generated by Chemical Vapor Deposition of Tetramethoxysilane on MFI Zeolite Catalyst

Daisuke Mitsuyoshi, Koji Kuroiwa, Yuta Kataoka, Takuya Nakagawa, Misaki Kosaka, Koshiro Nakamura, Satoshi Suganuma, Yasuhiro Araki, Naonobu Katada

Microporous and Mesoporous Materials, **242**, 118-126 (2017)

[3]   Enhancement of Catalytic Activity for Toluene Disproportionation by Loading Lewis Acidic Nickel Species on ZSM-5 Zeolite

Satoshi Suganuma, <u>Koshiro Nakamura</u>, Akihito Okuda, Naonobu Katada

Molecular Catalysis, **435**, 110-117 (2017)

[4]   Selective Formation of Active Cobalt Species for Direct Methylation of Benzene with Methane on MFI Zeolite by Co-presence of Secondary Elements

Hitoshi Matsubara, Etsushi Tsuji, Yasumi Moriwaki, Kazu Okumura, Kana Yamamoto, Koshiro Nakamura, Satoshi Suganuma, Naonobu Katada

Catalysis Letters, **149**, 2627-2635 (2019)

Acknowledgments